



# Distinguishing signatures of scalar leptoquarks at hadron and muon colliders

Priyotosh Bandyopadhyay<sup>1,a</sup>, Anirban Karan<sup>1,2,b</sup>, Rusa Mandal<sup>3,c</sup>, Snehashis Parashar<sup>1,d</sup>

<sup>1</sup> Indian Institute of Technology Hyderabad, Kandi, Sangareddy, Telangana 502284, India

<sup>2</sup> Instituto de Física Corpuscular (CSIC - Universitat de València), Apt. Correus 22085, 46071 Valencia, Spain

<sup>3</sup> Indian Institute of Technology, Gandhinagar, Gujarat 382355, India

Received: 16 June 2022 / Accepted: 14 September 2022  
© The Author(s) 2022

**Abstract** While the hunt for new states beyond the standard model (SM) goes on for various well motivated theories, the leptoquarks are among the most appealing scenarios at recent times due to a series of tensions observed in  $B$ -meson decays. We consider  $SU(2)$  singlet and triplet scalar leptoquarks separately, which contribute to charged and neutral current  $B$ -meson decays. Focusing on the single production of these two scalar leptoquarks, we perform a PYTHIA-based simulation considering all the dominant SM backgrounds at the current and future setups of the Large Hadron Collider (LHC). The mono- $b$ -jet +  $\cancel{p}_T$  finalstate gives the strongest signal for the singlet leptoquark at the 30 TeV LHC or Future Circular Collider (FCC), with a possibility of  $5\sigma$  signal significance with  $\gtrsim 1000 \text{ fb}^{-1}$  of integrated luminosity, for the chosen benchmark scenarios. The finalstate consisting of a  $c$ -jet and two  $\tau$ -jets provides highest reach for the singlet leptoquark, probing an  $\mathcal{O}(10^{-1})$  value of the Yukawa-type couplings for up to 3.0 TeV leptoquark mass. For the triplet leptoquark,  $1 - \text{jet} + 2\mu + \cancel{p}_T$  topology is the most optimistic signature at the LHC, probing leptoquark couplings to fermions at  $\mathcal{O}(10^{-1})$  value for the leptoquark mass range up to 4.0 TeV. The invariant mass edge distribution is found to be instrumental in determination of the leptoquark mass scale at the LHC. We also perform the analysis at the proposed multi-TeV muon collider, where an  $\mathcal{O}(10^{-1})$  leptoquark Yukawa coupling can be probed for a 5.0 TeV leptoquark mass.

## Contents

1	Introduction	.....
2	Framework	.....
2.1	Theory and benchmark points	.....
2.2	Set up for the LHC/FCC and muon colliders	.....
3	$S_1$ at the LHC/FCC	.....
3.1	Kinematic distributions and topologies	.....
3.2	Finalstates including $b$ and $\tau$ jets	.....
3.2.1	$1b - \text{jet} + 1\tau - \text{jet} + 1\ell + \cancel{p}_T$	.....
3.2.2	$1b - \text{jet} + 1\tau - \text{jet} + 2 - \text{jets} + \cancel{p}_T$	.....
3.2.3	$1b - \text{jet} + \cancel{p}_T$	.....
3.3	Finalstates including $c$ and $\tau$ jets	.....
3.3.1	$1c - \text{jet} + 1\tau - \text{jet} + \cancel{p}_T$	.....
3.3.2	$1c - \text{jet} + 2\tau - \text{jet} + \cancel{p}_T$	.....
3.4	Invariant mass edge distribution	.....
4	$S_3$ at the LHC/FCC	.....
4.1	Kinematic distributions and topologies	.....
4.2	$S_3^{4/3}$ component of $S_3$ : $1 - \text{jet} + 2\mu + \cancel{p}_T$	.....
4.3	$S_3^{2/3}$ component of $S_3$ : $1c - \text{jet} + \cancel{p}_T$	.....
4.4	$S_3^{1/3}$ component of $S_3$	.....
4.4.1	$1c - \text{jet} + 2\mu + \cancel{p}_T$	.....
4.4.2	$1c - \text{jet} + 1\mu + \cancel{p}_T$	.....
4.4.3	$2 - \text{jet} + \cancel{p}_T$	.....
4.4.4	$1 - \text{jet} + 1\mu + \cancel{p}_T$	.....
5	Lepton flavour violating decay signatures	.....
5.1	$1b - \text{jet} + 2 - \text{jet} + 2\mu$	.....
5.2	$1b - \text{jet} + 1\ell + 1\mu$	.....
6	Leptoquarks at muon collider	.....
6.1	Kinematic distributions and topologies	.....
6.2	$2 - \text{jet} + 2\mu$	.....
6.3	$2c - \text{jet} + 2\mu$	.....
6.4	$2b - \text{jet} + 2\mu$	.....
6.5	$2b - \text{jet} + 2 - \text{jet} + 2\mu$	.....

<sup>a</sup> e-mail: [bpriyo@phy.iith.ac.in](mailto:bpriyo@phy.iith.ac.in) (corresponding author)

<sup>b</sup> e-mail: [kanirban@ific.uv.es](mailto:kanirban@ific.uv.es)

<sup>c</sup> e-mail: [rusa.mandal@iitgn.ac.in](mailto:rusa.mandal@iitgn.ac.in)

<sup>d</sup> e-mail: [ph20resch11006@iith.ac.in](mailto:ph20resch11006@iith.ac.in)

7	Comparison of results and reach at colliders . . . . .
7.1	Discussion on $S_1$ . . . . .
7.2	Discussion on $S_3$ . . . . .
7.2.1	For the LHC/FCC . . . . .
7.2.2	For a muon collider . . . . .
7.3	Discussion on uncertainties . . . . .
8	Conclusion . . . . .
	Appendix A: NLO QCD $K$ -factors of SM backgrounds at the LHC/FCC . . . . .
	References . . . . .

## 1 Introduction

Leptoquarks among the most promising beyond the Standard Model (SM) candidates have been extensively searched at the experiments in past few years and the hunt is very much on at recent colliders. These colour charged bosons couple to quarks and leptons at the tree level and carry electromagnetic charge as well. Although the idea of quark-lepton unification was put forward in the 1970s [1, 2], leptoquarks have drawn a significant attention recent days in order to explain the tensions observed in  $B$ -decays by several experimental collaborations [3–8].

Leptoquark can be pair or singly produced at the colliders and because of its strong interaction nature, pair production generally dominates at the LHC [9–14]. However the single production, which is governed by the model dependent Yukawa-type couplings, can also be significant in higher mass region [15, 16]. Such Yukawa-type couplings are directly related to the low energy processes like meson decays. Hence, at present when no signatures of these new particles have been found at the LHC, which in turn is regularly pushing the lower limit of the allowed masses upwards, it is important to study the single production in connection with the possible hints of new physics (NP) seen in  $B$ -decays.

In this paper, we focus on two scalar leptoquarks namely  $S_3$  and  $S_1$  having  $(\bar{\mathbf{3}}, \mathbf{3}, 1/3)$  and  $(\bar{\mathbf{3}}, \mathbf{1}, 1/3)$  quantum numbers, respectively, under the SM gauge group  $(SU(3)_c, SU(2)_L, U(1)_Y)$ . This choice is motivated with the possibility to address the discrepancies observed in either or both the  $b \rightarrow s\mu\mu$  (neutral current (NC)) and  $b \rightarrow c\tau\bar{\nu}$  (charged current (CC)) transitions [17–29]. Phenomenology of scalar leptoquarks [30–53] and R-parity violating scalars (which resemble the leptoquark scenarios) [54–56] at the colliders has been studied in literature with main emphasis on the pair production. The distinct features of scalar and vector leptoquarks carrying all possible combinations of the SM gauge quantum numbers are explored at the lepton-photon collider [57], electron-proton collider [58] and at the LHC [59, 60] as well. The couplings to first generation of quarks are leptons are stringently constrained from Kaon and lepton physics [61–64] and the recent ATLAS searches performed with a

centre-of-mass energy of 13 TeV and an integrated luminosity of  $139\text{fb}^{-1}$  [65] exclude mass up to 1.8 TeV decaying into an electron and a quark. The limits are relatively weaker while looking for finalstates into third generation of fermions [66, 67].

The finalstate topologies studied in this work is directly related to the channels where certain tensions have been observed in  $B$ -decays and thus the phenomenology of  $S_1$  leptoquark aims at modes with  $\tau$  lepton and neutrinos in the finalstate whereas for  $S_3$  leptoquark mostly muons and neutrinos are present. This provides very interesting and distinguishable signatures for the direct searches which can probe the most favored parameter space. Apart from the current setup of the LHC, this work also presents outcomes for the potential of the high luminosity LHC and the high energy LHC projects [68] to measure the properties of the considered leptoquarks. In view of the European Strategy Update for Particle Physics released its recommendation to investigate the technical and financial feasibility of a future hadron collider (FCC) at CERN with a center-of-mass energy of at least 100 TeV [69], we provide the analysis for such a setup as well.

Recently, there is a growing interest in the community for a multi-TeV muon collider which can succeed the LHC [70–73]. Due to less synchrotron radiation of muon compared to electron, no initial state QCD radiation, centre-of-mass frame and significantly reduced background environment in contrast to hadron colliders, a muon collider has potential to look for new states beyond the SM [74–77]. The advantage is eminent for the NP mediators having direct connection to the  $b \rightarrow s\mu\mu$  anomalies [78, 79]. Hence, in this article, we explore the phenomenology of  $S_3$  leptoquark at muon collider as well. The pair production of leptoquark provides interesting signatures such as di-muon plus jets at muon collider which has spectacular sensitivity for the leptoquark coupling and mass parameters.

The rest of the paper is organized as follows. In Sect. 2, we discuss the theoretical framework behind the choice of the benchmark scenarios (in Sect. 2.1) and then specify the setup used for the phenomenological study at colliders (in Sect. 2.2). We perform the LHC simulation for the single production of the scalar leptoquark  $S_1$  in Sect. 3; starting with the kinematic distributions (in 3.1) and then with two separate sections (Sects. 3.2 and 3.3) differing due to the flavour of the jets in the finalstates. The invariant mass edge distribution for  $S_1$  is discussed in Sect. 3.4. Similar analysis for the phenomenology at the current and future LHC for the scalar leptoquark  $S_3$  is described in Sect. 4. Several subsections are devoted to study the signatures arising from the different components of this electroweak triplet leptoquark and we separately analyze lepton flavour violating signatures in the decay for  $S_3$  in Sect. 5. We perform the simulation at a multi-TeV muon collider for the scalar leptoquarks in Sect. 6.

Finally, Sect. 7 presents comparison of all the results for both of these leptoquarks highlighting the prospects at current and future colliders and our concluding remarks are mentioned in Sect. 8.

## 2 Framework

In this section starting with the interaction Lagrangians of the two scalar leptoquarks, we obtain the benchmark scenarios which can explain any of the two types of tensions observed in neutral and charged current  $B$ -decays while being consistent with other data. Then we describe the basic set up used in our analysis to study the collider phenomenology at the LHC, FCC as well as at the proposed multi-TeV muon collider.

### 2.1 Theory and benchmark points

We consider two scalar leptoquarks  $S_1(\bar{\mathbf{3}}, \mathbf{1}, 1/3)$  and  $S_3(\bar{\mathbf{3}}, \mathbf{3}, 1/3)$  separately, and write the interaction Lagrangians for them with the SM fermions as

$$\mathcal{L}_{S_1} = \overline{Q}^{ci} i\tau_2 Y_{S_1}^{i\alpha} L^\alpha S_1 + \overline{u}_R^{ci} Z_{S_1}^{i\alpha} \ell_R^\alpha S_1 + \text{h.c.}, \tag{1}$$

$$\mathcal{L}_{S_3} = \overline{Q}^{ci} Y_{S_3}^{i\alpha} i\tau_2 \boldsymbol{\tau} \cdot \mathbf{S}_3 L^\alpha + \text{h.c.}, \tag{2}$$

respectively, where we denote the left-handed SM quark (lepton) doublets as  $Q$  ( $L$ ), while  $u_R$  ( $d_R$ ) and  $\ell_R$  are the right-handed up (down)-type quark and lepton singlets, respectively. The notation  $f^c \equiv \mathcal{C}\bar{f}^T$  indicates the charge-conjugated field of the fermion  $f$ . Here  $Y_{LQ}$  and  $Z_{LQ}$  are completely arbitrary Yukawa-type matrices in flavour space and  $\tau_k$ ,  $k \in \{1, 2, 3\}$  are the Pauli matrices. Expanding the interaction terms in the mass-eigenstate basis we get

$$\mathcal{L}_{S_1} = \left[ \overline{u}_L^{ci} (V^* Y_{S_1})^{ij} \ell_L^j - \overline{d}_L^{ci} Y_{S_1}^{ij} v_L^j + \overline{u}_R^{ci} Z_{S_1}^{ij} \ell_R^j \right] S_1 + \text{h.c.}, \tag{3}$$

$$\begin{aligned} \mathcal{L}_{S_3} = & -\overline{d}_L^{ci} Y_{S_3}^{ij} v_L^j S_3^{1/3} - \sqrt{2} \overline{d}_L^{ci} Y_{S_3}^{ij} \ell_L^j S_3^{4/3} \\ & + \sqrt{2} \overline{u}_L^{ci} (V^* Y_{S_3})^{ij} v_L^j S_3^{-2/3} \\ & - \overline{u}_L^{ci} (V^* Y_{S_3})^{ij} \ell_L^j S_3^{1/3} + \text{h.c.} . \end{aligned} \tag{4}$$

The transformation from the fermion interaction eigenstates to mass eigenstates is simply given by  $u_L \rightarrow V^\dagger u_L$ , where  $V$  is the quark Cabibbo–Kobayashi–Maskawa (CKM) matrix [80,81] and we have neglected the unitary matrix in the neutrino sector. Note that, being a triplet under  $SU(2)_L$ ,  $S_3$  has three components differing in electric charges which are shown in the superscripts.

It is apparent from Eq. (3) that at tree level,  $S_1$  contributes to the  $b \rightarrow c\tau\bar{\nu}$  transition, whereas,  $S_3$  in Eq. (4) promotes both  $b \rightarrow s\mu\mu$  and  $b \rightarrow c\tau\bar{\nu}$  modes. Considering one leptoquark at a time, the minimal set of non-zero couplings required for the above mentioned leptoquarks to explain either of the  $b \rightarrow s\mu\mu$  or  $b \rightarrow c\tau\bar{\nu}$  anomalies are summarized in Table 1. Here the contribution to CC mode is via the following effective Hamiltonian

$$\begin{aligned} \mathcal{H}_{\text{eff}}^{\text{CC}} = & \frac{4G_F V_{cb}}{\sqrt{2}} \left[ \mathcal{C}_L^S (\bar{c} P_L b) (\bar{\tau} P_L \nu) \right. \\ & \left. + \mathcal{C}_L^T (\bar{c} \sigma^{\mu\nu} P_L b) (\bar{\tau} \sigma_{\mu\nu} P_L \nu) \right], \end{aligned} \tag{5}$$

where

$$\mathcal{C}_L^S(M_{S_1}) = -4\mathcal{C}_L^T(M_{S_1}) = -\frac{v^2}{4M_{S_1}^2} \frac{1}{V_{cb}} Y_{S_1}^{33} Z_{S_1}^{*23}. \tag{6}$$

The ratios, defined as  $R(D^{(*)}) \equiv \text{BR}(B \rightarrow D^{(*)} \tau \bar{\nu})/\text{BR}(B \rightarrow D^{(*)} \ell \bar{\nu})$ , with  $\ell = \{e, \mu\}$ , can then be expressed as [82]

$$\begin{aligned} R(D)/R(D)_{\text{SM}} \approx & 1 + 1.504 \text{Re} \left[ \mathcal{C}_L^{S*} \right] \\ & + 1.171 \text{Re} \left[ \mathcal{C}_L^{T*} \right] + 1.037 |\mathcal{C}_L^S|^2 \\ & + 0.939 |\mathcal{C}_L^T|^2, \end{aligned} \tag{7}$$

$$\begin{aligned} \mathcal{R}(D^*)/\mathcal{R}(D^*)_{\text{SM}} \approx & 1 - 0.114 \text{Re} \left[ \mathcal{C}_L^{S*} \right] \\ & - 5.130 \text{Re} \left[ \mathcal{C}_L^{T*} \right] - 0.037 |\mathcal{C}_L^S|^2 \\ & + 17.378 |\mathcal{C}_L^T|^2, \end{aligned} \tag{8}$$

where the Wilson coefficients are evaluated at the  $m_b$  scale using renormalization group equations and neglecting electroweak contributions:  $\mathcal{C}_L^{S(T)}(m_b) = 1.67(0.84) \times$

**Table 1** The benchmark points defined with the minimal set of coupling values required for the CC or NC anomalies for  $S_1$  and  $S_3$  leptoquarks, respectively. The symbol ‘✓’ (‘✗’) denotes agreement (disagreement) at  $\pm 1\sigma$  level for the corresponding observables

LQ	Mass (TeV)	NC	CC	Couplings	Benchmark points
$S_1$	1.5	✗	✓	$Y_{S_1}^{33} = 0.91, Z_{S_1}^{23} = -0.50$	BP1
	2.0			$Y_{S_1}^{33} = 1.10, Z_{S_1}^{23} = -0.74$	BP2
$S_3$	1.5	✓	✗	$Y_{S_3}^{22} = 0.50, Y_{S_3}^{32} = 0.003$	BP1
	2.0			$Y_{S_3}^{22} = 0.60, Y_{S_3}^{32} = 0.003$	BP2
	1.5			$Y_{S_3}^{22} = 0.008, Y_{S_3}^{32} = 0.20$	BP3

$\mathcal{C}_L^{S(T)}$  ( $\Lambda = \mathcal{O}(\text{TeV})$ ). The latest HFLAV average of  $R(D^{(*)})$  data indicates 14% enhancements [8] compared to the SM predictions and two desired benchmark values are quoted in Table 1. We have checked that such benchmark points are allowed by the one-loop induced  $Z \rightarrow \tau\tau$ ,  $Z \rightarrow \nu\nu$  decays [83–86] and  $B_s$  mixing bound [87]. Note that,  $S_3$  also generates SM-like V-A operator, however, the required couplings to explain the  $R(D^{(*)})$  anomalies are forbidden by  $Z \rightarrow \tau\tau$  and  $B_s$ -mixing data.

In case of the NC anomalies we generate the following contribution to the effective Hamiltonian

$$\mathcal{H}_{\text{eff}}^{\text{NC}} = -\frac{4G_F}{\sqrt{2}} \frac{\alpha_{\text{EM}}}{4\pi} V_{td} V_{ts}^* \left[ C_9^{\text{NP}} (\bar{s}\gamma^\mu P_L b)(\bar{\mu}\gamma_\mu \mu) + C_{10}^{\text{NP}} (\bar{s}\gamma^\mu P_L b)(\bar{\mu}\gamma_\mu \gamma_5 \mu) \right], \tag{9}$$

where

$$C_9^{\text{NP}} = -C_{10}^{\text{NP}} = \frac{v^2}{M_{S_3}^2} \frac{\pi}{\alpha_{\text{EM}} V_{tb} V_{ts}^*} Y_{S_3}^{*32} Y_{S_3}^{22}. \tag{10}$$

The existing tensions observed in this mode can be achieved via  $C_9^{\text{NP}} = -C_{10}^{\text{NP}} = -0.41_{-0.07}^{+0.07}$  [88] and such benchmark cases are shown in Table 1, which are allowed by the most constraining bounds arising from  $Z \rightarrow \mu\mu$ ,  $Z \rightarrow \nu\nu$  decays [83–86] and  $B_s$  mixing [87]. The subsequent sections are devoted for detailed collider phenomenology studies of such benchmark scenarios for these two leptoquarks  $S_1$  and  $S_3$  at the LHC/FCC and at a multi-TeV muon collider. We mention that among all five scalar leptoquarks, the weak doublet  $R_2(\mathbf{3}, \mathbf{2}, 7/6)$  can also accommodate CC anomalies [89,90] and, with the minimal choice of Yukawa-type couplings, it might give rise to the similar phenomenology as of  $S_1$ . However, the detailed analysis of  $R_2$  is left for our future work. Additionally, the collider phenomenology is very much dependent on the flavour structure of the leptoquark Yukawa-type couplings, and we stick to the minimal choice required to explain the observed tensions in  $B$ -decays. Altering the flavour structure of the entries of these couplings will give rise to completely different phenomenology which is beyond the focus of this work. The minimal choice of couplings are presented in Table 1. In order to understand the relevance of the magnitude of such chosen couplings, the variation of signal significance for the most promising cases will be discussed in Sect. 7.

### 2.2 Set up for the LHC/FCC and muon colliders

In this subsection we summarise the kinematic cuts and definition of the collider set up that are used in simulations. Implementing the models in SARAH [91], model files are generated for CalcHEP [92]. The “.lhe” event files are then generated and interfaced with PYTHIA6.4.5 [93] for hadronization with initial state radiation (ISR) and final state radiation

(FSR). The jet is formed using Fastjet-3.0.3 [94] with Cambridge/Aachen jet algorithm with a jet radius of 0.5. The additional basic cuts, written below, are also implemented.

- The calorimeter coverage is  $|\eta| < 4.5$ .
- The minimum jet transverse momentum  $p_T = 20$  GeV and jets are ordered in  $p_T$ .
- Leptons are selected with  $p_T \geq 20$  GeV and  $|\eta| < 2.5$ .
- $\Delta R_{\ell j} \geq 0.4$  and  $\Delta R_{jj} \geq 0.2$ , where  $\Delta R_{ij} = \sqrt{\Delta\eta_{ij}^2 + \Delta\Phi_{ij}^2}$  is the angle between the  $i$ -th and  $j$ -th particles, with  $\Delta\Phi_{ij}$  is the difference of the azimuthal angle and  $\Delta\eta_{ij}$  is the difference of the pseudo-rapidities.
- We demand that hadronic activity within a cone of  $\Delta R = 0.3$  of the leptons should be  $\leq 0.15 p_T^\ell$  GeV in the specified cone.
- As our benchmark points are with leptoquark masses of 1.5 TeV or 2.0 TeV, a hardness cut evaluated as the scalar sum of lepton, jet and missing transverse momentum,  $p_T^H = \Sigma(p_T^\ell + p_T^j + p_T) \geq 1.2$  TeV is implemented at the analysis level for both signal and backgrounds. For computational convergence and to get events at the high-momentum tail, the SM background events were generated with  $\sqrt{\hat{s}} \geq 1.2$  TeV.

Armed with the above mentioned collider set up, in the following sections we analyse the phenomenologies of the single production of  $S_1$ ,  $S_3$  leptoquarks at the LHC/FCC with three different choices of the centre-of-mass energies 14 TeV, 30 TeV and 100 TeV. In this article we focus on the single leptoquark production for probing the leptoquark Yukawa couplings. Finalstates coming from such production processes solely depend on the Yukawa couplings, absence of which make the finalstates cease to exist. However, leptoquark pair production dominated by the strong coupling constant can contaminate such finalstates arising from the single leptoquark productions. We define such contamination as model backgrounds, that can be estimated once we have the information of the leptoquark mass and excitations for a given choice of Yukawa-type coupling that we already have benchmarked. In Sect. 7.3 we discuss the impact of such effects and the corresponding uncertainties in the signal significance.

### 3 $S_1$ at the LHC/FCC

In this section, we first start with the singlet leptoquark  $S_1$ . In order to perform a collider analysis at the LHC/FCC, we choose the following set of centre-of-mass energy ( $E_{\text{CM}}$ ) values: 14 TeV, 30 TeV and 100 TeV and the dominant SM backgrounds are also taken into account accordingly. The benchmark points, quoted in Table 1, for two different  $S_1$

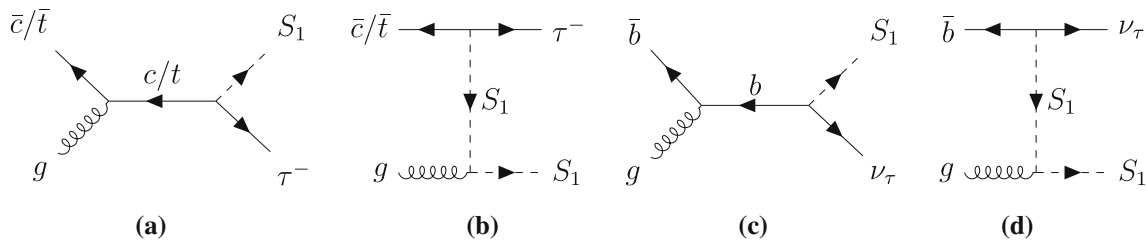


**Fig. 1** The tree level Feynman diagrams for  $c/t - g$  and  $b - g$  fusion producing  $S_1$  leptoquark associated with a lepton

**Table 2** The cross-sections at the LHC/FCC via  $c - g$ ,  $b - g$  and  $t - g$  channels for the two benchmark points of  $S_1$  leptoquark at three different centre-of-mass energies of 14 TeV, 30 TeV and 100 TeV. We chose

NNPDF\_lo\_as\_0130\_qed [95] as the parton distribution function and  $\sqrt{s}$  as renormalization/factorization scale, with the NLO QCD  $K$ -factor of 1.5

Benchmark Points ( $M_{S_1}$ )	$\sigma(c - g \rightarrow S_1 \tau)$ in fb with $E_{CM}$ in TeV			$\sigma(b - g \rightarrow S_1 \nu_\tau)$ in fb with $E_{CM}$ in TeV			$\sigma(t - g \rightarrow S_1 \tau)$ in fb with $E_{CM}$ in TeV		
	14 TeV	30 TeV	100 TeV	14 TeV	30 TeV	100 TeV	14 TeV	30 TeV	100 TeV
BP1 (1.5 TeV)	0.24	4.07	96.65	0.50	9.09	237.29	0.12	2.60	78.21
BP2 (2.0 TeV)	0.08	1.86	60.62	0.09	2.73	98.16	0.03	0.80	33.20

masses namely, 1.5 TeV and 2.0 TeV are motivated from the explanation to CC anomalies seen in  $B$ -decays. Such parameter spaces are also allowed by the recent searches at the LHC [66,67]. The main focus of this article is to probe the Yukawa-type coupling via single leptoquark production and the corresponding quark - gluon ( $g$ ) fusion production modes can be seen from the leading order Feynman diagrams in Fig. 1. The tree-level cross-sections for the  $c - g$  and  $b - g$  fusions are presented in Table 2 for three different centre-of-mass energies of 14 TeV, 30 TeV and 100 TeV respectively, where NNPDF\_lo\_as\_0130\_qed [95] is used as parton distribution function, and  $\sqrt{s}$ , the parton level centre-of-mass energy is used as the renormalization/factorization scale. It can be seen that the  $t - g$  fusion is not negligible at the  $E_{CM}$  of 30 TeV and 100 TeV due to enhanced parton distribution function contribution in NNPDF\_lo\_as\_0130\_qed [95]. Additionally, extrapolating the results from Refs. [15,96], we take the NLO QCD  $K$ -factor of 1.5 for the single scalar leptoquark production processes. For the purpose of the analysis, the SM backgrounds contributions are also quoted at NLO QCD, with the  $K$ -factors calculated using MadGraph5\_aMC@NLO [97], which are presented in Appendix A. The final event numbers and the signal significance are evaluated with NLO cross-sections and assuming Gaussian distribution the signal significance is calculated as  $\sigma = \frac{n_{sig}}{\sqrt{n_{sig} + n_{bg}}}$ , where  $n_{sig}$ ,  $n_{bg}$  are the signal and the background events numbers presented at certain integrated luminosity at some centre-of-mass energy.

The leptoquarks produced from these mentioned channels will decay into  $b\nu_\tau$ ,  $t\tau$  and  $c\tau$  finalstates with the branching ratios quoted in Table 3. Here we find that  $b\nu_\tau$ ,  $t\tau$  are the dominant modes which give rise to various finalstate topologies as discussed later in the subsections. Note that this min-

**Table 3** Decay branching fractions in % for the allowed benchmark points of  $S_1$  leptoquark

Decay Modes	Branching fractions	
	BP1 $M_{S_1} = 1.5$ TeV	BP2 $M_{S_1} = 2.0$ TeV
$S_1 \rightarrow b\nu_\tau$	43.9	41.4
$S_1 \rightarrow t\tau$	42.8	40.4
$S_1 \rightarrow c\tau$	13.3	18.6

imal choice of parameter space forbids a decay to  $c\mu$  mode which substantially reduces the SM backgrounds and can also nicely reconstruct the leptoquark invariant mass as found in [31]. The following subsections describe kinematical distributions and signal events and background events for several chosen topologies.

### 3.1 Kinematic distributions and topologies

Before going into the details of the collider simulation let us have a look at the different differential distributions to motivate the advanced cuts which will be used later on to reduce the SM backgrounds. Depending on the decays of  $S_1$  some finalstates may have more background than the rest. However, to reduce the light QCD-jet backgrounds we need more flavour tagging viz.  $b$ -jet and/or  $\tau$ -jet. We first consider the production channel  $c - g \rightarrow S_1 \tau$  (shown in Fig. 1a), where  $S_1$  can further decay to either  $b\nu$  or  $c\tau$  states. Thus, finalstates involving  $b$ -,  $c$ - and  $\tau$ -jets are possible and we discuss them separately. The dominant SM backgrounds arise from  $t\bar{t}$ , owing to the high cross-section, which contribute in the finalstates involving  $b/c/\tau$ -jets. The demand of only

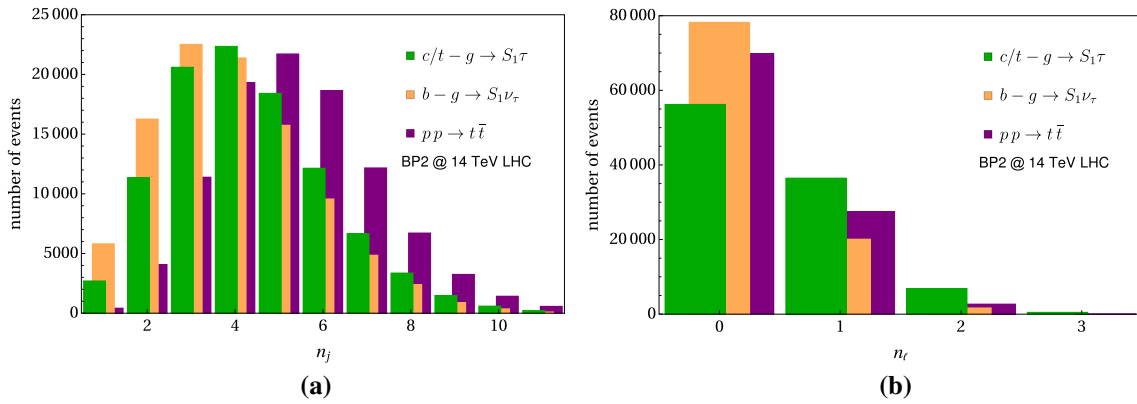


**Fig. 2** The jet multiplicity ( $n_j$  in a) and lepton multiplicity ( $n_\ell$  in b) distributions for the BP2 and SM background  $t\bar{t}$  at the LHC with centre-of-mass energy of 14 TeV

one  $b/c$ -jets, one or two  $\tau$ -jets, high cuts on missing transverse momentum ( $\cancel{p}_T$ ), and veto on the number of light jets can help us reduce such background contaminations. Each of such demands and cuts are categorically mentioned when we discuss each individual finalstate. If we consider the decay of  $S_1 \rightarrow t\tau$ , the finalstates involving leptons are suppressed due to the lower branching of  $W^\pm$  in the leptonic mode.

For this analysis we considered  $b$ -jet tagging efficiency of  $\sim 70\%$  via the secondary vertex reconstruction mechanism [98–100]. For  $\tau$ -jet we reconstruct the hadronic one-prong ( $\pi^\pm$ ) jet as  $\tau$ -jet with momentum dependent efficiencies as shown in [101,102]. The  $c$ -jet tagging efficiency is taken around 56% with a mistagging of 12%, which is very conservative considering non-loose tagging mechanism [103].

In Fig. 2a we display the jet multiplicity distribution ( $n_j$ ) for the two signal processes of  $c/t - g \rightarrow S_1\tau$  (green) and  $b - g \rightarrow S_1\nu_\tau$  (orange) for BP2 at the 14 TeV LHC, in comparison with the  $t\bar{t}$  SM background (purple). The distribution for  $b - g \rightarrow S_1\nu_\tau$  peaks at three jets, with the sources of jets being the daughter top quark of  $S_1$ , as well as the  $\tau$ -jet in the  $S_1 \rightarrow t\tau$  decay channel (if tagged). This peak increases to four jets for  $c/t - g \rightarrow S_1\tau$ , where the additional  $\tau$ -jet produced with  $S_1$  contributes. The  $t\bar{t}$  background distribution shows the peak at five jets, as both the top quarks and their daughter  $W^\pm$  bosons contribute. The ISR/FSR effects give the tails for these jet multiplicity distributions. Figure 2b shows the distribution of lepton multiplicity ( $n_\ell$ ) for the same processes, following the same colour codes. While both the signal processes and the background peaks at zero leptons, the  $b - g \rightarrow S_1\nu_\tau$  process has more events there owing to less sources of leptons in the production and decay products. The hard charged lepton ( $e/\mu$ ) mainly comes from the decay to top quark which is produced from the  $S_1$  decay. The source of the second lepton is mostly from the  $\tau$  decay or the semileptonic decays of  $b$  quark. On the other hand,  $c/t - g \rightarrow S_1\tau$  gives the least number of zero-lepton events, as the leptonic decay of the recoiled  $\tau$  can also contribute. The

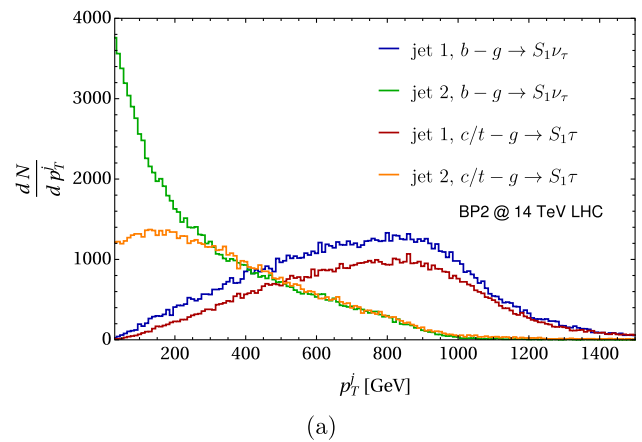


**Fig. 3** The  $p_T$  distribution of the two hardest jets ( $p_T^j$ ) from each of the production processes  $b - g \rightarrow S_1\nu_\tau$  and  $c/t - g \rightarrow S_1\tau$ , at the 14 TeV LHC, for BP2

background shows similar behaviour as the signal, as mainly the  $W^\pm$  bosons coming from the top quarks can contribute to the lepton multiplicity.

In Fig. 3 we depict the jet  $p_T$  ( $p_T^j$ ) distributions of the two hardest jets at the 14 TeV LHC, emanating from each of the two production modes considered. The jets from  $b - g \rightarrow S_1\nu_\tau$  process are shown in blue and green, while those from  $c/t - g \rightarrow S_1\tau$  are shown in red and orange. In each case, it is evident that the hardest jets (blue and red) peak at  $\sim 850$  GeV, which lies roughly around half of the leptoquark mass, as expected. In case of  $b - g \rightarrow S_1\nu_\tau$ , the second hardest jet’s source is the daughter  $W$ -boson of the top quark from  $S_1 \rightarrow t\tau$  decay, and so the  $p_T$  peak is observed at around 40 GeV. However, for  $c/t - g \rightarrow S_1\tau$ , the hadronic  $\tau$ -jet produced alongside the leptoquark accounts for the second hardest jet, showing a wide peak at  $\sim 150$  GeV.

We now move to the lepton  $p_T$  distributions as depicted in Fig. 4a, showing the  $p_T$  distribution of the hardest lepton  $p_T^\ell$  obtained from the two production processes  $b - g \rightarrow S_1\nu_\tau$

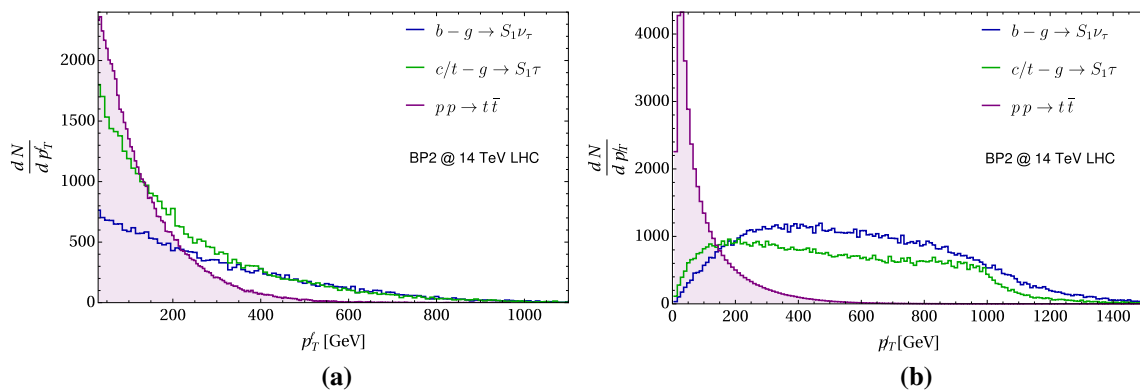


**Fig. 4** The lepton  $p_T$  ( $p_T^\ell$  in **a**) and missing transverse momentum ( $\cancel{p}_T$  in **b**) distributions for BP2 and the SM background  $t\bar{t}$  at the LHC with centre-of-mass energy of 14 TeV. The background in (a) and (b) are scaled with 1/2 and 1/100 respectively for convenience

(blue) and  $c/t - g \rightarrow S_1 \tau$  (green), for BP2 at the 14 TeV LHC. For comparison, the same distribution is shown in shaded purple for the  $t\bar{t}$  background, scaled down by 1/2 for illustrative purposes. The lack of a lepton as a direct decay product of the leptoquark means that in either of the signal production processes, the lepton  $p_T$  peaks at  $\sim 30$  GeV, same as the  $t\bar{t}$  case. However, the distributions in case of signal processes have more events at the tail, which can help us put advanced cut of  $p_T^\ell \geq 200$  GeV, to reduce the background contamination, later in our analysis. Figure 4b shows the missing transverse momentum  $\cancel{p}_T$  distribution for the three aforementioned signal and background processes with the same colour coding. It is evident that a large missing transverse momentum is observed which arises from the recoiled neutrino coming either at the production level for  $b - g \rightarrow S_1 \nu_\tau$  or at the later stage from  $c - g \rightarrow S_1 (\rightarrow b \nu_\tau) \tau$ . On the contrary, the missing transverse momentum  $\cancel{p}_T$  due to neutrinos in case of  $t\bar{t}$  peaks near  $\sim 50$  GeV, and the tail is much shorter. We can thus apply missing transverse momentum cut  $\cancel{p}_T \geq 500$  GeV for the considered finalstates later in our analysis which reduce the SM backgrounds substantially.

### 3.2 Finalstates including $b$ and $\tau$ jets

In this subsection we describe the finalstate topologies comprising  $b$ - and  $\tau$ -jets for  $S_1$  leptoquark production mainly via  $c - g$  and  $b - g$  fusions as well as with  $t - g$  fusion which contributes at high energy. Once produced in association with  $\tau$ -jet in  $c - g$  fusion, the  $S_1$  leptoquark further decays to  $b \nu_\tau$ ,  $t\tau$  states governed by the decay branching given in Table 3 giving rise to the following topologies composed of at least one  $b$ - and  $\tau$ -jet.

BP1, BP2:  $c/t - g \rightarrow S_1 \tau,$   
 $\rightarrow (b \nu_\tau) + \tau \rightarrow 1b - \text{jet}$   
 $+ 1\tau - \text{jet} + \cancel{p}_T, \quad (11)$

$$\rightarrow (t\tau) + \tau \rightarrow 1b - \text{jet}$$

$$+ 2\tau - \text{jet} + 1\ell + \cancel{p}_T, \quad (12)$$

$$\rightarrow (t\tau) + \tau \rightarrow 1b - \text{jet}$$

$$+ 2\tau - \text{jet} + 2 - \text{jets}. \quad (13)$$

Similarly,  $b - g \rightarrow S_1 \nu_\tau$  can give rise to the following topologies with  $b$ - and  $\tau$ -jet.

BP1, BP2:  $b - g \rightarrow S_1 \nu_\tau,$   
 $\rightarrow (b \nu_\tau) + \nu \rightarrow 1b - \text{jet} + \cancel{p}_T(14)$   
 $\rightarrow (t\tau) + \nu \rightarrow 1b - \text{jet}$   
 $+ 1\tau - \text{jet} + 1\ell + \cancel{p}_T, \quad (15)$   
 $\rightarrow (t\tau) + \nu \rightarrow 1b - \text{jet}$   
 $+ 1\tau - \text{jet} + 2 - \text{jets} + \cancel{p}_T. \quad (16)$

Note that, unlike the  $c/t - g$  fusion, for  $b - g$  fusion we can have mono  $b$ -jet plus missing energy as an unique signature Eq. (14). The  $b$ -jet and  $\tau$ -jet tagging are followed with the corresponding efficiencies [98–102], as mentioned earlier. From now onward, in the rest of the analysis, the light-jets are denoted as ‘jets’ ensuring no flavour tagging has been implemented. In the subsequent subsections we discuss all these finalstate signatures involving at least one  $b$ - and  $\tau$ -jet at the LHC/FCC with two different centre-of-mass energies namely 30 TeV and 100 TeV and we leave 14 TeV results as the signal significances are lower than  $3\sigma$  even with the integrated luminosity of  $3000 \text{ fb}^{-1}$ .

#### 3.2.1 $1b - \text{jet} + 1\tau - \text{jet} + 1\ell + \cancel{p}_T$

Here we consider Eqs. 15 and 12 which lead to  $1b - \text{jet} + 1\tau - \text{jet} + 1\ell + \cancel{p}_T$  finalstate topology. The complete finalstate including the advanced cuts and veto are given below.

$$n_{b-\text{jet}} = 1, n_{\tau-\text{jet}} \geq 1, n_j \geq 2, n_\ell \geq 1 \quad \text{and}$$

$$\cancel{p}_T \geq 500 \text{ GeV}, p_T^{j_1, j_2} \geq 200 \text{ GeV},$$

$$p_T^\ell \geq 200 \text{ GeV}, p_T^H \geq 1200 \text{ GeV}.$$

**Table 4** The number of events for  $1b\text{-jet} + \geq 1\tau\text{-jet} + \geq 1\ell + \cancel{p}_T \geq 500\text{ GeV}$  finalstate for the benchmark points and dominant SM backgrounds at the LHC/FCC with the centre-of-mass energies of 30 TeV and 100 TeV with integrated luminosities at  $1000\text{ fb}^{-1}$  and  $100\text{ fb}^{-1}$ , respectively. The required luminosities to achieve a  $5\sigma$  signal ( $\mathcal{L}_{5\sigma}$ ) are also shown for both the cases

$E_{CM}$ in TeV	Mode	$1b\text{-jet} + \geq 1\tau\text{-jet} + \geq 1\ell + \cancel{p}_T \geq 500\text{ GeV}$						
		Signal		Backgrounds				
		BP1	BP2	$t\bar{t}$	$VV$	$VVV$	$t\bar{t}V$	$tVV$
30	$c/t - g \rightarrow S_1 \tau$	56.08	39.76	643.35	1.36	0.00	30.66	7.84
	$b - g \rightarrow S_1 \nu$	7.44	3.24					
Total		63.52	43.00	683.21				
Significance ( $\sigma$ )		2.32	1.60					
$\mathcal{L}_{5\sigma}$ ( $\text{fb}^{-1}$ )		$\gg 3000$	$\gg 3000$					
100	$c/t - g \rightarrow S_1 \tau$	294.42	232.08	1313.83	7.67	7.04	91.84	28.02
	$b - g \rightarrow S_1 \nu$	23.96	18.53					
Total		318.36	250.61	1448.40				
Significance ( $\sigma$ )		7.57	6.08					
$\mathcal{L}_{5\sigma}$ ( $\text{fb}^{-1}$ )		43.58	67.63					

The event numbers at the centre-of-mass energies of 30 TeV and 100 TeV at the LHC/FCC with the respective integrated luminosities of  $1000\text{ fb}^{-1}$  and  $100\text{ fb}^{-1}$  are presented in Table 4. It can be seen that  $1b\text{-jet} + 1\tau\text{-jet} + 1\ell + \cancel{p}_T$  finalstate arises from both  $c/t$ -gluon and  $b$ -gluon fusion, where  $S_1$  decays to  $t\tau$  states. The top quark then provides the  $b$ -jet and the charged lepton via subsequent decays. When any of the two  $\tau$ -jets in Eq. (12) is tagged we obtain the mentioned finalstate from  $c/t - g$  fusion. However, for  $b - g$  fusion we have only one  $\tau$ -jet finalstate making the contribution significantly reduced in this case. The missing energy for the signal is relatively higher as can be seen from Fig. 4b and we apply a cut of  $\cancel{p}_T > 500\text{ GeV}$ . The benchmark points are with leptoquark masses of 1.5 and 2.0 TeV, so we apply a hardness cut of 1.2 TeV to reduce the background number of the events substantially, where the transverse variable total hardness defined as  $p_T^H = \Sigma(p_T^\ell + p_T^j + \cancel{p}_T)$ , is the scalar sum of lepton, jet and missing transverse momentum. The first two hard jets  $p_T$  and the charged lepton  $p_T$  are demanded to be  $\geq 200\text{ GeV}$  in order to reduce the SM backgrounds further as demonstrated in Fig. 3. Although 14 TeV numbers are not encouraging, the numbers presented in Table 4 at centre-of-mass energy of 30 TeV give rise to the signal significances of  $2.32\sigma$  and  $1.60\sigma$  at  $1000\text{ fb}^{-1}$  of integrated luminosity for BP1 and BP2, respectively, which again is not a very pleasant scenario. However, at the 100 TeV centre-of-mass energy of the LHC/FCC, we see promising numbers, with the signal significances of  $7.57\sigma$  and  $6.08\sigma$  obtained at  $100\text{ fb}^{-1}$  of integrated luminosity, for BP1 and BP2, respectively. In all cases,  $t\bar{t}$  remains the dominant background owing to the availability of a  $b$ -jet and the high cross-section, while  $t\bar{t}V$  also contributing significantly.

### 3.2.2 $1b\text{-jet} + 1\tau\text{-jet} + 2\text{-jets} + \cancel{p}_T$

Now we consider the  $1b\text{-jet} + 1\tau\text{-jet} + 2\text{-jets} + \cancel{p}_T$  finalstate, which is almost similar to the previous decay topologies with only exception of the  $W^\pm$ , coming from the top quark, decays hadronically (Eqs. 13, 16). Certainly, due to higher branching fraction in the hadronic mode, the event numbers for this finalstate are expected to increase substantially as compared to  $1b\text{-jet} + 1\tau\text{-jet} + 1\ell + \cancel{p}_T$  in Table 4. The complete finalstate with the advanced cuts is given as

$$n_{b\text{-jet}} = 1, n_{\tau\text{-jet}} \geq 1, n_j \geq 4, n_\ell = 0 \quad \text{and}$$

$$\cancel{p}_T \geq 500\text{ GeV}, p_T^{j_1, j_2} \geq 200\text{ GeV}, p_T^H \geq 1200\text{ GeV}.$$

Similar to  $1b\text{-jet} + 1\tau\text{-jet} + 1\ell + \cancel{p}_T$ , here also the 14 TeV numbers are insignificant. Therefore, in Table 5 we list only the number of events for the benchmark points as well as the dominant SM backgrounds for the centre-of-mass energies of 30 TeV and 100 TeV at integrated luminosities of  $1000\text{ fb}^{-1}$ ,  $100\text{ fb}^{-1}$ , respectively.

In this case, while the signal events increase as expected, we observe an overwhelming rise of the background contribution, owing to the abundance of zero-lepton events.  $t\bar{t}$  and  $t\bar{t}V$  remain the most dominant backgrounds, contributing to the demand of a  $b$ -jet. Such high backgrounds reduce our chances of obtaining a good signal strength at the 14 TeV LHC for both benchmark points and we do not list them here. The situation improves for BP1 when we move to the centre-of-mass energy of 30 TeV, where  $3.86\sigma$  signal significance can be obtained at  $1000\text{ fb}^{-1}$  of integrated luminosity. The required  $5\sigma$  discovery can be predicted to be made with a luminosity of  $1675.80\text{ fb}^{-1}$  for BP1. The BP2 signal however remains weak with  $2.21\sigma$  significance. The most promising

**Table 5** The number of events for  $1b - \text{jet} + \geq 1\tau - \text{jet} + \geq 2 - \text{jets} + / p_T \geq 500 \text{ GeV}$  finalstate for the benchmark points and dominant SM backgrounds at the LHC/FCC with the centre-of-mass energies of 30 TeV and 100 TeV for the integrated luminosities of  $1000 \text{ fb}^{-1}$  and  $100 \text{ fb}^{-1}$  for 100 TeV, respectively. The required luminosities to achieve a  $5\sigma$  signal ( $\mathcal{L}_{5\sigma}$ ) are also shown for both the cases

$E_{CM}$ in TeV	Mode	$1b - \text{jet} + \geq 1\tau - \text{jet} + \geq 2 - \text{jets} + \cancel{p}_T \geq 500 \text{ GeV}$						
		Signal		Backgrounds				
		BP1	BP2	$t\bar{t}$	$VV$	$VVV$	$t\bar{t}V$	$tVV$
30	$c/t - g \rightarrow S_1 \tau$	426.62	256.89	28097.22	128.64	28.06	737.05	94.04
	$b - g \rightarrow S_1 \nu$	239.59	123.33					
Total		666.21	380.22	29085.01				
Significance ( $\sigma$ )		3.86	2.21					
$\mathcal{L}_{5\sigma}$ ( $\text{fb}^{-1}$ )		1675.80	$\gg 3000$					
100	$c/t - g \rightarrow S_1 \tau$	1575.29	1105.74	59677.63	151.75	75.81	1682.02	320.77
	$b - g \rightarrow S_1 \nu$	830.63	546.74					
Total		2405.92	1664.48	61907.98				
Significance ( $\sigma$ )		9.49	6.60					
$\mathcal{L}_{5\sigma}$ ( $\text{fb}^{-1}$ )		27.78	57.37					

scenario again is the 100 TeV LHC/FCC, where  $9.49\sigma$  and  $6.60\sigma$  significance can be obtained for BP1 and BP2 respectively, with an integrated luminosity of  $100 \text{ fb}^{-1}$ .

### 3.2.3 $1b - \text{jet} + \cancel{p}_T$

In this case we consider the mode where  $S_1$  decays to  $b\nu_\tau$  states and this finalstate may only be composed of mono  $b$ -jet and missing energy, when  $S_1$  being produced from  $b - g$  fusion (Eq. 14). In order to obtain a cleaner signal and elimination of the SM background, further advanced cuts are applied on this finalstate. The full finalstate is given as follows:

$$n_{b-\text{jet}} = 1, n_j \leq 2, n_{\tau-\text{jet}} = 0, n_\ell = 0 \quad \text{and}$$

$$\cancel{p}_T \geq 500 \text{ GeV}, p_T^j \geq 400 \text{ GeV}, p_T^H \geq 1.2 \text{ TeV}$$

and

$$|M_{\ell\ell} - M_Z| \geq 5 \text{ GeV} + |M_{jj} - M_W| \geq 10 \text{ GeV}.$$

While we keep the cut on missing energy to be  $\geq 500 \text{ GeV}$  accounting for the recoiled neutrino or the neutrino coming from the  $S_1$  decay, we increase the leading jet  $p_T$  cut to  $400 \text{ GeV}$ . The hardness cut remains the same as the previous two cases. However, the absence of a top quark-induced contribution to this decay topology, we can put a veto on the di-jet invariant mass  $M_{jj}$ , demanding it to be at least  $10 \text{ GeV}$  away from the  $W$ -boson mass peak. Similar veto is applied to the di-lepton invariant mass  $M_{\ell\ell}$ , demanding a  $5 \text{ GeV}$  minimum separation from the  $Z$ -boson mass. This helps us reduce the background contribution further. Such a decay topology has a very unique signature, and we show the number of events and the SM backgrounds in Table 6 for the two centre-of-mass energies at the LHC/FCC. Similar to the previous cases the 14 TeV signal numbers are not very encouraging and we

do not list them here. The 30 TeV and 100 TeV event numbers are given in Table 6 at integrated luminosities of  $1000, 100 \text{ fb}^{-1}$ , respectively. At the 30 TeV LHC, results are a bit more promising for BP1 with a healthy  $4.9\sigma$  of signal significance, while the BP2 signal remains weak with a  $1.86\sigma$  significance. The  $5\sigma$  reach for BP1 can be achieved at a luminosity of  $1038.39 \text{ fb}^{-1}$ . At 100 TeV, the situation improves for BP2, as we reach a strength of  $3.92\sigma$  with  $100 \text{ fb}^{-1}$  luminosity, with a requirement of  $162.63 \text{ fb}^{-1}$  for the desired  $5\sigma$  strength. For BP1, we achieve  $7.93\sigma$  significance  $100 \text{ fb}^{-1}$  luminosity, with the  $5\sigma$  strength predicted to be obtainable at  $39.75 \text{ fb}^{-1}$  of luminosity. In all the cases,  $t\bar{t}$  remains the dominant background due to availability of a  $b$ -jet and higher cross-section, and the diboson ( $VV$ ) background is the next dominant one.

### 3.3 Finalstates including $c$ and $\tau$ jets

After studying the finalstates involving  $b$ -jets, we now aim to probe the other decay mode of  $S_1$ , namely to  $c \tau$  states. With the two dominant production channels via  $c - g$  and  $b - g$  fusions, we look for topologies composed of at least one  $c$ -jet and  $\tau$ -jet. The entire decay chain prompt us the following signals.

$$c/t - g \rightarrow S_1 \tau$$

$$\rightarrow (c \tau) + \tau \rightarrow 1c - \text{jet} + 2\tau - \text{jet}, \quad (17)$$

$$b - g \rightarrow S_1 \nu_\tau$$

$$\rightarrow (c \tau) + \nu \rightarrow 1c - \text{jet} + 1\tau - \text{jet} + \cancel{p}_T. \quad (18)$$

Below we list the event numbers for the benchmark points (defined in Table 1) for the above mentioned finalstates along with the dominant SM backgrounds. Just to remind, the  $c$ -jet tagging efficiency is taken around  $56\%$  with a mistagging

**Table 6** The number of events for  $1b - \text{jet} + \cancel{p}_T > 500 \text{ GeV}$  final-state for the benchmark points and dominant SM backgrounds at the LHC/FCC with the centre-of-mass energies of 30 TeV and 100 TeV for

the integrated luminosities of  $1000 \text{ fb}^{-1}$  and  $100 \text{ fb}^{-1}$ , respectively. The required luminosities to achieve a  $5\sigma$  signal ( $\mathcal{L}_{5\sigma}$ ) are also shown for both the cases

$E_{CM}$ in TeV	Mode	$1b - \text{jet} + \cancel{p}_T > 500 \text{ GeV}$						
		Signal		Backgrounds				
		BP1	BP2	$t\bar{t}$	$VV$	$VVV$	$t\bar{t}V$	$tVV$
30	$c/t - g \rightarrow S_1 \tau$	27.98	13.76	6439.58	650.04	50.14	74.10	25.86
	$b - g \rightarrow S_1 \nu$	401.73	146.02					
Total		429.71	159.78	7239.72				
Significance ( $\sigma$ )		4.90	1.86					
$\mathcal{L}_{5\sigma} (\text{fb}^{-1})$		1038.39	$\gg 3000$					
100	$c/t - g \rightarrow S_1 \tau$	66.33	39.59	11196.26	432.21	33.51	96.66	57.61
	$b - g \rightarrow S_1 \nu$	827.77	294.36					
Total		894.10	433.95	11816.25				
Significance ( $\sigma$ )		7.93	3.92					
$\mathcal{L}_{5\sigma} (\text{fb}^{-1})$		39.75	162.63					

of 12%, which is very conservative considering non-loose tagging mechanism [103].

### 3.3.1 $1c - \text{jet} + 1\tau - \text{jet} + \cancel{p}_T$

Table 7 presents the results for the  $1c - \text{jet} + 1\tau - \text{jet} + \cancel{p}_T$  finalstate, where  $c$ -gluon,  $b$ -gluon as well as  $t$ -gluon contribute. The complete finalstate comprised of the advanced cuts and veto is given as follows:

$$n_{c\text{-jet}} = 1, n_{\tau\text{-jet}} \geq 1, n_j \geq 2, n_\ell = 0 \quad \text{and}$$

$$\cancel{p}_T \geq 500 \text{ GeV},$$

$$p_T^{j_1, j_2} \geq 200 \text{ GeV}, p_T^{\tau\text{-jet}, c\text{-jet}} \geq 200 \text{ GeV},$$

$$p_T^H \geq 1.2 \text{ TeV}.$$

Since the  $c$ -jet originates directly from the leptoquark decay we demand a relatively hard cut of  $p_T > 200 \text{ GeV}$  for the  $c$ -jet. The  $\tau$ -jet however, can either come directly from the production channel (for  $c - g$  fusion) or from the leptoquark decay. Hence we also demand  $p_T > 200 \text{ GeV}$  for the  $\tau$ -jet. This almost implied that the first two  $p_T$  ordered jets are with  $p_T > 200 \text{ GeV}$ . The missing transverse momentum  $\cancel{p}_T \geq 500 \text{ GeV}$  is demanded as well since the relatively boosted neutrino arise at the production level. The number of events listed for the benchmark points and dominant SM backgrounds in Table 7 for 30 TeV and 100 TeV centre-of-mass energies at integrated luminosities of 1000,  $100 \text{ fb}^{-1}$ , respectively at the LHC/FCC. Once again, at the 14 TeV LHC, we do not even reach  $1\sigma$  for either benchmark point and we do not list them. Moving to the 30 TeV LHC, we get a  $3.52\sigma$  significance for BP1, with the  $5\sigma$  strength being obtainable with  $\sim 2020 \text{ fb}^{-1}$  luminosity. At the highest centre-of-mass energy of 100 TeV, both the BPs cross  $5\sigma$  significance, with  $9.40\sigma$  for BP1, and  $6.61\sigma$  for BP2.

High cross-section and more number of jets keep  $t\bar{t}$  as the substantially dominant background here.

### 3.3.2 $1c - \text{jet} + 2\tau - \text{jet} + \cancel{p}_T$

In Table 8 we now tag one more  $\tau$ -jet compared to the previous case and present  $1c - \text{jet} + 2\tau - \text{jet} + \cancel{p}_T \geq 500 \text{ GeV}$  finalstates for the benchmark points and dominant SM backgrounds for the two different centre-of-mass energies. Here, the complete finalstate including the advanced cuts and veto is described as follows:

$$n_{c\text{-jet}} = 1, n_{\tau\text{-jet}} \geq 2, n_j \geq 3, n_\ell = 0 \quad \text{and}$$

$$\cancel{p}_T \geq 500 \text{ GeV}, p_T^{j_1, j_2} \geq 200 \text{ GeV},$$

$$p_T^{\tau\text{-jet}, c\text{-jet}} \geq 200 \text{ GeV}, p_T^H \geq 1.2 \text{ TeV}.$$

Tagging one more  $\tau$ -jet and demanding high momentum for both of them definitely reduces the events numbers both for the signal as well as for the backgrounds. We see a overall drop in the significance. The signal remains very weak with  $< 1\sigma$  significance for both BPs, at the 14 TeV LHC, which are not listed. At the centre-of-mass energy of 30 TeV, the signal for BP1 shows a  $2.21\sigma$  strength, while BP2 stays weaker with  $1.44\sigma$  significance. Moving to 100 TeV, both benchmark points show promising outcomes, with  $8.65\sigma$  and  $6.13\sigma$  significance for BP1 and BP2, respectively at  $100 \text{ fb}^{-1}$  of integrated luminosity. Nonetheless, this set up will help us in reconstructing the invariant mass edge of  $c\tau$  which we discuss in the next in Sect. 3.4.

## 3.4 Invariant mass edge distribution

Ensuring the finalstates with excess events, we now look for invariant mass distributions for the resonance discovery of the

**Table 7** The number of events for  $1c - \text{jet} + \geq 1\tau - \text{jet} + \cancel{p}_T \geq 500$  GeV finalstate for the benchmark points and dominant SM backgrounds at the LHC/FCC, with centre-of-mass energies of 30 TeV and 100 TeV, for the integrated luminosities of  $1000 \text{ fb}^{-1}$  and  $100 \text{ fb}^{-1}$ , respectively. The required luminosities to achieve a  $5\sigma$  signal ( $\mathcal{L}_{5\sigma}$ ) are also shown for both cases

$E_{CM}$ in TeV	Mode	$1c - \text{jet} + \geq 1\tau - \text{jet} + \cancel{p}_T \geq 500$ GeV						
		Signal		Backgrounds				
		BP1	BP2	$t\bar{t}$	$VV$	$VVV$	$t\bar{t}V$	$tVV$
30	$c/t - g \rightarrow S_1 \tau$	355.17	192.99	21345.00	136.84	30.07	356.38	29.77
	$b - g \rightarrow S_1 \nu$	172.02	109.77					
Total		527.19	302.76	21898.07				
Significance( $\sigma$ )		3.52	2.03					
$\mathcal{L}_{5\sigma}$ ( $\text{fb}^{-1}$ )		2017.17	$\gg 3000$					
100	$c/t - g \rightarrow S_1 \tau$	1395.93	929.10	42636.18	199.77	54.66	953.79	129.25
	$b - g \rightarrow S_1 \nu$	619.95	479.67					
Total		2015.88	1408.77	43973.66				
Significance ( $\sigma$ )		9.40	6.61					
$\mathcal{L}_{5\sigma}$ ( $\text{fb}^{-1}$ )		28.29	57.17					

**Table 8** The number of events for  $1c - \text{jet} + 2\tau - \text{jet} + \cancel{p}_T \geq 200$  GeV finalstate for the benchmark points and dominant SM backgrounds at the LHC/FCC with centre-of-mass energies of 30 TeV and 100 TeV for the integrated luminosities of 1000,  $100 \text{ fb}^{-1}$ , respectively. The required luminosities to achieve a  $5\sigma$  signal ( $\mathcal{L}_{5\sigma}$ ) are also shown for both cases

$E_{CM}$ in TeV	Mode	$1c - \text{jet} + \geq 2\tau - \text{jet} + \cancel{p}_T$						
		Signal		Backgrounds				
		BP1	BP2	$t\bar{t}$	$VV$	$VVV$	$t\bar{t}V$	$tVV$
30	$c/t - g \rightarrow S_1 \tau$	55.28	35.07	619.31	10.93	4.00	30.65	2.34
	$b - g \rightarrow S_1 \nu$	4.35	3.21					
Total		59.64	38.28	667.23				
Significance( $\sigma$ )		2.21	1.44					
$\mathcal{L}_{5\sigma}$ ( $\text{fb}^{-1}$ )		$\gg 3000$	$\gg 3000$					
100	$c/t - g \rightarrow S_1 \tau$	329.07	222.62	1118.48	9.60	8.82	103.10	15.56
	$b - g \rightarrow S_1 \nu$	17.33	14.02					
Total		346.40	236.64	1255.56				
Significance( $\sigma$ )		8.65	6.13					
$\mathcal{L}_{5\sigma}$ ( $\text{fb}^{-1}$ )		33.38	66.62					

leptoquark. The decay branching fractions quoted in Table 3 show that the leptoquark  $S_1$  decays mostly to third generation fermions. It has been demonstrated in [31] that the third generation fermions give rise to a very rich finalstate; however, in the presence of a large number of jets, and specially the missing momentum from neutrino, the peaks are smeared. In case of a decay to  $c\mu$  finalstate a very clear invariant mass peak can be constructed [31]. In this paper due the absence of such mode we demonstrate how invariant mass edge can be constructed, which is similar to a situation arises in supersymmetric theories with neutralino decays [104, 105].

As schematically shown in Fig. 5a,  $S_1$  decays into a  $c$ -jet and a  $\tau$ , which is detected as hadronic  $\tau$ -jet [101, 102].

The neutrino in the finalstate contributes to missing energy but not to the  $\tau$ -jet energy, which is identified as hadronic one-prong ( $\pi^\pm$ ) jet. This results in a mass edge rather than a mass peak at the  $S_1$  mass in the  $c$ -jet- $\tau$ -jet invariant mass distribution as given in Eq. (19).

$$M_{\tau c}^{\max} \equiv m_{\pi c}^{\max} = \frac{1}{m_\tau} [(m_{S_1}^2 - m_\tau^2)(m_\tau^2 - m_\nu^2)]^{1/2} \simeq \frac{1}{m_\tau} (m_{S_1}^2 - m_\tau^2)^{1/2} m_\tau \simeq m_{S_1}. \quad (19)$$

The mass edge can be calculated from a three-body decay  $S_1$ , where the  $\tau$ -jet accumulates the energy of the pion ( $\pi^\pm$ ). This can be expressed in terms of the mass of the leptoquarks,

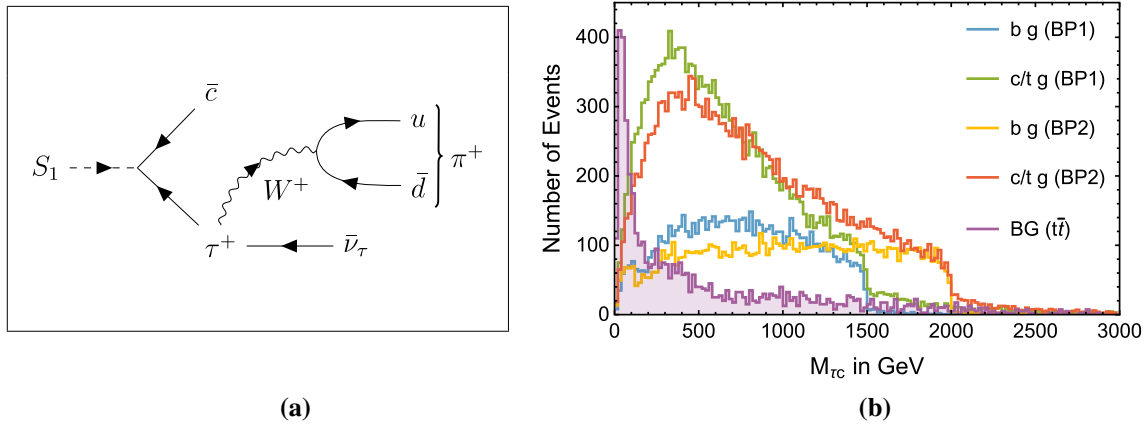


**Fig. 5** Panel **a** presents the Feynman diagram of  $S_1 \rightarrow \bar{c} \bar{\tau} \rightarrow \bar{c} \pi^+ \bar{\nu}_\tau$  and panel **b** shows the invariant mass distribution of  $c$ -jet and  $\tau$ -jet ( $M_{\tau c} \equiv m_{\pi c}$ ) for the chosen scenarios BP1, BP2 and the SM back-

ground  $t\bar{t}$  (scaled by 5) at 14 TeV centre-of-mass energy at the LHC. Invariant mass edges of  $m_{c\pi^+}^{\max}$  at the leptoquark masses  $M_{S_1}$  are clearly identifiable for both the benchmark scenarios

mass of  $\tau$  and the neutrino. As the leptoquark is at the TeV scale, from the collider perspective we can consider the last two particles as massless and this leaves us with the mass edge at  $\sim m_{S_1}$  as shown in Eq. (19). In Fig. 5b we show the distributions at 14 TeV LHC for the two benchmark points BP1, BP2 and the dominant SM background  $t\bar{t}$ . It is clear that the invariant mass of  $c$  and  $\tau$  (rather the  $\pi^+$ )  $m_{c\pi^+}^{\max}$ , gives mass edge at  $\sim 1.5$  TeV and 2.0 TeV for the respective benchmark points, where the contributions are coming from all three production modes  $b - g$  and  $c/t - g$  fusions. The dominant SM background  $t\bar{t}$  does not show any mass edge at these two regions.

We also present, in Table 9, the number of events for the interval  $(m_{\pi c} < m_{\text{edge}}) - (m_{\pi c} \geq m_{\text{edge}})$  with reconstructed invariant mass of  $\tau$ - and  $c$ - jets, denoted as  $M_{\tau c} \equiv m_{\pi c}$ , for the benchmark points and the total SM background at the LHC/FCC at two different centre-of-mass energies by identifying the  $\tau$ -jet as hadronic one prong ( $\pi^\pm$ ) jet. Additionally, we implement the  $W$ - and  $Z$ -boson vetoes on the di-jet and di-lepton invariant masses, and put the hardness cut of  $p_T^H \geq 1200$  GeV to obtain these numbers. The top quark backgrounds are further reduced by demanding  $n_{b\text{-jet}} = 0$ . Similar to the previous analysis, we present the numbers at the 30 TeV and 100 TeV results are for 1000, 100  $\text{fb}^{-1}$  integrated luminosities, respectively. Here  $m_{\text{edge}}$  represents the mass-edge (or mass-wall) that we see for BP1 and BP2 in Fig. 5b and thus a asymmetry around it is constructed by selecting events in the interval  $(m_{\pi c} < m_{\text{edge}}) - (m_{\pi c} \geq m_{\text{edge}})$ . In both benchmark points, we achieve a  $\sim 3.8\sigma$  significance at the centre-of-mass energy of 30 TeV. This increases to  $7.08\sigma$  for BP1, and  $7.36\sigma$  for BP2, when we move to the 100 TeV LHC/FCC. The background numbers in Table 9 includes contributions from all possible backgrounds i.e.  $t\bar{t}$ ,  $VV$ ,  $VVV$ ,  $t\bar{t}V$ , and  $tVV$ .

### 4 S3 at the LHC/FCC

In this section we discuss the collider phenomenology of the  $S_3$  leptoquark. Unlike  $S_1$ , the  $SU(2)_L$  triplet leptoquark  $S_3$  has three components namely  $S_3^{4/3}$ ,  $S_3^{1/3}$ ,  $S_3^{2/3}$  which are degenerate at the tree-level (see Eq. 4). Finding distinguishable signatures for these different excitations can be challenging. In this article we illustrate how production modes vary depending on the leptoquark excitations. In Table 1 we present three benchmark scenarios corresponding to two different mass scales 1.5 TeV and 2 TeV for the leptoquark, and three different Yukawa-type coupling combinations. Note that, BP3 has largest  $Y_{S_3}^{32}$  value which can lead to sizable interactions between the second and third generation of fermions. For this reason we separately discuss BP3 as lepton flavour violating (LFV) signatures in decay in Sect. 5.

We list the Feynman diagrams for dominant single production processes of  $S_3^{4/3}$ ,  $S_3^{1/3}$  and  $S_3^{2/3}$  via quark-gluon fusions in Fig. 6. The cross-sections at the LHC for the centre-of-mass energies of 14 TeV, 30 TeV and 100 TeV are listed in Table 10 for  $s - g$  fusion and in Table 11 for  $c - g$  fusion for the benchmark points BP1 and BP2. Similarly, the production cross-sections for BP3 from  $b - g$  and  $t - g$  fusion at the same three values of centre-of-mass energies are presented in Tables 12 and 13. Here NNPDF\_lo\_as\_0130\_qed [95] has been used as parton distribution function where top quark is also included. The parton-level centre-of-mass energy, i.e.  $\sqrt{\hat{s}}$  is used as renormalization/factorization scale. Again, similar to Sect. 3, these cross-sections are enhanced with the NLO QCD  $K$ -factor of 1.5 [15,96]. It is interesting to note that  $S_3^{4/3}$  can only be produced via  $s - g$  fusion, whereas,  $S_3^{2/3}$  is produced through  $c - g$  fusion for the chosen BP1 and BP2 scenarios. Due to different choices of couplings, in the case of BP3, the only production process for  $S_3^{4/3}$  ( $S_3^{2/3}$ )

**Table 9** The number of event combinations for  $(m_{\pi c} < m_{\text{edge}}) - (m_{\pi c} \geq m_{\text{edge}})$  with reconstructed invariant mass of  $\tau$ - and  $c$ - jets as  $M_{\tau c} \equiv m_{\pi c}$  for the benchmark points and the total SM background at the LHC/FCC with centre-of-mass energies of 30 TeV and 100 TeV for the integrated luminosities of 1000, 100 fb<sup>-1</sup>, respectively. The required luminosities to achieve a 5  $\sigma$  signal ( $\mathcal{L}_{5\sigma}$ ) are also shown for both the cases

$(m_{\pi c} < m_{\text{edge}}) - (m_{\pi c} \geq m_{\text{edge}})$					
$E_{\text{CM}}$	Mode	BP1	Background	BP2	Background
30 TeV	$c/t - g \rightarrow S_1 \tau$	358.97	31077.18	307.53	24119.70
	$b - g \rightarrow S_1 \nu$	315.35		287.93	
	Total	674.32		595.46	
Significance( $\sigma$ )		3.78		3.79	
$\mathcal{L}_{5\sigma}$ (fb <sup>-1</sup> )		1745.76		1742.63	
100 TeV	$c/t - g \rightarrow S_1 \tau$	868.43	56479.22	871.02	49375.35
	$b - g \rightarrow S_1 \nu$	840.59		791.48	
	Total	1709.02		1662.50	
Significance( $\sigma$ )		7.08		7.36	
$\mathcal{L}_{5\sigma}$ (fb <sup>-1</sup> )		49.80		46.16	

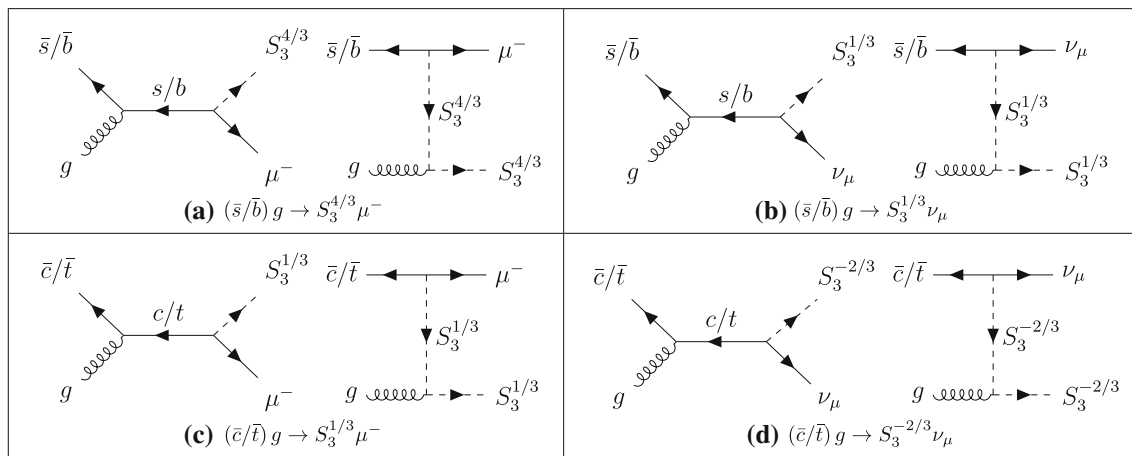


**Fig. 6** The tree level Feynman diagrams for  $(s/b) - g$  and  $(c/t) - g$  fusions producing different components of the leptoquark  $S_3$  in association with a lepton

**Table 10** The cross-sections (in fb) at the LHC via  $s - g$  fusion of  $S_3^{4/3}$  and  $S_3^{1/3}$ , for the two benchmark points, at three different centre-of-mass energies 14 TeV, 30 TeV and 100 TeV, respectively. NNPDF\_lo\_as\_0130\_qed [95] is considered as the parton distribution function with  $\sqrt{s}$  as renormalization/factorization scale with the NLO QCD  $K$ -factor of 1.5

Benchmark Points ( $M_{S_3}$ )	$\sigma(s - g \rightarrow S_3^{4/3} \mu)$ in fb with center of mass energies in TeV			$\sigma(s - g \rightarrow S_3^{1/3} \nu_\mu)$ in fb with center of mass energies in TeV		
	$E_{\text{CM}}=14$	$E_{\text{CM}}=30$	$E_{\text{CM}}=100$	$E_{\text{CM}}=14$	$E_{\text{CM}}=30$	$E_{\text{CM}}=100$
BP1 (1.5 TeV)	0.33	5.15	115.38	0.17	2.58	57.69
BP2 (2.0 TeV)	0.08	1.59	48.03	0.03	0.80	24.02

is via  $b - g$  ( $t - g$ ) fusion. We notice that  $S_3^{1/3}$  has contributions from both the production processes for the considered benchmark points. It is noteworthy that the production cross-section of  $S_3^{1/3}$  in any particular fusion process is almost half of the production cross-section of  $S_3^{4/3}$  and  $S_3^{2/3}$  leptoquarks. This is due to the reason that the interaction vertex of  $S_3^{4/3}$  and  $S_3^{2/3}$  with quarks and leptons carry an additional  $\sqrt{2}$  factor

as can be observed from Eq. (4). However, due to larger mass scale leptoquark (in TeV range), the cross-sections at 14 TeV centre-of-mass energy is not quite promising and we need to depend on the collisions at 30 TeV and 100 TeV centre-of-mass energies at the LHC/FCC.

Next, in Table 14 we list the decay branching fractions of the different excitations of  $S_3$  for the first two benchmark

**Table 11** The cross-sections (in fb) at the LHC via  $c - g$  fusion of  $S_3^{1/3}$  and  $S_3^{2/3}$ , for the two benchmark points, at three different centre-of-mass energies 14 TeV, 30 TeV and 100 TeV. NNPDF\_lo\_as\_0130\_qed [95] is considered as the parton distribution function with  $\sqrt{s}$  as renormalization/factorization scale with the NLO QCD  $K$ -factor of 1.5

Benchmark Points ( $M_{S_3}$ )	$\sigma(c - g \rightarrow S_3^{1/3} \mu)$ in fb with center of mass energies in TeV			$\sigma(c - g \rightarrow S_3^{2/3} \nu_\mu)$ in fb with center of mass energies in TeV		
	$E_{CM} = 14$	$E_{CM} = 30$	$E_{CM} = 100$	$E_{CM} = 14$	$E_{CM} = 30$	$E_{CM} = 100$
BP1 (1.5 TeV)	0.12	2.09	49.76	0.26	4.19	99.47
BP2 (1.5 TeV)	0.03	0.63	20.51	0.05	1.26	41.06

**Table 12** The cross-sections (in fb) at the LHC via  $b - g$  fusion of  $S_3^{4/3}$  and  $S_3^{1/3}$ , for the benchmark point BP3, at three different centre-of-mass energies 14 TeV, 30 TeV and 100 TeV. NNPDF\_lo\_as\_0130\_qed [95] is considered as parton distribution function with  $\sqrt{s}$  as renormalization/factorization scale, with the NLO QCD  $K$ -factor of 1.5

Benchmark Points ( $M_{S_3}$ )	$\sigma(b - g \rightarrow S_3^{4/3} \mu)$ in fb with center of mass energies in TeV			$\sigma(b - g \rightarrow S_3^{1/3} \nu_\mu)$ in fb with center of mass energies in TeV		
	$E_{CM} = 14$	$E_{CM} = 30$	$E_{CM} = 100$	$E_{CM} = 14$	$E_{CM} = 30$	$E_{CM} = 100$
BP3 (1.5 TeV)	0.05	0.90	23.56	0.03	0.45	11.81

**Table 13** The cross-sections (in fb) at the LHC via  $t - g$  fusion of  $S_3^{4/3}$  and  $S_3^{1/3}$ , for the benchmark point BP3, at three different centre-of-mass energies 14 TeV, 30 TeV and 100 TeV. NNPDF\_lo\_as\_0130\_qed [95] is considered as parton distribution function with  $\sqrt{s}$  as renormalization/factorization scale with the NLO QCD  $K$ -factor of 1.5

Benchmark Points ( $M_{S_3}$ )	$\sigma(t - g \rightarrow S_3^{1/3} \mu)$ in fb with center of mass energies in TeV			$\sigma(t - g \rightarrow S_3^{2/3} \nu_\mu)$ in fb with center of mass energies in TeV		
	$E_{CM} = 14$	$E_{CM} = 30$	$E_{CM} = 100$	$E_{CM} = 14$	$E_{CM} = 30$	$E_{CM} = 100$
BP3 (1.5 TeV)	0.006	0.14	3.90	0.015	0.26	7.77

points. We find that  $S_3^{4/3}$  decays to  $s \mu$  with 100% branching ratio for BP1 and BP2. Again, in both the BPs, the modes  $c \mu$  and  $s \nu_\mu$  share 50% branching ratios for  $S_3^{1/3}$ . The component  $S_3^{2/3}$  decays completely (100% branching fraction) to  $c \nu_\mu$  for BP1 and BP2 as well. The decay branching ratios in BP3 for the lepton flavour violating decays will be separately discussed in Sect. 5.

#### 4.1 Kinematic distributions and topologies

We compare various kinematic distributions for  $S_3$  leptoquark with the dominant SM background arising from  $t\bar{t}$  channel. For illustration we choose to discuss these distributions for BP1 at 100 TeV centre-of-mass energy. The jet multiplicity distribution ( $n_j$ ) for the signal (in orange) and  $t\bar{t}$  background (in purple) are displayed in Fig. 7a for the channel  $c - g \rightarrow S_3^{1/3} \mu$ . All the four production channels for different components of  $S_3$ , as shown in the Feynman diagrams in Fig. 6, exhibit similar jet multiplicity distribution peaking around three, whereas, the SM background  $t\bar{t}$  peaks at five jets, with more events in the higher multiplicity regions due to large ISR/FSR effects at the 100 TeV centre-of-mass energy. Similarly, Fig. 7b illustrates the lepton multiplicity

distributions ( $n_\ell$ ) for signal and  $t\bar{t}$  background for BP1 at 100 TeV centre-of-mass energy. As discussed in the case for  $S_1$ , the light charged leptons ( $e^\pm, \mu^\pm$ ) for  $t\bar{t}$  essentially come from  $W^\pm$  bosons which are produced with the decay of the top quarks to bottom quarks. As the branching fraction of  $W^\pm$  to light charged leptons ( $e^\pm, \mu^\pm$ ) is only about 22%, most of the  $W^\pm$  decay hadronically producing no-lepton (dominant) and mono-lepton signatures for the background (in purple). In BP1,  $S_3^{1/3}$  couples to both muon and  $\nu_\mu$  and thus,  $c - g \rightarrow S_3^{1/3} \mu$  (in blue) shows mono-lepton and di-lepton signatures, whereas,  $s - g \rightarrow S_3^{1/3} \nu_\mu$  (in green) shows non-leptonic and mono-leptonic signatures. Now, the component  $S_3^{2/3}$  does not couple to any charged lepton, giving almost always zero-lepton events (in orange) in the finalstate. Lastly, it is easy to see that the leptoquark  $S_3^{4/3}$  couples to muon only, and hence the process  $s - g \rightarrow S_3^{4/3} \mu$  has maximum di-lepton events out of all the signal processes considered (in red).

In Fig. 8, the  $p_T$  distribution of the two hardest jets emanating from two different fusion processes are shown for BP1 at the 100 TeV LHC/FCC. The hardest jet ( $j_1$ ) each from the processes  $c - g \rightarrow S_3^{1/3} \mu$  (blue) and  $s - g \rightarrow S_3^{4/3} \mu$  (orange) both follow an almost identical distribution, peak-

**Table 14** The decay branching ratios (in percentage) of  $S_3$  for the chosen benchmark points BP1 and BP2

Decay Modes	Branching ratios (%)	
	BP1 $M_{S_3} = 1.5$ TeV	BP2 $M_{S_3} = 2.0$ TeV
$S_3^{-4/3} \rightarrow s\mu$	100	100
$S_3^{-1/3} \rightarrow c\mu$	50	50
$S_3^{-1/3} \rightarrow sv_\mu$	50	50
$S_3^{2/3} \rightarrow cv_\mu$	100	100

ing at around half of the leptoquark mass, as expected ( $\sim 750$ ) GeV. As there is no recoiled  $\tau$ -jet in the production processes, the only source of the second hardest jets in each case (green for  $S_3^{1/3}$ , red for  $S_3^{4/3}$ ) are the ISR/FSR, and they are much softer. Distributions for  $S_3^{2/3}$  are not shown here to avoid repetition and overlapping, as they also follow the very same pattern.

We show the transverse momentum distributions for light charged leptons ( $e^\pm, \mu^\pm$ ) for all the production channels of  $S_3$  and  $t\bar{t}$  background in Fig. 9a, for BP1 at the 100 TeV LHC/FCC. As discussed above, the light charged leptons for  $t\bar{t}$  background can only come from the  $W^\pm$ , produced from the decay of top quark, the lepton  $p_T$  distribution (in purple) exhibits a peak around the half mass of the  $W$ -boson and becomes insignificant for higher  $p_T^{\text{lep}}$ . The component  $S_3^{2/3}$  does not couple to charged leptons and hence does not contribute here. Now for the mode  $s - g \rightarrow S_3^{1/3}\nu$  (in yellow), as the charged lepton arises only from the decay of  $S_3^{1/3}$ , the lepton  $p_T$  distribution peaks around half the mass of leptoquark (i.e. 750 GeV). In the other two modes (in blue and red), muons are produced at two stages: firstly, during the production of the leptoquark, and secondly, during its decay. So, the distributions show quite similar behaviour for

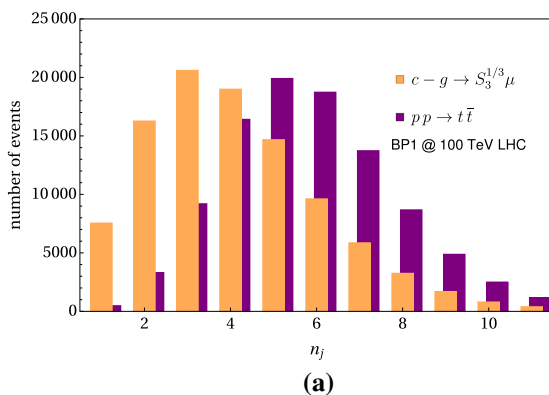


**Fig. 7** The jet multiplicity ( $n_j$  in **a**) and lepton multiplicity ( $n_\ell$  in **b**) distributions of  $S_3$  (for BP1) and the SM background  $t\bar{t}$  at the LHC/FCC with the centre-of-mass energy of 100 TeV. The jet multiplicity for sig-

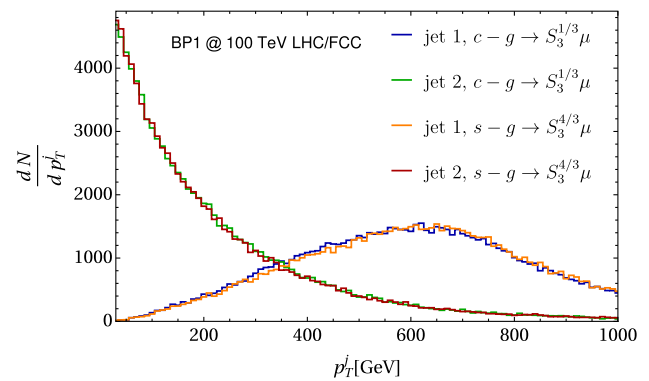
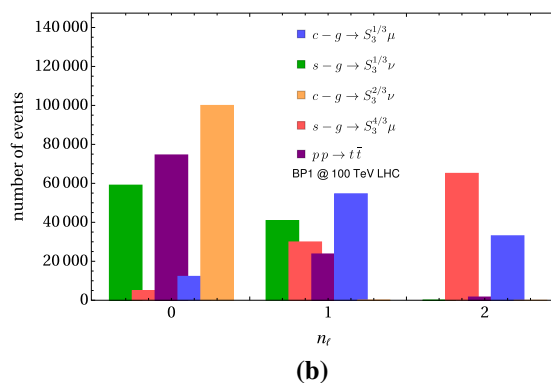


**Fig. 8** The jet  $p_T$  ( $p_T^j$ ) distributions from  $S_3^{1/3}$  and  $S_3^{4/3}$  production processes at the LHC/FCC with the centre-of-mass energy of 100 TeV for BP1.  $S_3^{2/3}$  shows the same distribution, so it is not shown in the plot

$S_3^{4/3}$  and  $S_3^{1/3}$ . However,  $S_3^{1/3}$  can decay to muon or neutrino, whereas,  $S_3^{4/3}$  has channel only to muon (see Table 14). For this reason the  $p_T^{\text{lep}}$  distribution for  $s - g \rightarrow S_3^{4/3}\mu$  (in red) remains above the mode  $c - g \rightarrow S_3^{1/3}\mu$  (in blue).

The missing  $p_T$  distributions for signals and dominant SM background have been presented in Fig. 9b, again for BP1 at the centre-of-mass energy of 100 TeV. During the production and decay of  $S_3^{4/3}$  (in red), no neutrino is involved, and thus the  $\cancel{p}_T$  peaks at around 30 GeV only, owing to neutrinos from SM sources. The production and decay of  $S_3^{2/3}$  (in green) create two neutrinos, moving nearly opposite to each other with different momentum. However, the first neutrino at the production carries most of the missing transverse momentum and we observe a nice bell-shaped curve peaking around half of the leptoquark mass (i.e. 750 GeV). During the production of  $S_3^{1/3}$  through  $s - g$  fusion (in yellow), neutrino appears at production level and again, there is 50% probability for  $S_3^{1/3}$  to decay to neutrino. Therefore, the  $\cancel{p}_T$



nal, shown in (a), represents  $c - g \rightarrow S_3^{1/3}\mu$  channel only. Since the other single-production channels of  $S_3$  show the same jet multiplicity distribution, they are not depicted in (a)

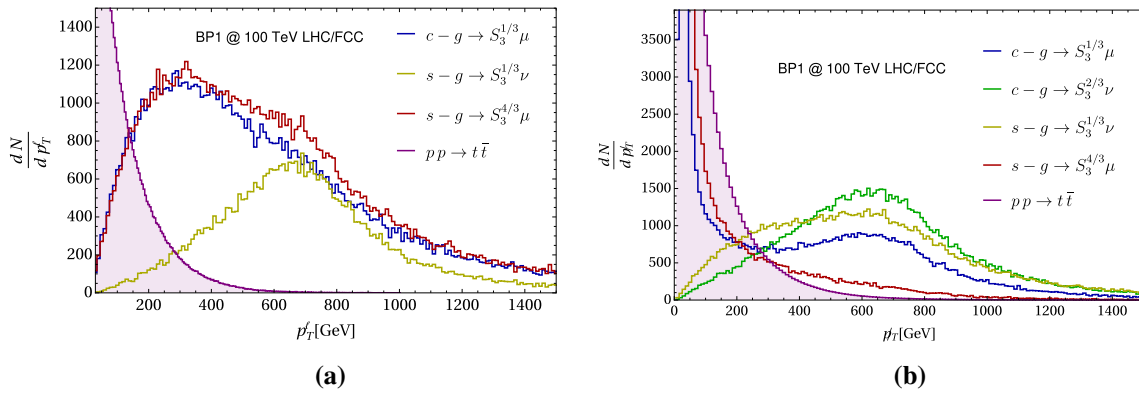


**Fig. 9** **a** Distributions of lepton  $p_T$  ( $p_T^\ell$ ) and **b** missing  $p_T$  ( $p_T^{\cancel{p}}$ ) of  $S_3$  (for BP1) with the SM background  $t\bar{t}$  at the LHC with centre-of-mass energy of 100 TeV. In **a**, background has been scaled by 1/10, while in **b** it has been scaled as 1/300.  $S_3^{2/3}$  is not shown in **a** as it does not couple to leptons

distribution curve becomes a bit flat and resembles with in  $S_1$  scenario. Finally, for  $c g \rightarrow S_3^{1/3} \mu$  mode (in blue), when  $S_3^{1/3}$  decays to muon the missing  $p_T$  shows a peak in low  $p_T$  region similar to the  $t\bar{t}$  background. Although, there is also a possibility for  $S_3^{1/3}$  to decay to a neutrino exhibiting a local maximum about the half of the leptoquark mass. Like muons, the neutrinos in  $t\bar{t}$  scenario also arise from leptonic decay of  $W^\pm$ , consequently the missing  $p_T$  distribution (in purple) peaks at lower  $p_T$  and decreases gradually with a longer tail, enabling us to demand large  $p_T$  to reduce the  $t\bar{t}$  background contamination.

We now focus on decay topologies arising from the single production channels for the two benchmark points BP1 and BP2. Our aim is to identify specific decay finalstates which can distinguish different components of the  $S_3$  leptoquark. Due to particular gauge structure of the Lagrangian (in Eq. 4), only  $S_3^{4/3}$  and  $S_3^{1/3}$  components of  $S_3$  will be produced in  $s - g$  fusion. Similarly,  $c - g$  fusion produces  $S_3^{2/3}$  and  $S_3^{1/3}$  components of  $S_3$  only. However, upon production, all these leptoquarks will decay to quarks and leptons. While  $S_3^{4/3}$  and  $S_3^{2/3}$  components decay to  $s\mu$  and  $c\nu_\mu$  respectively,  $S_3^{1/3}$  decays to both the  $s\nu_\mu$  and  $c\mu$  topologies giving rise to the following finalstates:

$$\text{BP1, BP2: } s - g \rightarrow S_3^{4/3} \mu \rightarrow (s \mu) + \mu \rightarrow 2\mu + 1 - \text{jet}, \quad (20)$$

$$s - g \rightarrow S_3^{1/3} \nu_\mu \rightarrow (s \nu_\mu) + \nu_\mu \rightarrow 1 - \text{jet} + \cancel{p}_T, \quad (21)$$

$$\rightarrow (c \mu) + \nu_\mu \rightarrow 1\mu + 1c - \text{jet} + \cancel{p}_T, \quad (22)$$

$$c - g \rightarrow S_3^{1/3} \mu \rightarrow (c \mu) + \mu \rightarrow 2\mu + 1c - \text{jet}, \quad (23)$$

$$\rightarrow (s \nu_\mu) + \mu$$

$$\rightarrow 1\mu + 1 - \text{jet} + \cancel{p}_T, \quad (24)$$

$$c - g \rightarrow S_3^{2/3} \nu_\mu \rightarrow (c \nu_\mu) + \nu_\mu \rightarrow 1c - \text{jet} + \cancel{p}_T. \quad (25)$$

As already mentioned, here ‘jet’ implies light-jets unless the flavour is mentioned. We note that the complete decay chain of the leptoquark  $S_3^{4/3}$  provides a unique finalstate of di-muon plus mono light jet. Similarly, we have unique signature for  $S_3^{2/3}$  through the finalstate consisting of mono  $c$ -jet with missing energy. On the other hand, four different finalstates are possible involving the production of  $S_3^{1/3}$  in quark-gluon fusion at LHC/FCC with BP1 and BP2. In the succeeding few subsections we describe the signal-background analyses for these six finalstates at centre-of-mass energies of 14 TeV, 30 TeV and 100 TeV.

#### 4.2 $S_3^{4/3}$ component of $S_3$ : $1 - \text{jet} + 2\mu + \cancel{p}_T$

As discussed earlier, leptoquark  $S_3^{4/3}$  gets produced in association with muon from  $s - g$  fusion via the Feynman diagram shown in Fig. 6a and eventually decays into  $s\mu$  with 100% branching fraction as presented in Table 14. This leads to the finalstate of mono-jet plus di-muon with suitable additional cuts as given below:

$$n_j \geq 1, n_\mu \geq 2, n_{\tau\text{-jet}} = 0 \quad \text{and}$$

$$p_T^{\ell_1} \geq 200 \text{ GeV}, p_T^{j_1} \geq 200 \text{ GeV},$$

$$\cancel{p}_T \leq 30 \text{ GeV}, p_T^H \geq 1200 \text{ GeV}.$$

The event numbers for the benchmark points BP1 and BP2 along with the dominant SM backgrounds for this finalstate are given in Table 15. The numbers are presented for three different centre-of-mass energies viz. 14 TeV, 30 TeV and 100 TeV. The integrated luminosity are taken to be  $1000 \text{ fb}^{-1}$  for the first two and  $100 \text{ fb}^{-1}$  for the last one. Since the lep-

**Table 15** The number of events for  $\geq 1 - \text{jet} + \geq 2\mu + \cancel{p}_T \leq 30 \text{ GeV}$  finalstate (Eq. 20) for the benchmark points and dominant SM backgrounds at the LHC/FCC with centre-of-mass energy of 14 TeV, 30 TeV and 100 TeV at an integrated luminosity of  $1000 \text{ fb}^{-1}$  for the first two and  $100 \text{ fb}^{-1}$  for 100 TeV. The required luminosities to achieve a  $5\sigma$  signal ( $\mathcal{L}_{5\sigma}$ ) are also shown for all three cases

$\sqrt{s}$ in TeV	Fusion	Mode	$\geq 1 - \text{jet} + \geq 2\mu + \cancel{p}_T$						
			Signal		Backgrounds				
			BP1	BP2	$t\bar{t}$	VV	VVV	$t\bar{t}V$	$tVV$
14	$s - g$	$S_3^{4/3}\mu$	174.08	46.53	14.47	171.22	20.83	53.75	11.57
		$S_3^{1/3}\nu$	0.00	0.00					
	$c - g$	$S_3^{1/3}\mu$	26.22	6.41					
		$S_3^{2/3}\nu$	0.00	0.00					
	Total		200.30	52.94	271.84				
	Significance ( $\sigma$ )		9.21	2.94					
$\mathcal{L}_{5\sigma} (\text{fb}^{-1})$		294.22	2897.62						
30	$s - g$	$S_3^{4/3}\mu$	2736.75	1032.44	210.43	1145.45	150.41	588.86	74.46
		$S_3^{1/3}\nu$	0.00	0.00					
	$c - g$	$S_3^{1/3}\mu$	443.89	163.39					
		$S_3^{2/3}\nu$	0.00	0.00					
	Total		3180.64	1195.83	2169.62				
	Significance ( $\sigma$ )		43.48	20.61					
$\mathcal{L}_{5\sigma} (\text{fb}^{-1})$		13.22	58.84						
100	$s - g$	$S_3^{4/3}\mu$	5360.33	2664.26	429.01	699.22	134.04	916.72	121.45
		$S_3^{1/3}\nu$	0.00	0.00					
	$c - g$	$S_3^{1/3}\mu$	935.26	440.97					
		$S_3^{2/3}\nu$	0.00	0.00					
	Total		6295.59	3105.23	2300.44				
	Significance ( $\sigma$ )		67.90	42.23					
$\mathcal{L}_{5\sigma} (\text{fb}^{-1})$		0.54	1.40						

toquark masses in the considered benchmark points (BP1 and BP2) are taken to be 1.5 TeV and 2.0 TeV, a hardness cut of 1.2 TeV has also been implemented here to reduce the background. Both the hardest jet and lepton  $p_T$  cut are demanded to be  $\geq 200 \text{ GeV}$ . Moreover, as there is no neutrino involved in this finalstate, we put an upper limit on the missing energy, namely  $\cancel{p}_T \leq 30 \text{ GeV}$ . As expected, the dominant contribution to this mode comes from  $s - g \rightarrow S_3^{4/3}\mu$ . Nevertheless, a small contribution arises from  $c - g \rightarrow S_3^{1/3}\mu$  as well, since it can also provide di-muon finalstate. The dominant background contribution at 14 and 30 TeV LHC/FCC comes from the  $VV$  process, which has higher chance of getting us a pair of muons in the finalstate. At 100 TeV,  $t\bar{t}V$  becomes dominant due to the higher jump in cross-section, while contributing towards the criteria of di-muons and no upper limit on light jets. The demand of di-muons, accompanied by the hardness cut and the small window of missing energy keeps the background numbers comparatively lower than our previous discussions on  $S_1$  in Sect. 3, which leads to encouraging signal strengths in all the three centre-of-

mass energies. At the 14 TeV LHC, a  $9.21\sigma$  significance is obtained for BP1 with  $1000 \text{ fb}^{-1}$  of luminosity, whereas for BP2 the strength is  $2.94\sigma$ . Moving to the higher centre-of-mass energy of 30 TeV, both the BPs give us promising outcomes, with  $43.48\sigma$  and  $20.61\sigma$  significances for BP1 and BP2, respectively. The strength is further enhanced at the 100 TeV LHC/FCC, where with  $100 \text{ fb}^{-1}$  luminosity we can obtain  $67.90\sigma$  significance for BP1, and  $42.23\sigma$  significance for BP2. In both 30 TeV and 100 TeV energies, the required  $5\sigma$  discovery is predicted with much earlier data.

### 4.3 $S_3^{2/3}$ component of $S_3$ : $1c - \text{jet} + \cancel{p}_T$

As we have pointed out earlier,  $S_3^{2/3}$  can be produced only via  $c - g$  fusion in association with a neutrino (Feynman diagram in Fig. 6d) and then decays to  $c\nu$  with 100% branching ratio. This leaves us with mono  $c$ -jet plus missing energy signature, which is very unique. The recoil of  $\nu$  against  $S_3^{2/3}$  leads to larger missing energy as already shown in Fig. 9b. The complete finalstate demanded in this case is written as

**Table 16** The number of events for  $1c - \text{jet} + \cancel{p}_T \geq 200 \text{ GeV}$  finalstate (Eq. 25) for the benchmark points and dominant SM backgrounds at the LHC/FCC with centre-of-mass energies of 14 TeV, 30 TeV and 100 TeV at an integrated luminosity of  $1000 \text{ fb}^{-1}$  for the first two and  $100 \text{ fb}^{-1}$  for 100 TeV. The required luminosities to achieve a  $5\sigma$  signal ( $\mathcal{L}_{5\sigma}$ ) are also shown for all three cases

$\sqrt{s}$ in TeV	Fusion	Mode	$1c - \text{jet} + \cancel{p}_T \geq 200 \text{ GeV}$		Backgrounds				
			Signal		$t\bar{t}$	$VV$	$VVV$	$t\bar{t}V$	$tVV$
			BP1	BP2					
14	$s - g$	$S_3^{4/3} \mu$	0.00	0.00	2.89	31.86	0.96	0.00	0.25
		$S_3^{1/3} \nu$	0.12	0.05					
	$c - g$	$S_3^{1/3} \mu$	0.00	0.00					
		$S_3^{2/3} \nu$	27.51	6.64					
	Total		27.63	6.69					
Significance( $\sigma$ )		3.47	1.02						
$\mathcal{L}_{5\sigma} (\text{fb}^{-1})$		2082.10	$\gg 5000$						
30	$s - g$	$S_3^{4/3} \mu$	0.00	0.00	0.00	173.93	6.01	1.27	0.00
		$S_3^{1/3} \nu$	2.12	0.80					
	$c - g$	$S_3^{1/3} \mu$	0.00	0.02					
		$S_3^{2/3} \nu$	366.42	131.13					
	Total		368.54	131.95					
Significance( $\sigma$ )		15.72	7.46						
$\mathcal{L}_{5\sigma} (\text{fb}^{-1})$		101.19	449.71						
100	$s - g$	$S_3^{4/3} \mu$	0.00	0.00	19.15	170.96	1.75	0.00	0.00
		$S_3^{1/3} \nu$	8.42	5.33					
	$c - g$	$S_3^{1/3} \mu$	0.19	0.16					
		$S_3^{2/3} \nu$	634.05	295.82					
	Total		642.66	301.31					
Significance( $\sigma$ )		22.25	13.57						
$\mathcal{L}_{5\sigma} (\text{fb}^{-1})$		5.05	13.58						

follows:

$$n_{c-\text{jet}} = 1, n_j = 1, n_\ell = n_{\tau-\text{jet}} = 0 \quad \text{and} \\ p_T^{c-\text{jet}} \geq 200 \text{ GeV}, \cancel{p}_T \geq 200 \text{ GeV}, p_T^H \geq 1200 \text{ GeV}.$$

In Table 16, the events for signal and the SM backgrounds are quoted again for the three different center mass energies with the same choices for integrated luminosity as of all other cases discussed in this work. We put veto on the charged lepton as well as on the  $\tau$ -jet, and demand only one  $c$ -jet with  $p_T \geq 200 \text{ GeV}$  along with  $\cancel{p}_T \geq 200 \text{ GeV}$  can be present. Besides, we do not allow any light jets, keeping the total number of jets equal to one, which results into a significant drop in all the background events. The results for 14 TeV are not very heartening for BP2, as the signal significance of just  $1.02\sigma$  can be reached. Meanwhile, BP1 shows a healthy signal of  $3.47\sigma$  significance at this energy, with an integrated luminosity of  $\sim 2082 \text{ fb}^{-1}$  being enough to probe the required  $5\sigma$  significance. At the 30 TeV energy, both these BPs cross  $5\sigma$  significance at  $1000 \text{ fb}^{-1}$  luminosity, with  $15.72\sigma$  and  $7.46\sigma$  strengths being reached by BP1

and BP2, respectively. At the highest energy of 100 TeV, these significances enhance to  $22.25\sigma$  for BP1, and  $13.57\sigma$  for BP2 with  $100 \text{ fb}^{-1}$  of integrated luminosity, while the required  $5\sigma$  strength can be obtained with very early data. For this finalstate,  $VV$  remains the strongest background, with fully invisible decay of  $Z$  and/or hadronic decays of  $Z, W^\pm$  with a  $c$ -jet.

#### 4.4 $S_3^{1/3}$ component of $S_3$

The component  $S_3^{1/3}$  of  $S_3$  leptoquark can be produced in association with a muon or a neutrino in  $c - g$  and  $s - g$  fusions. The produced leptoquark then disintegrates into either  $c\mu$  or  $s\nu_\mu$  with equal probability as shown in Table 14. Consequently, four different finalstates are possible in this scenario and we investigate them all sequentially.

##### 4.4.1 $1c - \text{jet} + 2\mu + \cancel{p}_T$

In this case, we consider  $S_3^{1/3}$  to be produced in accompany with a muon through  $c - g$  fusion and eventually decays into

**Table 17** The number of events for  $2\mu + 1c - \text{jet} + \cancel{p}_T \leq 30 \text{ GeV}$  finalstate (Eq. 23) for the benchmark points and dominant SM backgrounds at the LHC/FCC with centre-of-mass energy of 14 TeV, 30 TeV and 100 TeV at an integrated luminosity of  $1000 \text{ fb}^{-1}$  for the first two and  $100 \text{ fb}^{-1}$  for 100 TeV. The required luminosities to achieve a  $5\sigma$  signal ( $\mathcal{L}_{5\sigma}$ ) are also shown for all three cases

$\sqrt{s}$ in TeV	Fusion	Mode	$\geq 1c - \text{jet} + \geq 2\mu + \cancel{p}_T \leq 30 \text{ GeV}$						
			Signal		Backgrounds				
			BP1	BP2	$t\bar{t}$	VV	VVV	$t\bar{t}V$	$tVV$
14	$s - g$	$S_3^{4/3}\mu$	1.17	0.36	11.57	3.98	0.64	10.38	1.75
		$S_3^{1/3}\nu$	0.00	0.00					
	$c - g$	$S_3^{1/3}\mu$	16.55	4.17					
		$S_3^{2/3}\nu$	0.00	0.00					
	Total		17.72	5.53	28.32				
Significance( $\sigma$ )		2.61	0.79						
$\mathcal{L}_{5\sigma} (\text{fb}^{-1})$		3667.04	$\gg 5000$						
30	$s - g$	$S_3^{4/3}\mu$	29.06	11.97	90.19	60.26	8.01	94.53	8.62
		$S_3^{1/3}\nu$	0.00	0.00					
	$c - g$	$S_3^{1/3}\mu$	284.26	106.83					
		$S_3^{2/3}\nu$	0.00	0.00					
	Total		313.32	118.80	261.61				
Significance( $\sigma$ )		13.07	6.09						
$\mathcal{L}_{5\sigma} (\text{fb}^{-1})$		146.41	673.85						
100	$s - g$	$S_3^{4/3}\mu$	91.65	48.14	233.65	53.79	14.11	141.78	32.70
		$S_3^{1/3}\nu$	0.00	0.00					
	$c - g$	$S_3^{1/3}\mu$	600.77	291.15					
		$S_3^{2/3}\nu$	0.00	0.00					
	Total		692.42	339.29	476.03				
Significance( $\sigma$ )		20.26	11.88						
$\mathcal{L}_{5\sigma} (\text{fb}^{-1})$		6.09	17.71						

a  $c$ -quark and a muon as shown in Eq. (23). The complete finalstate with the advanced cuts is described below:

$$n_{c\text{-jet}} \geq 1, n_j \geq 1, n_\mu \geq 2, n_{\tau\text{-jet}} = 0 \quad \text{and}$$

$$p_T^{\ell 1} \geq 200 \text{ GeV}, p_T^{j1} \geq 200 \text{ GeV},$$

$$\cancel{p}_T \leq 30 \text{ GeV}, p_T^H \geq 1200 \text{ GeV}.$$

The signal-background analysis for this finalstate topology at LHC/FCC is illustrated in Table 17. Due to the absence of neutrinos in the entire decay chain ideally there should not be any missing energy and we impose the missing transverse momentum upper limit  $\cancel{p}_T \leq 30 \text{ GeV}$ . We demand at least one  $c$ -jet, and one muon of the two having  $p_T \geq 200 \text{ GeV}$ , along with  $\tau$ -jet veto for the finalstate. Apart from the mentioned process, this finalstate gets very small contribution arising from  $s - g \rightarrow S_3^{4/3}\mu$  channel (discussed in Sect. 4.2) as well, due to the mistagging of light-jet as  $c$ -jet. The applied cut on the total hardness, as well as the specific demand for di-muons keep the backgrounds relatively low, with the dominant contributions coming from  $t\bar{t}$  and  $t\bar{t}V$ . Now, about the outcomes, the 14 TeV scenario is not very inspiring since sig-

nificances of  $2.61\sigma$  and  $0.79\sigma$  can only be reached with  $1000 \text{ fb}^{-1}$  of integrated luminosity for the two respective benchmark points which implies the necessity of very high luminosity to attain  $5\sigma$  reach. However, the situation improves with 30 TeV of centre-of-mass energy where the signal significances of  $13.07\sigma$  and  $6.09\sigma$  can be obtained with  $1000 \text{ fb}^{-1}$  luminosity for BP1 and BP2 respectively which indicates requirement of only  $\sim 150 \text{ fb}^{-1}$  and  $\sim 675 \text{ fb}^{-1}$  integrated luminosities for  $5\sigma$  reach. On the other hand, the results are very uplifting for 100 TeV centre-of-mass energy as  $20.26\sigma$  and  $11.88\sigma$  of signal significances could be gained for BP1 and BP2, respectively, at  $100 \text{ fb}^{-1}$  of integrated luminosity only. Therefore significance of  $5\sigma$  is reachable with very early data.

#### 4.4.2 $1c - \text{jet} + 1\mu + \cancel{p}_T$

While considering the production of  $S_3^{1/3}$  along with a neutrino via  $s - g$  fusion and its disintegration into  $c$ -quark and a muon, the finalstate  $1c - \text{jet} + 1\mu + \cancel{p}_T$  arises (see Eq. 22).

**Table 18** The number of events for  $1\mu + 1c - \text{jet} + \cancel{p}_T \geq 500$  GeV finalstate (Eq. 22) for the benchmark points and dominant SM backgrounds at the LHC/FCC with centre-of-mass energy of 14 TeV, 30 TeV and 100 TeV at an integrated luminosity of  $1000 \text{ fb}^{-1}$  for the first two and  $100 \text{ fb}^{-1}$  for 100 TeV. The required luminosities to achieve a  $5\sigma$  signal ( $\mathcal{L}_{5\sigma}$ ) are also shown for all three cases

$\sqrt{s}$ in TeV	Fusion	Mode	$1c - \text{jet} + 1\mu + \cancel{p}_T \geq 500$ GeV						
			Signal		Backgrounds				
			BP1	BP2	$t\bar{t}$	$VV$	$VVV$	$t\bar{t}V$	$tVV$
14	$s - g$	$S_3^{4/3}\mu$	0.09	0.00	212.72	12.95	0.64	8.48	2.27
		$S_3^{1/3}\nu$	21.39	6.68					
	$c - g$	$S_3^{1/3}\mu$	2.10	0.72					
		$S_3^{2/3}\nu$	0.00	0.00					
	Total		23.58	7.40	237.07				
Significance( $\sigma$ )		1.46	0.47						
$\mathcal{L}_{5\sigma} (\text{fb}^{-1})$		$\gg 5000$	$\gg 5000$						
30	$s - g$	$S_3^{4/3}\mu$	3.71	1.71	4311.08	179.28	24.07	114.96	21.17
		$S_3^{1/3}\nu$	440.00	192.28					
	$c - g$	$S_3^{1/3}\mu$	54.55	28.94					
		$S_3^{2/3}\nu$	0.00	0.00					
	Total		498.26	222.93	4650.56				
Significance( $\sigma$ )		6.94	3.19						
$\mathcal{L}_{5\sigma} (\text{fb}^{-1})$		518.49	2451.56						
100	$s - g$	$S_3^{4/3}\mu$	21.71	19.88	9127.84	199.77	47.62	291.62	66.96
		$S_3^{1/3}\nu$	1155.23	662.25					
	$c - g$	$S_3^{1/3}\mu$	256.21	157.54					
		$S_3^{2/3}\nu$	0.00	0.00					
	Total		1433.15	839.67	9733.81				
Significance( $\sigma$ )		13.56	8.17						
$\mathcal{L}_{5\sigma} (\text{fb}^{-1})$		13.59	37.49						

The demands are almost the same as the previous one except we have only one muon in this finalstate and due to the presence of a high energetic neutrino here, we put a lower bound on the missing transverse momentum as  $\cancel{p}_T \geq 500$  GeV. The complete finalstate is given as:

$$n_{c\text{-jet}} = 1, n_j \geq 1, n_\mu = 1, n_{\tau\text{-jet}} = 0 \quad \text{and}$$

$$p_T^{\ell_1} \geq 200 \text{ GeV}, p_T^{c\text{-jet}} \geq 200 \text{ GeV},$$

$$\cancel{p}_T \geq 500 \text{ GeV}, p_T^H \geq 1200 \text{ GeV}.$$

The signal and background analysis at the LHC/FCC for this decay topology is presented in Table 18. The demand for only one muon keeps the background numbers higher than the previous case with two muons. With 14 TeV centre-of-mass energy and  $1000 \text{ fb}^{-1}$  of luminosity, both the BPs give very weak signals, with strengths of  $1.46\sigma$  and  $0.47\sigma$  respectively for BP1 and BP2. The situation improves for BP1 at the centre-of-mass energy of 30 TeV, where  $6.94\sigma$  signal significance can be achieved with a luminosity of  $1000 \text{ fb}^{-1}$ . BP2 here shows a  $3.19\sigma$  significance, with  $\sim 2450 \text{ fb}^{-1}$  luminosity required to reach the desired  $5\sigma$ . Promising outcomes are

obtained at the 100 TeV LHC/FCC, where  $13.56\sigma$  and  $8.17\sigma$  significances are predicted for BP1 and BP2, respectively with  $100 \text{ fb}^{-1}$  luminosity. Owing to the high cross-section and no upper limit on jets,  $t\bar{t}$  still contributes dominantly as background.

#### 4.4.3 2 - jet + $\cancel{p}_T$

The finalstate of  $1 - \text{jet} + \cancel{p}_T$  ensues from the production of  $S_3^{1/3}$  in association with a neutrino via  $s$ -gluon fusion followed by its disintegration into a  $s$ -quark and a neutrino (see Eq. 21). However, we cannot avoid a ISR/FSR jet and to avoid the reduction on the signal cross-section, we allow one such ISR/FSR jet in the finalstate. The complete finalstate with advanced cuts is as follows:

$$1 \leq n_j \leq 2, n_{b\text{-jet}} = n_{\tau\text{-jet}} = n_\ell = 0 \quad \text{and}$$

$$p_T^{j_1} \geq 400 \text{ GeV}, \cancel{p}_T \geq 500 \text{ GeV}, p_T^H \geq 1200 \text{ GeV}.$$

The signal and backgrounds for this finalstate are simulated in Table 19. Due to the fact that this finalstate incor-

**Table 19** The number of events for  $2 - \text{jet} + \cancel{p}_T \geq 500 \text{ GeV}$  finalstate (Eq. 21) for the benchmark points and dominant SM backgrounds at the LHC/FCC with centre-of-mass energy of 14 TeV, 30 TeV and 100 TeV

at an integrated luminosity of  $1000 \text{ fb}^{-1}$  for the first two and  $100 \text{ fb}^{-1}$  for 100 TeV. The required luminosities to achieve a  $5\sigma$  signal ( $\mathcal{L}_{5\sigma}$ ) are also shown for all three cases

$\sqrt{s}$ in TeV	Fusion	Mode	$2 - \text{jet} + \cancel{p}_T \geq 500 \text{ GeV}$						
			Signal		Backgrounds				
			BP1	BP2	$t\bar{t}$	$VV$	$VVV$	$t\bar{t}V$	$tVV$
14	$s - g$	$S_3^{4/3} \mu$	0.11	0.03	289.41	1335.87	57.15	4.39	3.39
		$S_3^{1/3} \nu$	47.01	12.35					
	$c - g$	$S_3^{1/3} \mu$	2.25	0.54					
		$S_3^{2/3} \nu$	118.31	29.34					
	Total		167.68	42.26					
Significance( $\sigma$ )		3.89	1.02						
$\mathcal{L}_{5\sigma} (\text{fb}^{-1})$		1652.15	$\gg 5000$						
30	$s - g$	$S_3^{4/3} \mu$	2.16	1.29	2441.14	8349.32	435.17	34.49	22.73
		$S_3^{1/3} \nu$	614.52	227.99					
	$c - g$	$S_3^{1/3} \mu$	42.86	14.00					
		$S_3^{2/3} \nu$	1648.86	604.69					
	Total		2308.40	847.97					
Significance( $\sigma$ )		19.80	7.70						
$\mathcal{L}_{5\sigma} (\text{fb}^{-1})$		63.76	421.75						
100	$s - g$	$S_3^{4/3} \mu$	12.93	8.75	6304.84	7095.89	527.31	69.28	46.70
		$S_3^{1/3} \nu$	1094.90	525.45					
	$c - g$	$S_3^{1/3} \mu$	133.38	58.56					
		$S_3^{2/3} \nu$	3157.52	1465.86					
	Total		4398.72	2058.62					
Significance( $\sigma$ )		32.39	16.22						
$\mathcal{L}_{5\sigma} (\text{fb}^{-1})$		2.38	9.50						

porates two neutrinos, we have imposed a very high missing energy cut as  $\cancel{p}_T \geq 500 \text{ GeV}$ . We also impose veto on charged leptons ( $e^\pm, \mu^\pm$ ),  $b$ -jets, and  $\tau$ -jet. Apart from the single jet from the leptoquark ( $s$  quark), we keep room for one ISR/FSR jet, so that the total number of jets in the finalstate can be maximum of two.

Demand of lesser jets, veto on  $b$ -jets, and high  $\cancel{p}_T$  cut means  $VV$  is the dominant background here, over the subdominant  $t\bar{t}$ . On the contrary, the signal gets a huge contribution from the mode  $c - g \rightarrow S_3^{2/3} \nu$  as the  $c$ -jet mimics the light jet. A tiny contribution from  $c - g \rightarrow S_3^{1/3} \mu$  arises here as well. The simulation is performed with the centre-of-mass energies of 14 TeV, 30 TeV and 100 TeV at an integrated luminosity of  $1000 \text{ fb}^{-1}$  for the first two and  $100 \text{ fb}^{-1}$  for 100 TeV. At the 14 TeV LHC, BP1 gives us a fairly strong  $3.89\sigma$  significance, which means  $5\sigma$  can be reached with  $\sim 1650 \text{ fb}^{-1}$  of luminosity. BP2 signal remains very weak with  $\sim 1\sigma$  significance. The situation becomes hopeful when we move to the 30 TeV LHC, where  $19.80\sigma$  and  $7.70\sigma$  significances are predicted at  $1000 \text{ fb}^{-1}$  luminosity, for BP1

and BP2, respectively. These strengths are further enhanced at 100 TeV, with significances of  $32.39\sigma$  and  $16.22\sigma$  for BP1 and BP2, respectively with  $100 \text{ fb}^{-1}$  luminosity. The required  $5\sigma$  significance here is predicted to be obtained with much earlier data.

#### 4.4.4 $1 - \text{jet} + 1\mu + \cancel{p}_T$

If the leptoquark  $S_3^{1/3}$  is produced in  $c$ -gluon fusion associated with a muon and eventually decays to a  $s$ -quark and a neutrino, the finalstate  $1 - \text{jet} + 1\mu + \cancel{p}_T$  appears as quoted in Eq. 24. The complete requirements and cuts for this finalstate are given below:

$$n_j \geq 1, n_\mu \geq 1, n_{b\text{-jet}} = n_{\tau\text{-jet}} = 0 \quad \text{and}$$

$$p_T^{\ell_1} \geq 200 \text{ GeV}, p_T^{j_1} \geq 200 \text{ GeV},$$

$$\cancel{p}_T \geq 500 \text{ GeV}, p_T^H \geq 1200 \text{ GeV}.$$

The event numbers along with different SM backgrounds have been shown in Table 20. As this finalstate involves one neutrino, a cut on missing transverse momentum is applied

**Table 20** The number of events for  $\geq 1 - \text{jet} + \geq 1\mu + \cancel{p}_T \geq 500 \text{ GeV}$  finalstate (Eq. 24) for the benchmark points and dominant SM backgrounds at the LHC/FCC with centre-of-mass energy of 14 TeV, 30 TeV and 100 TeV at an integrated luminosity of  $1000 \text{ fb}^{-1}$  for the first two and  $100 \text{ fb}^{-1}$  for 100 TeV. The required luminosities to achieve a  $5\sigma$  signal ( $\mathcal{L}_{5\sigma}$ ) are also shown for all three cases

$\sqrt{s}$ in TeV	Fusion	Mode	$\geq 1 - \text{jet} + \geq 1\mu + \cancel{p}_T \geq 500 \text{ GeV}$						
			Signal		Backgrounds				
			BP1	BP2	$t\bar{t}$	$VV$	$VVV$	$t\bar{t}V$	$tVV$
14	$s - g$	$S_3^{4/3}\mu$	6.57	2.69	295.20	226.96	32.51	13.52	6.05
		$S_3^{1/3}\nu$	36.81	10.88					
	$c - g$	$S_3^{1/3}\mu$	55.58	14.85					
		$S_3^{2/3}\nu$	0.00	0.00					
	Total		98.96	28.42	574.24				
Significance( $\sigma$ )		3.81	1.16						
$\mathcal{L}_{5\sigma} (\text{fb}^{-1})$		1718.72	$\gg 5000$						
30	$s - g$	$S_3^{4/3}\mu$	163.71	87.84	5549.70	2426.37	419.14	159.67	52.52
		$S_3^{1/3}\nu$	760.50	313.38					
	$c - g$	$S_3^{1/3}\mu$	974.61	463.29					
		$S_3^{2/3}\nu$	0.00	0.00					
	Total		1898.82	804.96	8607.40				
Significance( $\sigma$ )		18.52	8.30						
$\mathcal{L}_{5\sigma} (\text{fb}^{-1})$		72.85	363.15						
100	$s - g$	$S_3^{4/3}\mu$	970.04	604.41	10675.32	2153.36	536.16	349.62	151.04
		$S_3^{1/3}\nu$	1999.71	1076.01					
	$c - g$	$S_3^{1/3}\mu$	2396.01	1328.94					
		$S_3^{2/3}\nu$	0.00	0.00					
	Total		5365.76	3009.36	13865.50				
Significance( $\sigma$ )		38.69	23.17						
$\mathcal{L}_{5\sigma} (\text{fb}^{-1})$		1.67	4.66						

as  $\cancel{p}_T \geq 500 \text{ GeV}$  along with  $p_T \geq 200 \text{ GeV}$  for both the muon and the light-jet. Additionally, no  $b$ -jet and  $\tau$ -jet are demanded to reduce the SM backgrounds, and the hardness cut of  $p_T^H \geq 1.2 \text{ TeV}$  comes into play here as well. No upper limit on the number of jets means  $t\bar{t}$  still contributes dominantly to the background. At the 14 TeV LHC, the BP1 signal is fairly healthy with a  $3.81\sigma$  significance obtainable at  $1000 \text{ fb}^{-1}$  of integrated luminosity, with the  $5\sigma$  being achievable with luminosity of  $\sim 1720 \text{ fb}^{-1}$ . BP2 however, gives a weak signal of  $1.16\sigma$  significance. Moving to the centre-of-mass energy of 30 TeV, we obtain encouraging signals with significances of  $18.52\sigma$  for BP1, and  $8.30\sigma$  for BP2 with  $1000 \text{ fb}^{-1}$  luminosity. These are enhanced further at the 100 TeV predictions, where with  $100 \text{ fb}^{-1}$  luminosity, BP1 and BP2 signals carry significances of  $38.69\sigma$  and  $23.17\sigma$  respectively, indicating the feasibility of a  $5\sigma$  probe with  $< 5 \text{ fb}^{-1}$  integrated luminosity.

### 5 Lepton flavour violating decay signatures

In this section we discuss the signatures involving second and third generation fermion decays corresponding to the benchmark choice BP3 as quoted in Table 1. Due to different choice of coupling values, it can be seen from Table 21 that, we have different decay channels for the three components of  $S_3$  as compared to the two previously investigated cases BP1 and BP2, discussed in Table 14. In this case,  $S_3$  is produced in association with a muon or a neutrino through via  $b - g$  and  $t - g$  fusions. Now, the components  $S_3^{4/3}$  and  $S_3^{2/3}$  decay to  $b\mu$  and  $t\nu_\mu$  states, respectively, with 100% probability. Whereas,  $S_3^{1/3}$  disintegrates into  $t\mu$  and  $b\nu_\mu$  with equal probabilities i.e. 50% each. The further decay of  $t$ -quark to a  $b$ -quark and a  $W$ -boson, and finally the  $W$ -boson decay modes will give rise to two jets or lepton plus missing energy signatures. The complete decay chains of these processes are as following.

$$\text{BP3: } b - g \rightarrow S_3^{4/3}\mu \rightarrow (b\mu) + \mu \rightarrow 1b\text{-jet} + 2\mu, \tag{26}$$

**Table 21** The decay branching ratios (in percentage) of  $S_3$  for BP3

Decay Modes	Branching ratios BP3 $M_{S_3} = 1.5$ TeV
$S_3^{-4/3} \rightarrow b\mu$	100
$S_3^{-1/3} \rightarrow t\mu$	50
$S_3^{-1/3} \rightarrow bv_\mu$	50
$S_3^{2/3} \rightarrow tv_\mu$	100

$$b - g \rightarrow S_3^{1/3} v_\mu \rightarrow (t \mu) + v_\mu \rightarrow 1b\text{-jet} + 1\ell + 1\mu + \cancel{p}_T, \tag{27}$$

$$\rightarrow (t \mu) + v_\mu \rightarrow 1b - \text{jet} + 2 - \text{jet} + 1\mu + \cancel{p}_T, \tag{28}$$

$$\rightarrow (b v_\mu) + v_\mu \rightarrow 1b\text{-jet} + \cancel{p}_T, \tag{29}$$

$$t - g \rightarrow S_3^{1/3} \mu \rightarrow (b v_\mu) + \mu \rightarrow 1b - \text{jet} + 1\mu + \cancel{p}_T, \tag{30}$$

$$\rightarrow (t \mu) + \mu \rightarrow 1b - \text{jet} + 2 - \text{jet} + 2\mu, \tag{31}$$

$$\rightarrow (t \mu) + \mu \rightarrow 1b - \text{jet} + 1\ell + 2\mu + \cancel{p}_T, \tag{32}$$

$$t - g \rightarrow S_3^{2/3} v_\mu \rightarrow (t v_\mu) + v_\mu \rightarrow 1b - \text{jet} + 1\ell + \cancel{p}_T. \tag{33}$$

We can see that, the production channel of  $S_3^{4/3}$  provides unique signature as one  $b$ -jet plus di-muon. Whereas, for  $S_3^{2/3}$  we get two finalstates depending on the decay of the top-quark, which arises from  $S_3^{2/3}$ . However, six different finalstates are possible for the two production processes of  $S_3^{1/3}$ . It is interesting to notice that unlike BP1 and BP2 scenarios of  $S_3$  leptoquark, some finalstates for BP3 exhibit lepton flavour violating signatures (different lepton flavours in the finalstate) though the Lagrangian (in Eq. 2) does not contain any explicit lepton flavour violating interaction.

Next, we analyze these finalstates at the LHC/FCC adopting the similar procedures described in previous sections at 14 TeV and 30 TeV centre-of-mass energies with an integrated luminosity of  $1000 \text{ fb}^{-1}$ , also at 100 TeV collision with  $100 \text{ fb}^{-1}$  of integrated luminosity. The signal numbers for all the above mentioned finalstates are very low for 14 TeV results and do not list them here. The events at 30 TeV and 100 TeV centre-of-mass energies are noticeable, however, in most cases, they fail to attain a  $5\sigma$  signal strength within the proposed lifetime of LHC/FCC.

### 5.1 $1b - \text{jet} + 2 - \text{jet} + 2\mu$

The only encouraging scenario is the finalstate of  $1b\text{-jet} + 2\text{-jet} + 2\mu$ , which according to the topologies quoted above arises from  $S_3^{1/3}$  component (Eq. 31). However, due to presence of initial state radiations and large production cross-section of  $S_3^{4/3}$  (see Table 12), this component contributes dominantly via Eq. (26). As no neutrino is present in this finalstate, we have applied a cut in the missing transverse momentum  $\cancel{p}_T < 30 \text{ GeV}$ . Moreover, a total hardness cut  $p_T^H \geq 1200 \text{ GeV}$  is also applied, like the previous analysis for  $S_1$  and  $S_3$ . The complete finalstate is written below:

$$n_{b\text{-jet}} = 1, n_j \leq 3, n_\mu \geq 2, n_\ell \geq 2, n_{\tau\text{-jet}} = 0 \quad \text{and}$$

$$\cancel{p}_T \leq 30 \text{ GeV}, p_T^H \geq 1200 \text{ GeV} \quad \text{and} \quad |M_{jj} - M_W| \geq 10 \text{ GeV}, |M_{\ell\ell} - M_Z| \geq 5 \text{ GeV}.$$

While  $t\bar{t}$  is the dominant background in this case, the contribution is very low, owing to the stringent cuts on missing energy and hardness. It is interesting to note that, this background contribution decreases when we move from 30 to 100 TeV energies. This is accounted for by the less number of events with  $\cancel{p}_T \leq 30 \text{ GeV}$  and  $n_{\text{jet}} \leq 2$  at 100 TeV, compared to 30 TeV, due to the increase in jets coming from ISR/FSR. Additionally, we reintroduce the  $W$ - and  $Z$ -boson resonance vetoes on the di-jet and di-lepton invariant mass, helping us reduce the background further. The numbers for the signal and the SM background events are given in Table 22. The signal significances of  $6.73\sigma$  at 30 TeV with  $1000 \text{ fb}^{-1}$  integrated luminosity and  $9.83\sigma$  at 100 TeV with luminosity of  $100 \text{ fb}^{-1}$  can be attained for this benchmark point (BP3). The required luminosity for a  $5\sigma$  discovery is  $552.68 \text{ fb}^{-1}$  at 30 TeV, which reduces to  $25.85 \text{ fb}^{-1}$  at 100 TeV.

### 5.2 $1b - \text{jet} + 1\ell + 1\mu$

Instead of the demand of two muons in the finalstate, we have also investigated the situations with one muon, namely, the finalstates quoted in Eqs. (27), (28) and (30). Among these the scenario in Eq. (27) is promising and the results are shown in Table 23. In this case, the complete finalstate with the appropriate cuts is described as follows:

$$n_{b\text{-jet}} = 1, n_j \leq 2, n_\mu = 1, n_e = 1, n_\ell = 2, n_{\tau\text{-jet}} = 0 \quad \text{and}$$

$$p_T^H \geq 1200 \text{ GeV}$$

and

$$|M_{jj} - M_W| \geq 10 \text{ GeV}, |M_{\ell\ell} - M_Z| \geq 5 \text{ GeV}.$$

Here the  $S_3^{1/3}$  is produced in association with a neutrino from  $b - g$  fusion and decays into a muon and top quark that further decomposes semi-leptonically into a bottom quark,

**Table 22** The number of events for  $1b - \text{jet} + 2 - \text{jet} + \geq 2\mu + \cancel{p}_T \leq 30 \text{ GeV}$  for BP3 and dominant SM backgrounds at the LHC/FCC with centre-of-mass energy of 30 TeV and 100 TeV at an integrated luminosity of  $1000 \text{ fb}^{-1}$  and  $100 \text{ fb}^{-1}$ , respectively. The required luminosities to achieve a  $5\sigma$  signal ( $\mathcal{L}_{5\sigma}$ ) are also shown for both the cases

$\sqrt{s}$ in TeV	Fusion	Mode	$1b - \text{jet} + 2 - \text{jet} + \geq 2\mu + \cancel{p}_T \leq 30 \text{ GeV}$					
			Signal	Backgrounds				
			BP3	$t\bar{t}$	VV	VVV	$t\bar{t}V$	$tVV$
30	$b - g$	$S_3^{4/3} \mu$	55.41	12.02	0.00	0.00	0.00	0.78
		$S_3^{1/3} \nu$	0.00					
	$t - g$	$S_3^{1/3} \mu$	0.23					
		$S_3^{2/3} \nu$	0.00					
	Total		55.64	12.80				
Significance( $\sigma$ )		6.73						
$\mathcal{L}_{5\sigma} (\text{fb}^{-1})$		552.68						
100	$b - g$	$S_3^{4/3} \mu$	100.07	3.83	0.00	0.00	0.00	0.00
		$S_3^{1/3} \nu$	0.00					
	$t - g$	$S_3^{1/3} \mu$	0.32					
		$S_3^{2/3} \nu$	0.00					
	Total		100.39	3.83				
Significance( $\sigma$ )		9.83						
$\mathcal{L}_{5\sigma} (\text{fb}^{-1})$		25.85						

**Table 23** The number of events for  $1b - \text{jet} + 1\ell + 1\mu$  for BP3 and dominant SM backgrounds at the LHC/FCC with centre-of-mass energy of 30 TeV and 100 TeV at an integrated luminosity of  $1000 \text{ fb}^{-1}$  and  $100 \text{ fb}^{-1}$ , respectively. The required luminosities to achieve a  $5\sigma$  signal ( $\mathcal{L}_{5\sigma}$ ) are also shown for both the cases

$\sqrt{s}$ in TeV	Fusion	Mode	$1b - \text{jet} + 1\ell + 1\mu$					
			Signal	Backgrounds				
			BP3	$t\bar{t}$	VV	VVV	$t\bar{t}V$	$tVV$
30	$b - g$	$S_3^{4/3} \mu$	80.70	625.32	12.32	14.04	65.14	8.62
		$S_3^{1/3} \nu$	2.43					
	$t - g$	$S_3^{1/3} \mu$	0.53					
		$S_3^{2/3} \nu$	0.02					
	Total		83.68	725.44				
Significance( $\sigma$ )		2.94						
$\mathcal{L}_{5\sigma} (\text{fb}^{-1})$		2889.44						
100	$b - g$	$S_3^{4/3} \mu$	148.16	628.19	26.90	10.58	37.06	15.56
		$S_3^{1/3} \nu$	5.24					
	$t - g$	$S_3^{1/3} \mu$	0.78					
		$S_3^{2/3} \nu$	0.03					
	Total		154.21	718.29				
Significance( $\sigma$ )		5.22						
$\mathcal{L}_{5\sigma} (\text{fb}^{-1})$		91.73						

a light charged lepton and a neutrino. In this finalstate, we demand this accompanying lepton to be an electron. However, due to the higher cross-section and the high probability of having a  $b$ -jet and at least one muon, we still have dominant contribution from the  $b - g \rightarrow S_3^{4/3}$  process. In this case, we do not put a cut on the  $\cancel{p}_T$  to avoid the risk of losing signal events. The backgrounds are reduced by the  $W$ - and  $Z$ -boson vetoes, along with the hardness cut and the demand of  $\leq 2$  total jets. In both the centre-of-mass energies of 30 and 100 TeV,  $t\bar{t}$  remains the dominant background, contributing to the  $b$ -jet criteria. The signal strength at this finalstate is feeble compared to Table 22, as we only obtain a  $2.94\sigma$  significance at the 30 TeV LHC with  $1000 \text{ fb}^{-1}$  of integrated luminosity. However, the situation is more promising at 100 TeV centre-of-mass energy, where we have a  $5.22\sigma$  signal strength at  $100 \text{ fb}^{-1}$  of integrated luminosity, with the requirement of  $91.73 \text{ fb}^{-1}$  for a  $5\sigma$  probe.

However, for the two other topologies (Eqs. 28 and 30) the signal numbers are quite low and the SM  $t\bar{t}$  background numbers are significant which in turn reduces the signal strength considerably. The situations further worsen in the topologies where no muon is present, which are Eq. (29) for the  $S_3^{1/3}$  component, and Eq. (33) for the  $S_3^{2/3}$  part. In these cases, we do not obtain any significant signal strength due to the overwhelming SM background numbers. Hence we infer that unlike the previous cases with BP1 and BP2, here for BP3, different components of the  $S_3$  leptoquark can not be discriminated via looking at distinguishable signatures.

## 6 Leptoquarks at muon collider

This section is devoted to explore leptoquarks at a proposed muon collider about which a growing interest is noticed at recent times. The reach of a multi-TeV muon collider is expected to be  $90 \text{ ab}^{-1}$  with the centre-of-mass energy of 30 TeV [106]. Due to the absence of initial state QCD radiation, reduced synchrotron radiation compared to electron collider and known centre-of-mass frame, makes it a superior precision machine. In this section, we study the feasibility of producing leptoquarks in pair at muon collider. It is important to mention here that, in the case of  $\mu^+\mu^-$  collisions, it is not possible to have a single leptoquark produced at the final state. The possibility of resonant production of a single leptoquark from a muon-quark fusion is mentioned in Ref. [107], which can arise only when the quark contribution in the muon PDF is considered. These contributions are very tiny, and in the context of this paper, such small estimates are not very relevant for a detailed collider study. Hence, the pair production is the only possibility, where Yukawa-type couplings involving second generation leptons can play the major role via  $t$ -channel process. The initial setup and the kinematic cuts remain the same as described in Sect. 2.2.

For our choices of benchmark points, given in Table 1, these production processes occur through the Feynman diagrams shown in Fig. 10. It is worthwhile to remind that the benchmark points are motivated from the tensions observed in  $B$ -decays, where the leptoquark  $S_1$  couples only to third generation leptons aiming to reduce the  $b \rightarrow c\tau\bar{\nu}$  discrepancy [8] and as a result,  $S_1$  gets produced only through a photon and a  $Z^0$ -boson mediated  $s$ -channel diagram (Fig. 10a). While by construction of the benchmark points the leptoquark  $S_3$  couples to muons contributing to  $b \rightarrow s\mu\mu$  anomalies [3–7] and will be the prime candidate of our study at muon collider. Apart from the  $s$ -channel diagrams,  $S_3$  can be produced via the quark mediated  $t$ -channel diagrams (Fig. 10b, c) as well. The  $t$ -channel diagram for  $S_3^{4/3}$  component of  $S_3$  goes through a  $s$ -quark (BP1, BP2) or a  $b$ -quark (BP3), whereas for  $S_3^{1/3}$  component a  $c$ -quark (BP1, BP2) or a  $t$ -quark (BP3) serves the purpose. It is noteworthy that  $S_3^{2/3}$  does not couple to any charged lepton due to the structure of the interaction Lagrangian in Eq. (4), and hence it is produced at muon collider through the  $s$ -channel diagrams (Fig. 10a) only.

As BP1 and BP2, quoted in Table 1, differ mainly in the mass of the leptoquark, in this section we choose to present the results only for BP1 for simplicity, and BP3 as well. The variation of production cross-sections for  $S_3$  leptoquark with the centre-of-mass energy of the muon collider is presented in Fig. 11a, b for BP1 and BP3, respectively. The contributions arising from different components of  $S_3$  leptoquark are separately presented with different colour codes as specified in the plot legend. For BP1,  $S_3^{4/3}$  shows prepotent effects while  $S_3^{1/3}$  remains sub-dominant. In this case, the effects of  $t$ -channel diagrams are superior to the contributions from  $s$ -channel processes. However, for BP3,  $S_3^{2/3}$  dominates at low centre-of-mass energy and as energy starts increasing,  $S_3^{4/3}$  becomes the main contributor to the total cross-section mostly via  $s$ -channel contribution. Due to smaller values of leptoquark Yukawa-type couplings in BP3,  $t$ -channel processes are suppressed compared to BP1. Note that the interference of  $t$ - and  $s$ -channel diagrams in Fig. 11c introduces negative contribution, which are large at lower energies and are substantial even at higher energies. This keeps the cross-sections of  $S_3^{4/3}$  and  $S_3^{1/3}$  of the same order and results into a crossover of cross-sections for  $S_3^{4/3}$  and  $S_3^{2/3}$  around 6.5 TeV. It is easy to see from the two figures that the total production cross-section for  $S_3$  in BP1 scenario is much higher than the BP3 case as the  $Y_{S_3}^{22}$  coupling is significantly smaller in BP3 compared to BP1 (see Table 1). On the other hand, we have chosen the hardness cut of 1.2 TeV in our simulation, as discussed in Sect. 3.2.1, in such a way that the effects of  $s$ -channel processes could be neglected. Thus contributions from the  $S_3^{2/3}$  in Fig. 11a, b and similarly for  $S_1$  leptoquark become negligible.

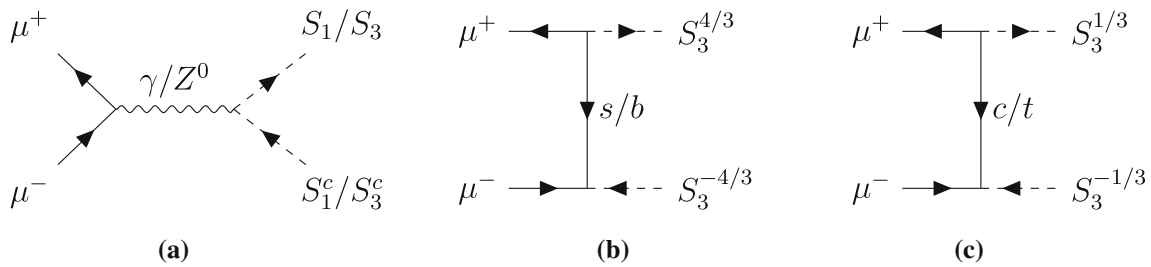


**Fig. 10** The tree-level Feynman diagrams for the pair production of  $S_1$  and  $S_3$  leptoquarks at a muon collider for the benchmark points specified in Table 1

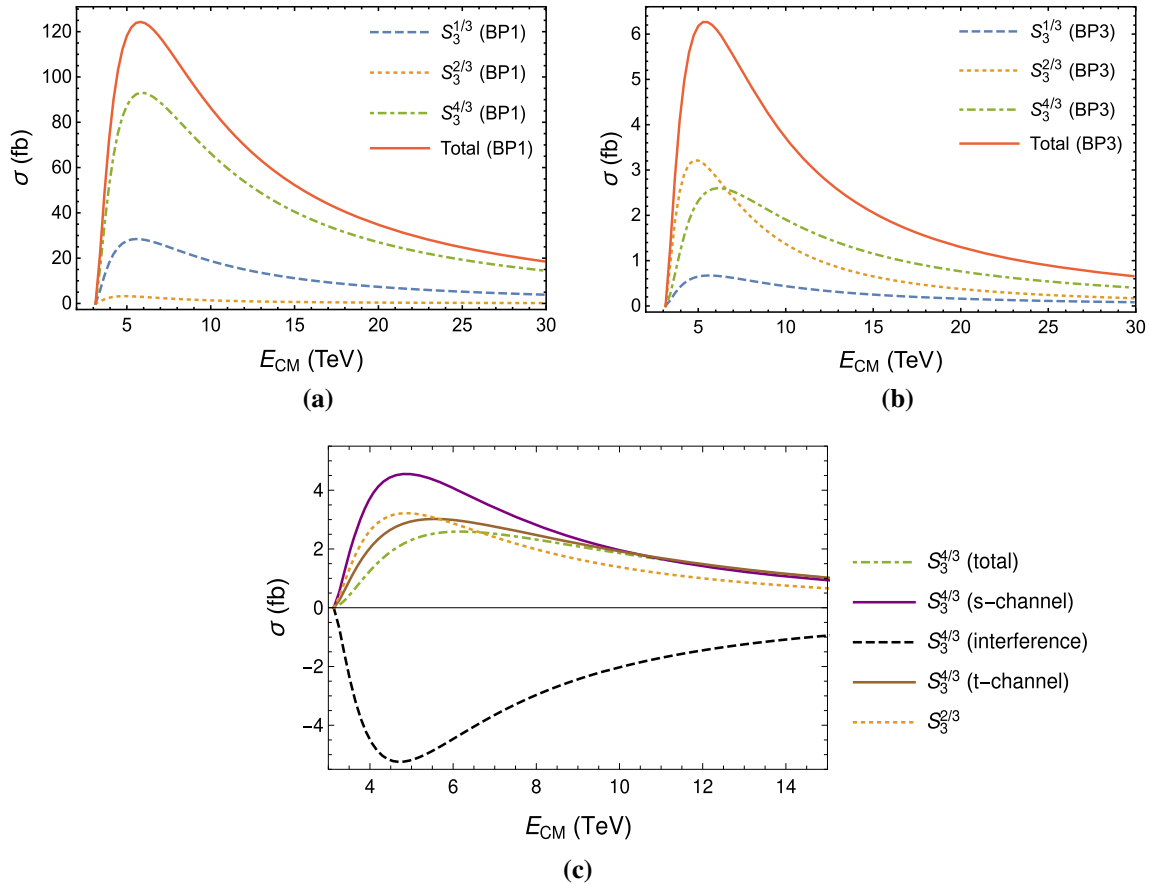


**Fig. 11** The variation of cross-sections for the pair production of  $S_3$  leptoquark with the centre-of-mass energy at a multi-TeV muon collider for BP1 (in **a**) and BP3 (in **b**). The blue (dashed), yellow (dotted) and green (dot-dashed) curves indicate individual contributions arising from  $S_3^{1/3}$ ,  $S_3^{2/3}$  and  $S_3^{4/3}$  components of  $S_3$  respectively, and the red (solid) line signifies the total production cross-section for  $S_3$  leptoquark. The

panel **c** zooms the BP3 case in the low energy region showing separately the  $s$ -channel (in purple solid),  $t$ -channel (in brown solid), interference of  $s$ - and  $t$ - channels (in black dashed) for  $S_3^{4/3}$ , as well as the total contributions of  $S_3^{4/3}$  (in green dot-dashed) and  $S_3^{2/3}$  (in yellow dotted) in the production cross-sections

For our analysis, we pick two centre-of-mass energies of 8 TeV and 30 TeV with the integrated luminosities of  $1000 \text{ fb}^{-1}$  and  $10000 \text{ fb}^{-1}$ , respectively. The cross-sections for pair production of different components of  $S_3$  at these two centre-of-mass energies are tabulated in Table 24. Interestingly enough, the cross-sections for pair production of  $S_3^{1/3}$  are significantly smaller than that of  $S_3^{4/3}$ . Although appar-

ently it seems that the ratio of these two cross-sections at some particular centre-of-mass energy will be  $1 : 4$  due to the extra  $\sqrt{2}$  factor in the interaction vertex of  $S_3^{4/3}$  with quarks and leptons, the presence of  $s$ -channel diagrams and masses of  $t$ -channel propagators cause a deviation from this  $1 : 4$  ratio. On the other hand, the cross-sections for  $S_3^{4/3}$  and  $S_3^{1/3}$  in BP3 case are around 40 times smaller than that in BP1

**Table 24** The cross-sections for pair production of  $S_3$  at a multi-TeV muon collider for two different benchmark points BP1 and BP3 (specified in Table 1) at the centre-of-mass energies of 8 TeV and 30 TeV. Here  $\sqrt{s}$  is used as the renormalization/factorization scale

Benchmark Points ( $M_{S_3}$ )	$\sigma(\mu^+\mu^- \rightarrow S_3^{4/3}S_3^{-4/3})$ in fb with $E_{CM}$ in TeV		$\sigma(\mu^+\mu^- \rightarrow S_3^{1/3}S_3^{-1/3})$ in fb with $E_{CM}$ in TeV		$\sigma(\mu^+\mu^- \rightarrow S_3^{2/3}S_3^{-2/3})$ in fb with $E_{CM}$ in TeV	
	8 TeV	30 TeV	8 TeV	30 TeV	8 TeV	30 TeV
	BP1 (1.5 TeV)	80.74	14.75	23.36	3.95	1.94
BP3 (1.5 TeV)	2.32	0.41	0.55	0.08	1.94	0.17

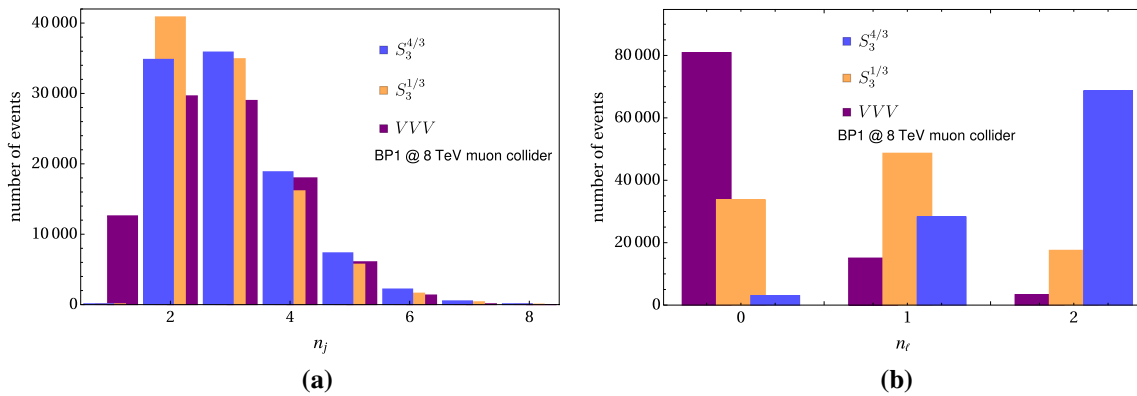


**Fig. 12** The jet multiplicity ( $n_j$  in a) and lepton multiplicity ( $n_\ell$  in b) distributions for the pair production of  $S_3^{4/3}$  and  $S_3^{1/3}$  for BP1 along with the SM background from triple gauge boson at a muon collider with 8 TeV centre-of-mass energy

due to magnitude of  $Y_{S_3}^{22}$  as mentioned previously. The production cross-section for  $S_3^{2/3}$  at muon collider remains the same in BP1 and BP3 since this process involves  $s$ -channel gauge interactions only.

### 6.1 Kinematic distributions and topologies

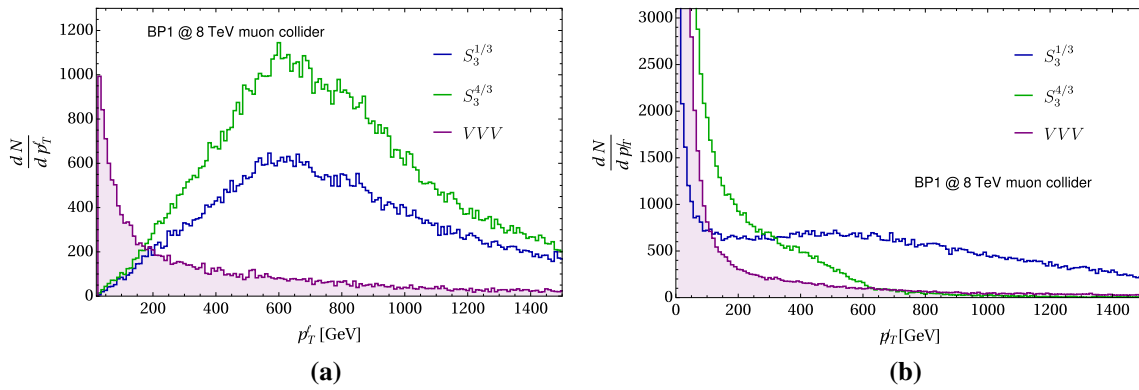
As discussed in the previous Sect. 4.1, we start with the comparison of various kinematic distributions of the  $S_3$  leptoquark and the dominant SM backgrounds at muon collider in order to understand the different interplay between hadron and muon collider. To demonstrate, we select BP1 scenario with 8 TeV of centre-of-mass energy. At this point, it is interesting to mention that triple gauge boson modes act as dominant SM background for BP1 and it can be easily observed from the results quoted in Tables 25 and 26 which will be discussed in the next subsection.

Figure 12a describes the jet multiplicity distribution ( $n_j$ ) for pair production of  $S_3^{4/3}$  (in blue) and  $S_3^{1/3}$  (in orange) along with the dominant SM background of triple gauge boson (in purple) with 8 TeV centre-of-mass energy. While all three distributions peak at around two or three jets, there are negligible number of mono-jet events for the signal processes, as both the pair produced leptoquarks must give one jet each. In contrast, the  $VVV$  background has significant number of monojet events, owing to pure leptonic decay modes of the vector bosons. In parallel, we have shown the

lepton multiplicity distributions ( $n_\ell$ ) for  $S_3^{4/3}$ ,  $S_3^{1/3}$  and triple gauge boson background in Fig. 12b. As expected,  $S_3^{4/3}$  displays peak with two leptons while  $S_3^{1/3}$  exhibits substantial contributions mainly to no-lepton and mono-lepton channels. This is due to the reason that  $S_3^{4/3}$  component of  $S_3$  in BP1 decays to  $s\mu$  mode with 100% branching ratio (see Table 14), whereas,  $S_3^{1/3}$  component decays to  $c\mu$  and  $sv$  with equal probability. However, the SM background coming from triple gauge bosons diminishes gradually with increase in lepton number at the final state as the weak gauge bosons mostly decay into jets.

The jet transverse momentum ( $p_T^j$ ) distribution at 8 TeV muon collider has been depicted in Fig. 13, where the two leading jets from the pair production of each of the components  $S_3^{1/3}$  and  $S_3^{4/3}$  are depicted. In both cases, the hardest jets ( $j_1$ ), shown in blue for  $S_3^{1/3}$  and orange for  $S_3^{4/3}$  peak around half of the leptoquark mass (i.e. 750 GeV), as expected. The second hardest jets ( $j_2$ ) are shown in green for  $S_3^{1/3}$  and red for  $S_3^{4/3}$ , and both of them reach their maxima at about 400 GeV.

The transverse momentum ( $p_T^\ell$ ) distributions for light charged leptons in the pair production channels of  $S_3^{4/3}$  and  $S_3^{1/3}$  along with the SM background arising from triple gauge boson have been depicted in Fig. 14a. Distributions for both the signals (blue for  $S_3^{1/3}$  and green for  $S_3^{4/3}$ ) reach their maxima at 600 GeV, which is slightly lower than half of the leptoquark mass (i.e. 750 GeV). However, the distribution



**Fig. 14** The lepton  $p_T$  ( $p_T^\ell$  in **a**) and missing  $p_T$  ( $\cancel{p}_T$  in **b**) distributions for  $S_3^{4/3}$ ,  $S_3^{1/3}$  and the SM background from triple gauge boson at a muon collider with centre-of-mass energy of 8 TeV

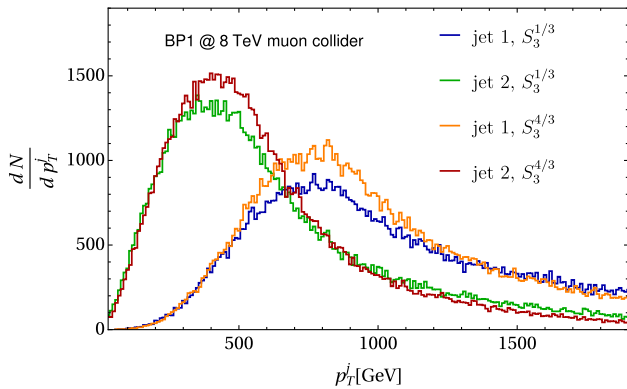


**Fig. 13** The jet  $p_T$  distribution of the pair production of  $S_3^{4/3}$  and  $S_3^{1/3}$  in BP1 at muon collider with 8 TeV centre-of-mass energy

for the dominant SM background (in purple) peak at around 40 GeV, and shows a long tail with very less events. Similarly the missing transverse momentum  $\cancel{p}_T$  distributions are displayed in Fig. 14b. The distribution for  $VVV$  background again peaks at around 40 GeV, showing a long, thin tail. The  $\cancel{p}_T$  distributions for  $S_3^{4/3}$  dies out comparatively quicker as it does not involve any neutrino in its decay channel.  $S_3^{1/3}$ , which decays into  $s\nu$  with 50% branching ratio, shows a relatively large tail.

$$\text{BP1 : } \mu^+\mu^- \rightarrow S_3^{+4/3} S_3^{-4/3} \rightarrow 2\text{-jet} + 2\mu, \quad (34)$$

$$\mu^+\mu^- \rightarrow S_3^{+1/3} S_3^{-1/3} \rightarrow 2c\text{-jet} + 2\mu, \quad (35)$$

$$\text{BP3 : } \mu^+\mu^- \rightarrow S_3^{+4/3} S_3^{-4/3} \rightarrow 2b\text{-jet} + 2\mu, \quad (36)$$

$$\mu^+\mu^- \rightarrow S_3^{+1/3} S_3^{-1/3} \rightarrow 2b\text{-jet} + 4\text{-jet} + 2\mu. \quad (37)$$

Now we proceed to study the detailed phenomenology of the two benchmark scenarios BP1 and BP3. After the pair production,  $S_3^{4/3}$  decays into  $s\mu$  ( $b\mu$ ) with 100% branching fraction whereas,  $S_3^{1/3}$  decays into  $c\mu$  and  $s\nu$  ( $t\mu$  and  $b\nu$ ) finalstates each with 50% branching fractions for BP1

(BP3), as displayed in Table 14 (Table 21). Thus, for  $S_3^{4/3}$ , we have di-jet plus di-muon (Eq. 34) and two  $b$ -jets plus di-muon (Eq. 36) signals at the muon collider for BP1 and BP3, respectively. However, for  $S_3^{1/3}$ , several finalstates are plausible depending on its decay channels. Here, we only focus on those finalstates with no missing energy. It helps us to reduce the contamination from  $S_3^{2/3}$  which despite of having a very low production cross-section, finally decays into finalstates with one neutrino for both the benchmark cases. Therefore for  $S_3^{1/3}$ , we consider two  $c$ -jets plus di-muon and two  $b$ -jets plus tetra-jet with di-muon topologies for BP1 and BP3, respectively. In the following few subsections we describe the simulated results for these four finalstates. We remind that we do not look for signals of  $S_3^{2/3}$  in this section, as it gets produced through  $s$ -channel contributions only. As far as backgrounds are concerned, the  $\mu^+\mu^- \rightarrow Z\ell^+\ell^-$  process can contribute to the aforementioned finalstates, along with the usual backgrounds of  $t\bar{t}$ ,  $VV$ ,  $VVV$ , and  $t\bar{t}V$ . Similar to our analysis at the LHC, a cut on the total hardness variable  $p_T^H \geq 1.2$  TeV is applied to both the signal and the background, which reduces the background contribution to the finalstates.

### 6.2 2-jet + 2 $\mu$

This finalstate arises for  $S_3^{4/3}$  in BP1 scenario (see Eq. 34). The complete finalstate with other cuts is given as:

$$n_j = 2, n_\mu = 2 \quad \text{and} \quad p_T^H \geq 1200 \text{ GeV}.$$

Here, similar to many of the finalstates in the LHC/FCC analysis, we have put the hardness cut  $p_T^H \geq 1.2$  TeV to reduce the background contamination. The signal and background analyses for this finalstate at 8 TeV and 30 TeV centre-of-mass energies with  $1000 \text{ fb}^{-1}$  and  $10000 \text{ fb}^{-1}$  of integrated luminosities are tabulated in Table 25. Triple gauge boson is the dominant background here, although tiny. The signal gets some contribution from  $S_3^{1/3}$  mode, where the

**Table 25** The number of events for  $2 - \text{jet} + 2\mu$  finalstate (Eq. 34) for the benchmark points and dominant SM backgrounds at a multi-TeV muon collider with the centre-of-mass energy of 8 TeV and 30 TeV at

an integrated luminosity of  $1000 \text{fb}^{-1}$  and  $10000 \text{fb}^{-1}$ , respectively. The required luminosities to achieve a  $5\sigma$  signal ( $\mathcal{L}_{5\sigma}$ ) are also shown for both the cases

$\sqrt{s}$ in TeV	Mode	$2 - \text{jet} + 2\mu$		Backgrounds				
		Signal		$t\bar{t}$	$VV$	$VVV$	$t\bar{t}V$	$Z\ell^+\ell^-$
		BP1	BP3					
8	$S_3^{4/3}$	23304.06	779.94	0.11	0.00	85.72	2.00	5.91
	$S_3^{1/3}$	1784.73	30.55					
	Total	25088.79	810.49	93.74				
	Significance( $\sigma$ )	158.09	26.95					
$\mathcal{L}_{5\sigma}$ ( $\text{fb}^{-1}$ )		1.00	34.19					
30	$S_3^{4/3}$	23988.13	506.18	0.00	0.00	139.01	2.16	25.73
	$S_3^{1/3}$	1628.46	34.66					
	Total	25616.59	540.84	166.90				
	Significance( $\sigma$ )	159.53	20.32					
$\mathcal{L}_{5\sigma}$ ( $\text{fb}^{-1}$ )		9.82	604.89					

$c$ -jets are misidentified with light-jets. The results are very inspiring here since we can achieve  $\sim 158\sigma$  of signal significance for BP1 at both of the centre-of-mass energies with the specified luminosities. Therefore, significance of  $5\sigma$  can be achieved at very early stage for both the centre-of-mass energies. It is also interesting to notice that with the specified luminosities at both the centre-of-mass energies one can attain more than  $20\sigma$  significance for BP3 as well, in which the  $b$ -jet remains untagged. It is worth mentioning here that the reduction in production cross-sections at higher energy is compensated by our choice of enhanced luminosity ( $10000 \text{fb}^{-1}$ ) at 30 TeV simulation. Thus the signal significance turns out to be very similar between 8 TeV and 30 TeV collisions for both the benchmark points.

### 6.3 $2c - \text{jet} + 2\mu$

The finalstate  $2c - \text{jet} + 2\mu$  emerges for BP1 scenario when the  $S_3^{1/3}$  component of  $S_3$  is produced in pair and each of them decays into  $c\mu$  states (in Eq. 35). As mentioned earlier, this is not the only finalstate accessible at muon collider for  $S_3^{1/3}$  with BP1, rather we choose this finalstate since it does not involve any missing energy. BP3 can contribute only when the  $b$ -jets are miss-tagged as  $c$ -jets, thus is subdominant. The complete finalstate is described as follows:

$$n_{c\text{-jet}} = 2, n_{b\text{-jet}} = 0, n_\mu = 2 \quad \text{and} \quad p_T^H \geq 1200 \text{ GeV}.$$

In addition to the hardness cut,  $b$ -jet veto potentially reduces BP3 contribution along with the dominant  $t\bar{t}$  background. The results for this finalstate at the centre-of-mass energies of 8 TeV and 30 TeV with the respective integrated luminosities of  $1000 \text{fb}^{-1}$  and  $10000 \text{fb}^{-1}$  are illustrated in Table 26. As the production cross-section of  $S_3^{1/3}$  is consid-

erably smaller than that of  $S_3^{4/3}$ , and furthermore the branching fraction of  $S_3^{1/3}$  to  $c\mu$  is only 50%, the signal numbers for this finalstate remain substantially low compared to the  $2 - \text{jet} + 2\mu$  finalstate. Although, these number of events are large enough compared to the SM backgrounds which are negligible after imposition of suitable cuts, and thus rendering  $\sim 28\sigma$  signal significance at both the centre-of-mass energies. Interestingly, it requires only  $34 \text{fb}^{-1}$  and  $302 \text{fb}^{-1}$  of integrated luminosities to obtain a  $5\sigma$  signal significance at the two energies respectively. It is worth mentioning that BP3 scenario can also provide  $5\sigma$  significance for this finalstate with luminosity less than  $10000 \text{fb}^{-1}$  at both the centre-of-mass energies.

### 6.4 $2b - \text{jet} + 2\mu$

The finalstate of two  $b$ -jets with two muons emerges at muon collider when the  $S_3^{4/3}$  component of  $S_3$  leptoquark are produced in pair in BP3 scenario (Eq. 36). BP1 fails to contribute much as it renders  $s$ -jets in the finalstate as well due to demand of only two jets, which are  $b$ -jets. Thus finalstate looks like:

$$n_{b\text{-jet}} = 2, n_\mu = 2 \quad \text{and} \quad p_T^H \geq 1200 \text{ GeV}.$$

The signal and background analyses for this finalstate at the similar previously specified setups for the centre-of-mass energy and integrated luminosity are presented in Table 27. We see from Table 24 that the production cross-sections for both  $S_3^{4/3}$  and  $S_3^{1/3}$  in BP3 are significantly low compared to BP1 case, and hence the signal significance would also be reduced. However, as the SM backgrounds in this case are also negligible and thus this finalstate results are inspiring too. In fact, one can attain  $\sim 26.5\sigma$  ( $20\sigma$ ) significance at

**Table 26** The number of events for  $2c - \text{jet} + 2\mu$  finalstate (Eq. 35) for the benchmark points and dominant SM backgrounds at a multi-TeV muon collider with the centre-of-mass energy of 8 TeV and 30 TeV at

an integrated luminosity of  $1000 \text{ fb}^{-1}$  and  $10000 \text{ fb}^{-1}$ , respectively. The required luminosities to achieve a  $5\sigma$  signal ( $\mathcal{L}_{5\sigma}$ ) are also shown for both the cases

$\sqrt{s}$ in TeV	Mode	$2c - \text{jet} + 2\mu$		Backgrounds				
		Signal		$t\bar{t}$	$VV$	$VVV$	$t\bar{t}V$	$Z\ell^+\ell^-$
		BP1	BP3					
8	$S_3^{4/3}$	0.81	4.29	0.00	0.00	0.97	0.00	0.00
	$S_3^{1/3}$	747.86	0.07					
Total		748.67	4.36	0.97				
Significance( $\sigma$ )		27.34	1.88					
$\mathcal{L}_{5\sigma} (\text{fb}^{-1})$		33.43	7009.62					
30	$S_3^{4/3}$	2.95	28.85	0.00	0.00	7.63	0.00	0.00
	$S_3^{1/3}$	831.41	0.17					
Total		834.36	29.02	7.63				
Significance( $\sigma$ )		28.75	4.79					
$\mathcal{L}_{5\sigma} (\text{fb}^{-1})$		302.37	10897.8					

**Table 27** The number of events for  $2b - \text{jet} + 2\mu$  finalstate (Eq. 36) for the benchmark points and dominant SM backgrounds at a multi-TeV muon collider with the centre-of-mass energy of 8 TeV and 30 TeV at

an integrated luminosity of  $1000 \text{ fb}^{-1}$  and  $10000 \text{ fb}^{-1}$ , respectively. The required luminosities to achieve a  $5\sigma$  signal ( $\mathcal{L}_{5\sigma}$ ) are also shown for both the cases

$\sqrt{s}$ in TeV	Mode	$2b - \text{jet} + 2\mu$		Backgrounds				
		Signal		$t\bar{t}$	$VV$	$VVV$	$t\bar{t}V$	$Z\ell^+\ell^-$
		BP1	BP3					
8	$S_3^{4/3}$	0.00	680.58	0.11	0.00	0.78	1.50	0.00
	$S_3^{1/3}$	0.00	20.98					
Total		0.00	701.56	2.39				
Significance( $\sigma$ )		0.00	26.44					
$\mathcal{L}_{5\sigma} (\text{fb}^{-1})$		—	35.76					
30	$S_3^{4/3}$	2.95	368.00	0.00	0.00	0.69	1.81	0.00
	$S_3^{1/3}$	0.00	25.17					
Total		2.95	393.17	2.5				
Significance( $\sigma$ )		1.26	19.76					
$\mathcal{L}_{5\sigma} (\text{fb}^{-1})$		$\gg 10000$	639.90					

8 TeV (30 TeV) energy with the specified integrated luminosity. It implies that less than  $50 \text{ fb}^{-1}$  ( $650 \text{ fb}^{-1}$ ) of luminosity is required to achieve the  $5\sigma$  significance for this finalstate. Note that there is no significant signal events for this finalstate in BP1 scenario as apart from the demand of two  $b$ -jets, a limit on total number of light jets  $n_j = 2$  is applied here.

### 6.5 $2b - \text{jet} + 2 - \text{jet} + 2\mu$

This particular finalstate appears if  $S_3^{1/3}$  is produced at muon collider in pair in BP3 scenario and then both of them decay through  $t\mu$  channel (Eq. 37). The top quark would disintegrate into a  $b$ -quark and a  $W$ -boson, and eventually the  $W$ -boson will produce two light jets. Thus, from the pair

production of  $S_3^{1/3}$ , for BP3, we get  $2b - \text{jet} + 4 - \text{jet} + 2\mu$  finalstate. However, the light jets coming from the  $W^\pm$  can be boosted and often form a Fatjet [76,108], which renders us to choose  $2b - \text{jet} + 2 - \text{jet} + 2\mu$  finalstate. Interestingly, for BP1, the partonic finalstates is  $2c + 2\mu$  (Eq. 35) owing to dominant branching of  $S_3^{1/3}$  into  $c\mu$  and though subdominant but can contribute to the desired finalstate when the  $c$ -jet is miss-tagged as  $b$ -jet with additional jets coming from FSR. A serious contribution from  $S_3^{4/3}$  cannot be avoided due to large cross-section of  $S_3^{4/3}$  pair and 100% branching to  $b\mu$ . Thus the finalstate looks like as

$$n_j \geq 4(n_{b\text{-jet}} = 2), n_\mu = 2 \quad \text{and} \quad p_T^H \geq 1200 \text{ GeV}.$$

**Table 28** The number of events for  $2b - \text{jet} + 4 - \text{jet} + 2\mu$  final-state (Eq. 37) for the benchmark points and dominant SM backgrounds at a multi-TeV muon collider with the centre-of-mass energy of 8 TeV

and 30 TeV at an integrated luminosity of  $1000 \text{fb}^{-1}$  and  $10000 \text{fb}^{-1}$ , respectively. The required luminosities to achieve a  $5\sigma$  signal ( $\mathcal{L}_{5\sigma}$ ) are also shown for both the cases

$\sqrt{s}$ in TeV	Mode	$2b - \text{jet} + 4 - \text{jet} + 2\mu$						
		Signal		Backgrounds				
		BP1	BP3	$t\bar{t}$	$VV$	$VVV$	$t\bar{t}V$	$Z\ell^+\ell^-$
8	$S_3^{4/3}$	112.22	204.48	0.43	0.00	0.00	2.27	0.00
	$S_3^{1/3}$	7.24	21.51					
Total		119.46	225.99	2.70				
Significance( $\sigma$ )		10.80	14.94					
$\mathcal{L}_{5\sigma}$ ( $\text{fb}^{-1}$ )		214.00	111.95					
30	$S_3^{4/3}$	20.64	19.88	0.02	0.00	0.00	2.78	0.00
	$S_3^{1/3}$	0.39	3.42					
Total		21.03	23.30	2.80				
Significance( $\sigma$ )		4.30	4.56					
$\mathcal{L}_{5\sigma}$ ( $\text{fb}^{-1}$ )		$\gg 10000$	$\gg 10000$					

The results for this finalstate at 8 TeV and 30 TeV centre-of-mass energies with the respective  $1000 \text{fb}^{-1}$  and  $10000 \text{fb}^{-1}$  of integrated luminosities are quoted in Table 28. At 8 TeV centre-of-mass energy with  $1000 \text{fb}^{-1}$  of data one can reach  $\sim 15\sigma$  of signal significance for BP3 indicating a need of  $\sim 110 \text{fb}^{-1}$  of integrated luminosity to achieve a  $5\sigma$  signal significance. Surprisingly, one can reach  $10.8\sigma$  signal significance at the same energy with  $1000 \text{fb}^{-1}$  of data for BP1 case as well contributing through the  $2 - \text{jet} + 2\mu$  channel. However, the results for 30 TeV is not heartening at all since we need integrated luminosity of more than  $10000 \text{fb}^{-1}$  to achieve  $5\sigma$  significance.

### 7 Comparison of results and reach at colliders

In order to identify the best outcomes of the previous sections and their implications in future searches at the colliders, in this section we explore the particular regions in the NP parameter space where more than  $5\sigma$  signal significance can be reached with the specific choices of centre-of-mass energy and integrated luminosity. For this purpose we select those finalstates which have very small model background (i.e. the contamination from other production channels). Then we observe the variation of significance with the parameters of the NP model, namely, the mass of the leptoquark and its couplings with quarks and leptons keeping the centre-of-mass energy and integrated luminosity fixed at the specific choices. It should be noted that though the SM backgrounds remain unaltered for any specific centre-of-mass energy and luminosity, the model background (along with signal) varies with the change in the parameters of the NP model. At this point it is worth mentioning that the significance presented

in this section are slightly smaller than those quoted in the corresponding tables in previous sections, as we separate out the contributions arising from different production modes and then except the desired signal channel we treat the rest of the signal numbers as background events.

#### 7.1 Discussion on $S_1$

Compiling the results for various different finalstates of  $S_1$  leptoquark at the LHC, discussed in Sect. 3, as a first step, we note down the variations of different production cross-sections and branching fractions as functions of three parameters, namely,  $M_{S_1}$ ,  $Y_{S_1}^{33}$  and  $Z_{S_1}^{23}$ . Then we weigh the signals and model backgrounds presented in any table accordingly to calculate the signal significance for different values of these three NP parameters. In this case, we find from the results quoted in Sect. 3.2, which aim at the finalstate composed of a  $b$ -jet and  $\tau$ -jet, the signal numbers in Tables 4 and 6 are dominated by one particular production channel  $c/t - g \rightarrow S_1\tau$  and  $b - g \rightarrow S_1\nu$ , respectively. When it comes to the finalstates with a  $c$ -jet, similar pattern is seen in Table 8 as discussed in Sect. 3.3. In the other two finalstates described in Tables 5 and 7, all the production channels contribute comparably, and hence it is not possible to single out any particular contribution with reasonable signal significance. Hence, we examine the cases described in Tables 4, 6, and 8 in the subsequent paragraphs.

The finalstate mentioned in Table 4 is  $1b - \text{jet} + 1\tau - \text{jet} + 1\ell + \cancel{p}_T$ , for which the  $c/t - g \rightarrow S_1\tau$  acts as signal and  $b - g \rightarrow S_1\nu$  serves as model background. While, the  $S_1$  production through  $c - g$  fusion depends on  $Z_{S_1}^{23}$ , the other two production modes involve  $Y_{S_1}^{33}$  only. Now as the decay vertex of  $S_1$  for this finalstate (i.e.  $S_1 \rightarrow t\tau$ ) con-

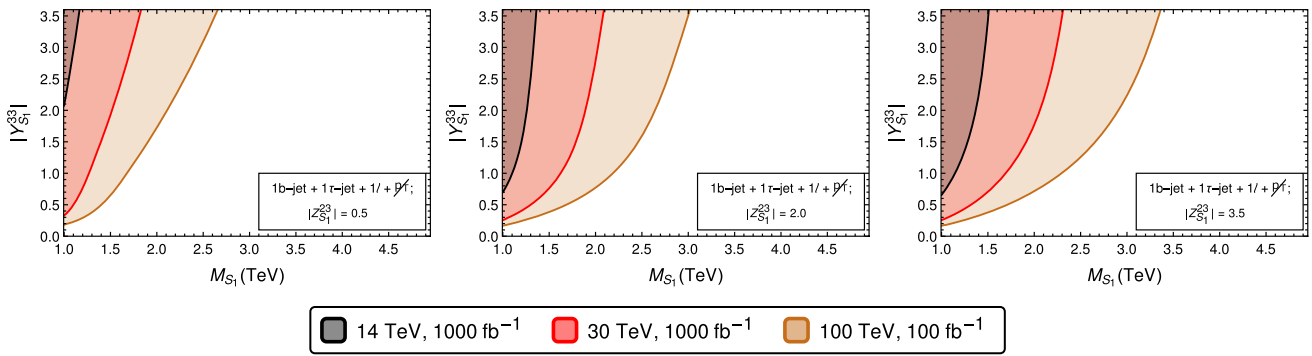


**Fig. 15** The regions with more than  $5\sigma$  signal significance in  $M_{S_1} - |Y_{S_1}^{33}|$  plane for the finalstate  $1b - \text{jet} + 1\tau - \text{jet} + 1\ell + \cancel{p}_T$  (see Table 4) at different centre-of-mass energies at the LHC/FCC. The three different plots (from left) correspond to  $|Z_{S_1}^{23}|$  values equal to 0.5, 2.0 and 3.5, respectively. The yellow curve represents the reach for  $5\sigma$  signal sig-

nificance at 100 TeV centre-of-mass energy with  $100 \text{ fb}^{-1}$  of integrated luminosity. The red and black curves highlight the same signal significance at 30 TeV and 14 TeV centre-of-mass energies, respectively, with  $1000 \text{ fb}^{-1}$  of integrated luminosity

tains  $Y_{S_1}^{33}$  alone, the total rate depends on both  $Y_{S_1}^{33}$  and  $Z_{S_1}^{23}$  couplings. The combined effects of all these facts are displayed in Fig. 15 in the  $M_{S_1} - |Y_{S_1}^{33}|$  plane, where the three sub-figures represent three different values of the coupling  $|Z_{S_1}^{23}|$  i.e., 0.5, 2.0 and 3.5, respectively. In each plot the yellow region indicates more than  $5\sigma$  signal significance with 100 TeV centre-of-mass energies and  $100 \text{ fb}^{-1}$  integrated luminosity, whereas the red and grey regions depict the same significance at 30 TeV and 14 TeV collisions, respectively, with an integrated luminosity of  $1000 \text{ fb}^{-1}$ . Now, it is easy to understand that increasing the mass of leptoquark will decrease the signal events requiring larger values for  $|Y_{S_1}^{33}|$  to reach the same significance. An interesting point to note here that each of the black, red and yellow curves gradually move toward the right side with enhancement in  $|Z_{S_1}^{23}|$  value indicating that with higher value of  $|Z_{S_1}^{23}|$ , one needs smaller  $|Y_{S_1}^{33}|$  coupling to reach the same significance for any particular mass of the leptoquark. This is due to the fact that higher  $|Z_{S_1}^{23}|$  value increases the production cross-section for the signal via  $c - g$  fusion while the model background, arising from the other production channels, being independent of  $Z_{S_1}^{23}$  remains unaltered. We find that the 14 TeV results can only probe  $Y_{S_1}^{33} \sim 2.5$  and above for low leptoquark mass that is close to 1 TeV–1.2 TeV, for the smallest  $Z_{S_1}^{23}$  value of 0.5. Increase in  $Z_{S_1}^{23}$  leads to the feasibility of probing  $Y_{S_1}^{33} \sim 1$  in the same low mass range of the leptoquarks. On the other hand, for this finalstate, considering the highest value of  $Z_{S_1}^{23} = 3.5$ , the 30 TeV and 100 TeV searches can reach up to leptoquark masses of 1.8 TeV and 2.4 TeV, respectively, probing  $Y_{S_1}^{33} \sim 1$ . It is also inferred from this discussion that, a minimal change in the chosen benchmark values of the Yukawa-type couplings can alter the signal significance substantially. For example, in reference to the finalstate studied in Table 4 and discussed in Fig. 15 for the  $S_1$

leptoquark, we find that, if we fix  $m_{S_1} = 1.5 \text{ TeV}$ , a change of  $\pm 0.1$  in the value of  $Y_{S_1}^{33} = 0.91$  (in BP1) can change the signal significance by  $\pm(12\% - 13\%)$  at the 30 TeV LHC. On the other hand, a similar change of  $\pm 0.1$  in the value of  $|Z_{S_1}^{23}| = 0.5$  (in BP1) alters the signal significance at the 30 TeV LHC by  $\pm(15\% - 16\%)$ .

The next finalstate we consider to explore the reaches of  $S_1$  at the LHC/FCC is  $1b - \text{jet} + \cancel{p}_T$ , corresponding to the results shown in Table 6. In this case  $b - g \rightarrow S_1 \nu$  process provides the signal, whereas, events from  $c/t - g \rightarrow S_1 \tau$  act as model background. Therefore, the production vertex for signal as well as the decay vertex of  $S_1$  depend only on one coupling  $Y_{S_1}^{33}$ , while the model background channels involve both  $Y_{S_1}^{33}$  and  $Z_{S_1}^{23}$ . The  $5\sigma$  reach of signal significance for this finalstate for three different  $|Z_{S_1}^{23}|$  values equal to 0.5, 2.0 and 3.5 are presented in Fig. 16 in three different panels, respectively. The colour codes are the same as of Fig. 15. In this case, unlike the previous scenario, we notice that the black, red and yellow curves shift upwards as we look at the three plots from left to right indicating necessity of higher  $|Y_{S_1}^{33}|$  values with the increase in  $|Z_{S_1}^{23}|$  coupling to maintain the same significance for any particular mass of the leptoquark. The reason behind this is that the cross-section for model background from  $c - g$  fusion is enhanced with the increase in  $|Z_{S_1}^{23}|$  value while the signal events remain unaffected. For  $|Z_{S_1}^{23}| = 0.5$ , we find that this finalstate can probe  $Y_{S_1}^{33} \sim 1$  when the leptoquark mass is around 1.2 TeV scale at the 14 TeV LHC, and can go up to 1.6 TeV, 2 TeV masses with higher centre-of-mass energies of 30 TeV and 100 TeV, respectively.

Next we move to the finalstate comprising of  $1c - \text{jet} + 2\tau - \text{jet} + \cancel{p}_T$ , whose signal and background event numbers are described in Table 8. This finalstate essentially shows a complementary behaviour to the previous two for which we

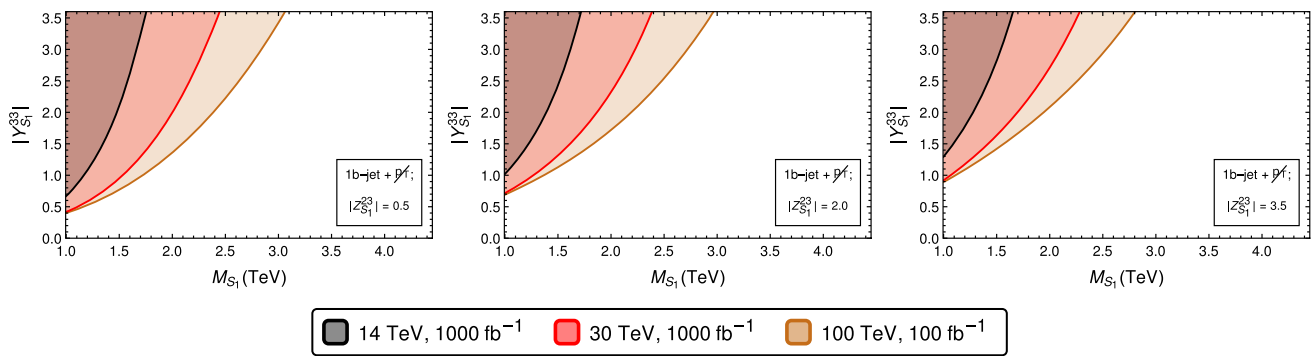


**Fig. 16** The regions with more than  $5\sigma$  signal significance in  $M_{S_1} - |Y_{S_1}^{33}|$  plane for the finalstate  $1b - \text{jet} + \cancel{p}_T$  (see Table 6) at different centre-of-mass energies at the LHC/FCC. The three different plots (from left) correspond to  $|Z_{S_1}^{23}|$  values equal to 0.5, 2.0 and 3.5, respectively. The yellow curve represents the reach for  $5\sigma$  signal significance at 100

TeV centre-of-mass energy with  $100 \text{ fb}^{-1}$  of integrated luminosity. The red and black curves highlight the same signal significance at 30 TeV and 14 TeV centre-of-mass energies, respectively, with  $1000 \text{ fb}^{-1}$  of integrated luminosity

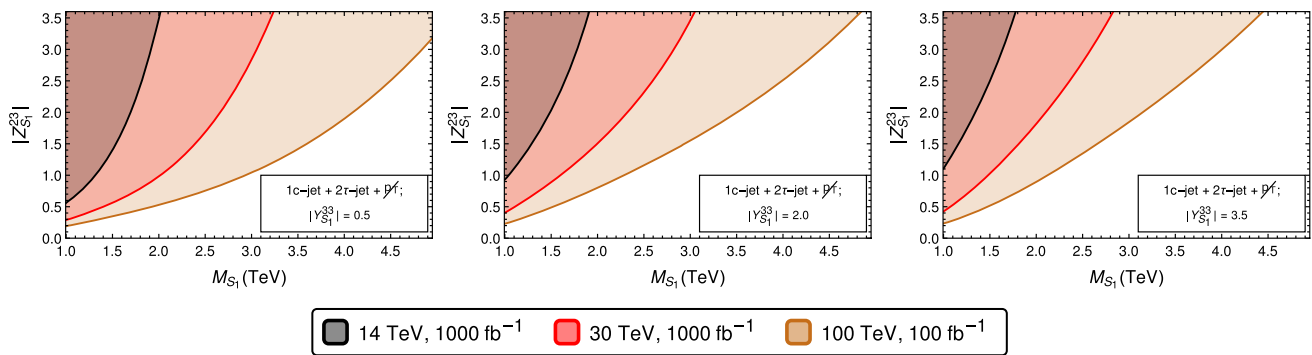


**Fig. 17** The regions with more than  $5\sigma$  signal significance in  $M_{S_1} - |Z_{S_1}^{23}|$  plane for the finalstate  $1c - \text{jet} + 2\tau - \text{jet} + \cancel{p}_T$  (see Table 8) at different centre-of-mass energies at the LHC/FCC. The three different plots (from left) correspond to  $|Y_{S_1}^{33}|$  values equal to 0.5, 2.0 and 3.5, respectively. The yellow curve represents the reach for  $5\sigma$  signal sig-

nificance at 100 TeV centre-of-mass energy with  $100 \text{ fb}^{-1}$  of integrated luminosity. The red and black curves highlight the same signal significance at 30 TeV and 14 TeV centre-of-mass energies, respectively, with  $1000 \text{ fb}^{-1}$  of integrated luminosity

studied the reach for the  $S_1$  leptoquark. Similar to Table 4, the  $c/t - g \rightarrow S_1 \tau$  mode acts as the signal while  $b - g \rightarrow S_1 \nu$  provides the model background. In the  $c - g \rightarrow S_1 \tau$  case, the production cross-section depends on  $Z_{S_1}^{23}$ , while the production of  $t - g \rightarrow S_1 \tau$  has a  $Y_{S_1}^{33}$  dependence. The model background i.e.  $b - g \rightarrow S_1 \nu$  production also varies with  $Y_{S_1}^{33}$ . However, in all three cases, the decay vertex  $S_1 \rightarrow c\tau$  is purely dependent on  $Z_{S_1}^{23}$ . Thus, the cumulative effects of the  $Z_{S_1}^{23}$  and  $Y_{S_1}^{33}$  couplings are presented for this case in the  $M_{S_1} - |Z_{S_1}^{23}|$  plane, depicted in Fig. 17. The three panels of Fig. 17 correspond to the  $5\sigma$  reach in this finalstate for three different  $Y_{S_1}^{33}$  values equalling 0.5, 2.0, and 3.5, respectively. While this finalstate shows a similar behaviour of the lines moving upwards with the increase in  $Y_{S_1}^{33}$ , which we observed in case of Fig. 16. This is accounted for by the enhancement of model background from the  $b - g \rightarrow S_1 \nu$  due to the increment in  $Y_{S_1}^{33}$ . However, compared to Fig. 16, we witness

the possibility of a  $5\sigma$  reach for a larger parameter space. For the lowest  $Y_{S_1}^{33}$  value of 0.5, the 14 TeV LHC can probe  $Z_{S_1}^{23} \sim 1$  up to a leptoquark mass value of  $\sim 1.3$  TeV. For higher centre-of-mass energies of 30 TeV and 100 TeV, this reach increases to the leptoquark masses of  $\sim 2$  TeV and  $\sim 3$  TeV, respectively. From the combined analysis of these three aforementioned finalstates, we see that, compared to  $Y_{S_1}^{33}$ , the  $Z_{S_1}^{23}$  coupling can be probed at similar orders, with a  $5\sigma$  significance for a wider range of the leptoquark mass.

### 7.2 Discussion on $S_3$

We learn from the phenomenological study performed in Sects. 4, 5 and 6 that the leptoquark  $S_3$  is quite interesting as various different components of it give rise to quite unique signatures at colliders. The circumstance to discriminate these components becomes easier when we look for the analysis performed with BP1 and BP2 at the LHC/FCC. As

the production cross-section is low in the case of BP3, we have obtained lower signal significance for it compared to the other two scenarios (BP1 and BP2), and thus is not a very favorable case to study the reach at the colliders. In subsequent subsections, we discuss the outcomes both at hadron and muon colliders separately.

### 7.2.1 For the LHC/FCC

It can be noted from Table 1 that in the case of BP1 and BP2, as  $Y_{S_3}^{32}$  is very tiny, the phenomenology is mainly determined by the coupling  $Y_{S_3}^{22}$ . This simplifies the situation due to the fact that as long as  $|Y_{S_3}^{22}|$  is greater than 0.03 (10 times larger than  $Y_{S_3}^{32}$ ), the effect of  $Y_{S_3}^{32}$  is insignificant. That means keeping all the other parameters unchanged, the branching fractions for different components of  $S_3$  remain almost unaltered. Therefore, ignoring the effects of tiny  $Y_{S_3}^{32}$ , we adopt  $|Y_{S_3}^{22}| \geq 0.03$ , and hence, we are left with only two parameters in this case, which are  $M_{S_3}$  and  $Y_{S_3}^{22}$ .

Now we first consider the two finalstates  $1 - \text{jet} + 2\mu + \cancel{p}_T$  and  $1c - \text{jet} + \cancel{p}_T$ , tabulated in Tables 15 and 16, respectively. For the first one, the signal events emerge from  $s - g \rightarrow S_3^{4/3}\mu$  mode and the model background comes from  $c - g \rightarrow S_3^{1/3}\mu$  channel making this finalstate an unique signature for the  $S_3^{4/3}$  component. The second case corresponds to the signature for  $S_3^{2/3}$  where the signal events arises from  $c - g \rightarrow S_3^{2/3}\nu$  mode, while the model background appears from  $s - g \rightarrow S_3^{1/3}\nu$  channel. The  $5\sigma$  reach for these two finalstates with varying  $M_{S_3}$  and  $Y_{S_3}^{22}$  are presented in the left and right panels of Fig. 18, respectively. The yellow region signifies signal significance of more than  $5\sigma$  at 100 TeV centre-of-mass energy with  $100\text{fb}^{-1}$  integrated luminosity, and the respective red and the grey region indicate the same significance at the 30 TeV and 14 TeV centre-of-mass energies with  $1000\text{fb}^{-1}$  of luminosity. It can be seen that the finalstate  $1 - \text{jet} + 2\mu + \cancel{p}_T$  probes larger parameter space than the finalstate  $1c - \text{jet} + \cancel{p}_T$  as higher significance can be attained with the former one for same values of  $M_{S_3}$  and  $Y_{S_3}^{22}$ . We find that the 14 TeV results for  $1 - \text{jet} + 2\mu + \cancel{p}_T$  is quite promising as it can probe  $Y_{S_3}^{22} \sim 1$  until 1.8 TeV mass of the leptoquark  $S_3$  and with higher centre-of-mass energies like 30 TeV and 100 TeV, the same coupling value can be probed until  $\sim 3$  TeV and  $\sim 4$  TeV mass of  $S_3$ , respectively. In the case of  $1c - \text{jet} + \cancel{p}_T$  finalstate, with  $Y_{S_3}^{22} \sim 1$ , the mass reach for  $S_3$  for the three centre-of-mass energies 14 TeV, 30 TeV and 100 TeV are  $\sim 1.7$  TeV,  $\sim 2.7$  TeV and  $\sim 3.5$  TeV, respectively. It is worthwhile to point out that both these two channels have much higher reach in the  $S_3$  mass axis compared to the cases discussed in the previous subsection (Sect. 7.1) for  $S_1$  leptoquark for an  $\mathcal{O}(1)$  value of the corresponding Yukawa type coupling(s). The effect of devi-

ation from the chosen benchmark values of the Yukawa-type couplings on the signal significance is very pronounced in case of  $S_3$  as well. Taking the example of the finalstate analyzed in Table 15, as well as discussed in Fig. 18a, a change of  $\pm 0.1$  in the value of  $Y_{S_3}^{22} = 0.5$  (in BP1) can affect the obtained signal significance at the 30 TeV LHC by  $\pm 28\%$ , for the fixed choice of  $m_{S_3} = 1.5$  TeV.

Having discussed the status of the two components of  $S_3$ , namely,  $S_3^{4/3}$  and  $S_3^{2/3}$ , we now focus on the finalstates corresponding to  $S_3^{1/3}$  component. For this purpose we select the two following decay topologies:  $1c - \text{jet} + 2\mu + \cancel{p}_T$  (see Table 17) and  $1c - \text{jet} + 1\mu + \cancel{p}_T$  (see Table 18). The finalstate  $1c - \text{jet} + 2\mu + \cancel{p}_T$  mainly arises from the channel  $c - g \rightarrow S_3^{1/3}\mu$  where the mode  $s - g \rightarrow S_3^{4/3}\mu$  acts as model background. Likewise, the finalstate  $1c - \text{jet} + 1\mu + \cancel{p}_T$  is generated from the production channel  $s - g \rightarrow S_3^{1/3}\nu$  whereas the modes  $s - g \rightarrow S_3^{4/3}\mu$  and  $c - g \rightarrow S_3^{1/3}\mu$  function as model backgrounds. The left and right panels of Fig. 19 illustrate the  $5\sigma$  reach for these two finalstates, respectively, at three different centre-of-mass energies and the similar luminosity choices as described in the last paragraphs. We can see from the left panel of Fig. 19 that the presence of  $c$ -jet in the finalstate reduces the signal significance compared to the left panel of Fig. 18 that has a similar finalstate except for a replacement of the  $c$ -jet with a light-jet. This is due to the fact that we have an enhancement factor for the  $S_3^{4/3}$  channel (i.e.,  $1 - \text{jet} + 2\mu + \cancel{p}_T$ ) arising from the interaction vertex and also a suppression factor in  $1c - \text{jet} + 2\mu + \cancel{p}_T$  originating from the branching fraction of  $S_3^{1/3}$ . As depicted in Fig. 19, the finalstate with two muons (left panel) yield a better reach than that with one muon (right panel), due to it having less SM background events. In the di-muon finalstate, for  $Y_{S_3}^{22} \sim 1$ , we can probe the leptoquark mass up to  $\sim 1.6$  TeV,  $\sim 2.4$  TeV, and  $\sim 3.0$  TeV, respectively for the centre-of-mass energies of 14 TeV, 30 TeV and 100 TeV. For the single muon finalstate, these mass reaches reduce to  $\sim 1.5$  TeV,  $\sim 2.0$  TeV, and  $\sim 2.5$  TeV.

### 7.2.2 For a muon collider

We continue to explore the similar outcomes at a multi-TeV muon collider. Here, the most encouraging finalstate is  $2 - \text{jet} + 2\mu$  (see Table 25) where we find enormously healthy signal numbers that arise from the  $S_3^{4/3}$  component of  $S_3$ , rendering a huge significance for such a signal. Thus one can achieve the  $5\sigma$  signal significance with very small value of  $|Y_{S_3}^{22}|$  coupling and for large mass of the  $S_3$  leptoquark. A similar scenario occurs for  $2b - \text{jet} + 2\mu$  finalstate in BP3 too. Therefore, we focus on  $2c - \text{jet} + 2\mu$  finalstate in BP1 scenario. As already shown in Table 26,  $S_3^{1/3}$  provides signal events for this finalstate while  $S_3^{4/3}$  behaves as a model background. The  $5\sigma$  reach plot, in the  $M_{S_3} - |Y_{S_3}^{22}|$  plane, for this

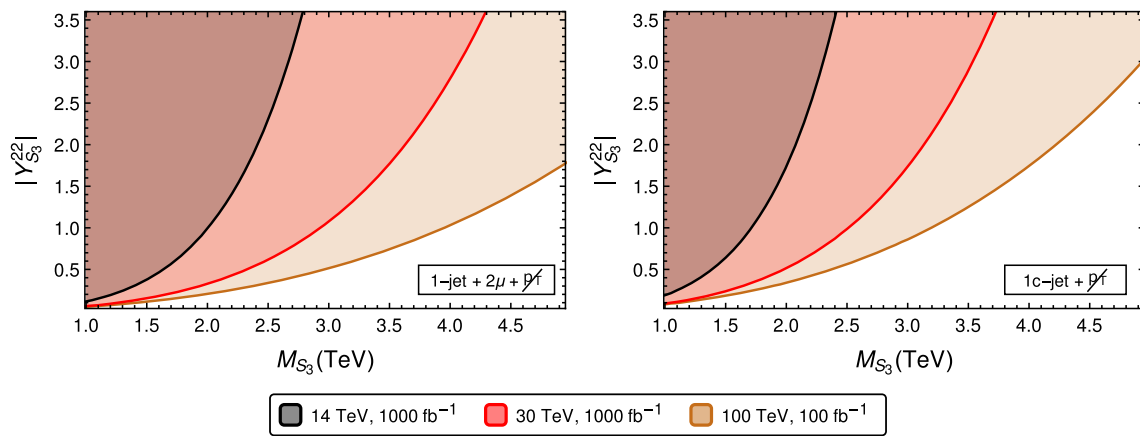


**Fig. 18** The regions with more than  $5\sigma$  signal significance in  $M_{S_3} - |Y_{S_3}^{22}|$  plane for the finalstates  $1 - \text{jet} + 2\mu + \cancel{p}_T$  (in left panel) and  $1c - \text{jet} + \cancel{p}_T$  (in right panel) at different centre-of-mass energies at the LHC/FCC. The yellow curve represents the reach for  $5\sigma$  signal significance at 100 TeV centre-of-mass energy with  $100 \text{ fb}^{-1}$  of integrated

luminosity. The red and black curves highlight the same signal significance at 30 TeV and 14 TeV centre-of-mass energies, respectively, with  $1000 \text{ fb}^{-1}$  of integrated luminosity. The signal and SM background numbers for these two final states are highlighted in Tables 15 and 16, respectively

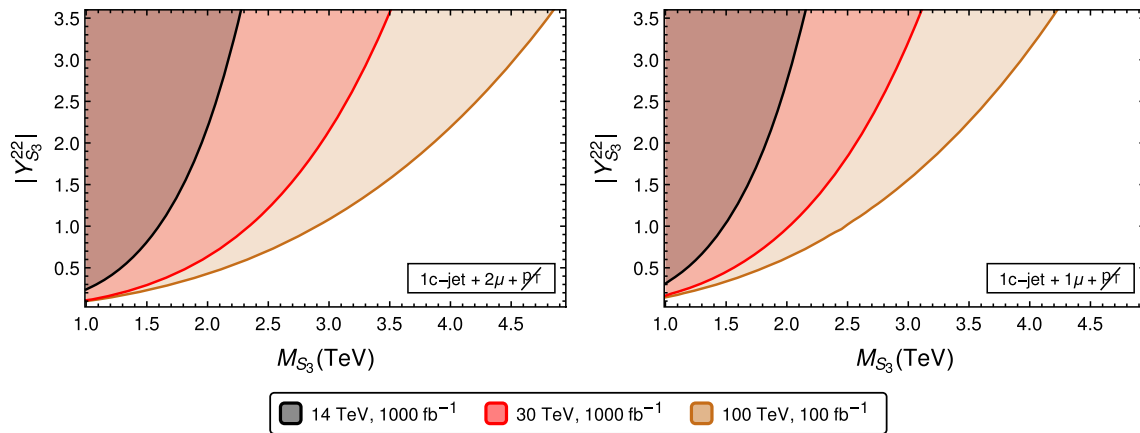


**Fig. 19** The regions with more than  $5\sigma$  signal significance in  $M_{S_3} - |Y_{S_3}^{22}|$  plane for the finalstates  $1c - \text{jet} + 2\mu + \cancel{p}_T$  (in left panel) and  $1c - \text{jet} + 1\mu + \cancel{p}_T$  (in right panel) at different centre-of-mass energies at the LHC/FCC. The yellow curve represents the reach for  $5\sigma$  signal significance at 100 TeV centre-of-mass energy with  $100 \text{ fb}^{-1}$  of integrated

luminosity. The red and black curves highlight the same signal significance at 30 TeV and 14 TeV centre-of-mass energies, respectively, with  $1000 \text{ fb}^{-1}$  of integrated luminosity. The signal and SM background numbers for these two final states are highlighted in Tables 17 and 18, respectively

finalstate is depicted in Fig. 20. The yellow region signifies the parameter space with signal significance of more than  $5\sigma$  level with the centre-of-mass energy being 30 TeV and an integrated luminosity of  $10000 \text{ fb}^{-1}$ , whereas the same signal significance with 8 TeV centre-of-mass energy and  $1000 \text{ fb}^{-1}$  integrated luminosity is shown in grey. It should be kept in mind that at 8 TeV centre-of-mass energy, leptoquark of mass greater than 4 TeV can not be produced in pairs. Therefore, we find a sharp rise of the black curve while approaching the mass of 4 TeV indicating no sensitivity after that mass scale. On the other hand, the  $5\sigma$  reach for 30 TeV energy with an integrated luminosity of  $10000 \text{ fb}^{-1}$  (shown

by the yellow curve) remains almost flat for the small value of  $|Y_{S_3}^{22}|$  until very large mass of the leptoquark. It is apparent from the discussions that the muon collider has much more sensitivity to probe the small coupling values up to the very large mass of the leptoquark compared to the hadron collider.

### 7.3 Discussion on uncertainties

In this subsection we discuss the systematic uncertainties in context of hadron colliders that might affect the signal significance of the finalstates which are discussed in this article. These include systematic uncertainties [109,110] due to

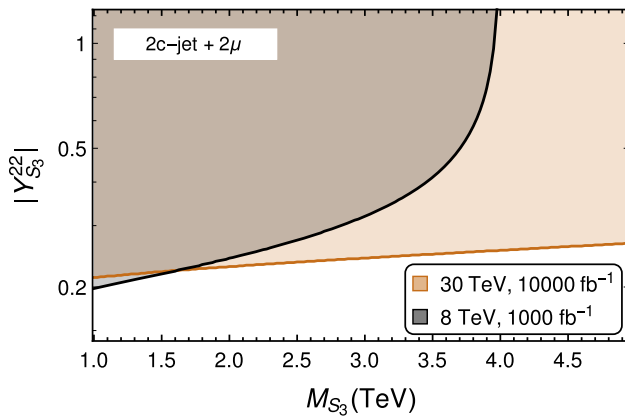


**Fig. 20** The regions with more than  $5\sigma$  significance in  $M_{S_3} - |Y_{S_3}^{22}|$  plane for the finalstate  $2c\text{-jet} + 2\mu$  (see Table 26) at two different centre-of-mass energies at a multi-TeV muon collider. The yellow (black) curve represents the reach for  $5\sigma$  signal significance at 30 TeV (8 TeV) centre-of-mass energy with  $10000\text{ fb}^{-1}$  ( $1000\text{ fb}^{-1}$ ) integrated luminosity

$b$ -jet tagging of 15% [111],  $c$ -jet tagging of 7.5 % [112],  $\tau$ -jet tagging of 8% [113], jet scale uncertainty of 3% [114], luminosity uncertainty 2% and the parton distribution function uncertainty of 10% [115]. We add them in quadrature to estimate the systematic uncertainties for  $b\text{-jet} + \tau\text{-jet}$ ,  $c\text{-jet} + \tau\text{-jet}$ ,  $b\text{-jet} + c\text{-jet}$ ,  $b\text{-jet}$  and  $c\text{-jet}$  finalstates as 20%, 15%, 20%, 18% and 13%, respectively. This can affect the signal significance roughly +25% to -25% depending on the finalstates.

Finally we proceed to estimate the contamination arising from the leptoquark pair production mainly mediated by the strong interaction processes. For our chosen finalstates such contamination can happen when one or more  $b$ -,  $c$ -,  $\tau$ -jets or charged leptons are missed from the pair production and in principle fake as a signal originating from the single leptoquark production. Given the fact, we can measure the leptoquark mass via the invariant mass reconstruction of  $c\mu$ ,  $s\mu$ , or mass edge of  $c\tau$  (as shown in Sect. 3.4) or via the invariant mass edge of  $c$ -jet and missing energy, we can estimate such model backgrounds for a given benchmark point. Determination of jet charges along with the finalstates can also identify the different excitations of leptoquarks [58,59], which in turn can isolate singlet and triplet leptoquarks. The appraisal of model contamination can thus be more precise. We find such contamination can reduce the signal significance from a few percent to at most 25%. However, note that the leptoquark pair production although mainly generated from strong interaction processes, the subsequent decays of leptoquarks are governed by the leptoquark Yukawa-type couplings. In that regard, one may also include such effect into signal contributions, which will further enhance the signal significance. Therefore, we think for any early hint of a leptoquark signature these effects might as well be considered as a signal. Then later in case we are certain about the existence of the

leptoquark, for the precision measurement of the leptoquark Yukawa-type coupling, pair production can be regarded as model contamination.

### 8 Conclusion

In this article we study the phenomenology of two scalar leptoquarks via single production channels mediated by quark gluon fusions. The leptoquarks carry color as well as electromagnetic charge, while the leptoquark  $S_1$  is singlet and  $S_3$  is triplet under the weak gauge group. The decays of these leptoquarks are dictated by specific non-vanishing couplings to fermions where the choice is governed by the series of discrepancies observed in  $B$ -decays. Rather constraining the parameter space explaining such tensions, we have demonstrated that our analysis is general enough and can easily be adopted to any scenario from the collider search perspective.

The pair productions of the leptoquarks at hadron collider are mostly dominated via QCD processes like gluon fusions, however, the single leptoquark productions which can probe the Yukawa-type couplings of the leptoquark to a quark and a lepton become efficient at high energies. The current and upcoming searches at the LHC/FCC play the key role here. Whereas, interestingly a multi-TeV muon collider can be effective in probing these same Yukawa-type couplings through pair productions of the leptoquarks. We first consider different finalstates bearing distinguishable signatures arising from the  $S_1$  leptoquark and three different components of the  $S_3$  leptoquark. In case of a TeV mass range  $S_1$ , we find among several decay topologies,  $1b\text{-jet} + 1\tau\text{-jet} + 1\ell + \cancel{p}_T$  and  $1b + \cancel{p}_T$  are the most promising ones that include a  $b$ -jet, which can probe the Yukawa-type coupling  $Y_{S_1}^{33}$  as low as 0.2 and 0.4, respectively, for  $Z_{S_1}^{23} = 0.5$  at the LHC/FCC at 30 TeV and 100 TeV energies with upgraded luminosity. Whereas, the finalstate of  $1c\text{-jet} + 2\tau\text{-jet} + \cancel{p}_T$  can probe minimum values of  $Z_{S_1}^{23} = 0.3$  and 0.2, at 30 TeV and 100 TeV centre-of-mass energies, respectively for  $Y_{S_1}^{33} = 0.5$ . In this finalstate, the 100 TeV FCC is shown to have the possibility of probing  $S_1$  mass exceeding 5 TeV, for large enough  $Z_{S_1}^{23}$  values  $\sim 3.0$ . We have also illustrated that when  $S_1$  is produced in association with a visible particle (say a charged lepton), the further decay  $S_1 \rightarrow \bar{c}\tau^+ \rightarrow \bar{c}\pi^+\bar{\nu}$  leads to invariant mass edge at the  $S_1$  mass, which can be instrumental in determination of the leptoquark mass scale at the LHC. In all the finalstates pertaining to  $S_1$ , the number of signal and SM background events are presented at centre-of-mass energies of 30 TeV and 100 TeV, owing to the low signal significance at the 14 TeV LHC.

The phenomenology is richer in the case of  $S_3$  leptoquark where three different components, namely  $S_3^{4/3}$ ,  $S_3^{2/3}$  and  $S_3^{1/3}$  are produced with the same tree-level mass. For our choices of the benchmark points these components often decay into finalstates consisting of muons compared to tau leptons as observed in the case of  $S_1$ . We notice that  $S_3^{4/3}$  and  $S_3^{2/3}$  components have distinct signatures;  $1 - \text{jet} + 2\mu + \cancel{p}_T \leq 30 \text{ GeV}$  and  $1c - \text{jet} + \cancel{p}_T \geq 200 \text{ GeV}$ , respectively, which can probe very low values ( $\lesssim \mathcal{O}(10^{-1})$ ) of the Yukawa-type coupling  $Y_{S_3}^{22}$  for a TeV mass scale  $S_3$  at the upcoming upgrades of the LHC. On the other hand  $S_3^{1/3}$  has four modes to search for, and focusing on the most encouraging ones  $2\mu + 1c - \text{jet} + \cancel{p}_T \leq 30 \text{ GeV}$  and  $1\mu + 1c - \text{jet} + \cancel{p}_T \geq 500 \text{ GeV}$ , we find similar small values of  $Y_{S_3}^{22}$  can be explored at the LHC/FCC. Additionally, we also briefed about the lepton flavour violating signatures in the decay caused due to the off-diagonal Yukawa-type coupling  $Y_{S_3}^{32}$ . In majority of the finalstates from single production of  $S_3$  leptoquarks, the signal and background event numbers are presented at three different centre-of-mass energies of 14 TeV, 30 TeV, and 100 TeV at the LHC/FCC. However, in case of the lepton flavour violating finalstates, the 14 TeV event numbers are not listed, citing low signal significance. The results exhibit a maximum reach of more than 5 TeV mass of the  $S_3$  leptoquark at the 100 TeV FCC, if the Yukawa-type coupling of leptoquarks are large, namely, close to the perturbativity limit.

We also explore the possibilities for direct searches of the leptoquarks at a multi-TeV muon collider considering two different centre-of-mass energies; 8 TeV and 30 TeV. Here in most cases, we rely on the pair productions via  $t$ -channel processes (through quarks) to probe the relevant Yukawa-type couplings, except for the  $S_3^{2/3}$  component of  $S_3$  which can only be produced via  $s$ -channel exchange of photon and  $Z$ -boson. The situation for  $S_1$  leptoquark is very similar to that of  $S_3^{2/3}$  component, as  $S_1$  does not couple to muon for the chosen benchmark scenarios and thus can only be produced through the mentioned  $s$ -channel processes. Therefore, with the main intention to probe the Yukawa-type couplings of the leptoquarks, we analyze the pair productions of  $S_3^{4/3}$  and  $S_3^{1/3}$  components via  $t$ -channel contributions. The distinctive feature of these two components are found to be prominent here as well. For  $S_3^{4/3}$ , the finalstate consisting of  $2 - \text{jet} + 2\mu$  (for BP1) and  $2b - \text{jet} + 2\mu$  (for BP3) can probe the  $Y_{S_3}^{22}$  coupling up to its perturbativity limit for  $\mathcal{O}(10 \text{ TeV})$  mass leptoquark with a very early data at muon collider. The reach calculated for the topology  $2c + 2\mu$  shows a lower sensitivity of  $Y_{S_3}^{22} \sim 0.2$ . To conclude, we find that the prospect of the scalar leptoquarks and their different  $SU(2)_L$  components can be distinguished and segregated with the complementarity of hadron and muon colliders.

**Acknowledgements** The authors thank Rahul Sinha for useful suggestions. P.B. and A.K. acknowledge SERB CORE Grant CRG/2018/004971 and MATRICS Grant MTR/2020/000668 for the financial support. The work of R.M. is partly supported by the Alexander von Humboldt Foundation and the University of Siegen under the Young Investigator Research Group (Nachwuchsforscherinnen-gruppe) grant. S.P. acknowledges the Council of Scientific and Industrial Research (CSIR), India for funding his research (File no: 09/1001(0082)/2020-EMR-I). A.K also acknowledges the partial support by MCIN/AEI/10.13039/501100011033 Grant No. PID2020-114473GB-I00, and Grant PROMETEO/2021/071 (Generalitat Valenciana.)

**Data Availability Statement** This manuscript has no associated data or the data will not be deposited. [Authors' comment: In this article we have studied the collider signatures of leptoquarks at multiple benchmark scenarios, using Monte-Carlo event samples generated by Pythia. No experimental or astrophysical data has been analysed or produced in this article].

**Open Access** This article is licensed under a Creative Commons Attribution 4.0 International License, which permits use, sharing, adaptation, distribution and reproduction in any medium or format, as long as you give appropriate credit to the original author(s) and the source, provide a link to the Creative Commons licence, and indicate if changes were made. The images or other third party material in this article are included in the article's Creative Commons licence, unless indicated otherwise in a credit line to the material. If material is not included in the article's Creative Commons licence and your intended use is not permitted by statutory regulation or exceeds the permitted use, you will need to obtain permission directly from the copyright holder. To view a copy of this licence, visit <http://creativecommons.org/licenses/by/4.0/>.

Funded by SCOAP<sup>3</sup>. SCOAP<sup>3</sup> supports the goals of the International Year of Basic Sciences for Sustainable Development.

## Appendix A: NLO QCD $K$ -factors of SM backgrounds at the LHC/FCC

In Table 29, we present the NLO QCD  $K$ -factors for the five dominant SM backgrounds considered at the analysis for the LHC/FCC. The calculation is performed in MadGraph5\_AMC@NLO [97], following prescriptions from Ref. [116]. The renormalization and factorization scales are set as the dynamic variable of  $\sqrt{\hat{s}}$ , and the PDF considered is

**Table 29** NLO QCD  $K$ -factors of the SM backgrounds at three different centre-of-mass energies at the LHC/FCC. NNPDF\_lo\_as\_0130\_qed [95] has been taken as the PDF, with a dynamic scale choice of  $\sqrt{\hat{s}}$  using MadGraph5\_AMC@NLO [97]

Background	$K$ -factors at three $E_{CM}$ values		
	14 TeV	30 TeV	100 TeV
$t\bar{t}$	1.52	1.51	1.52
$VV$	1.49	1.58	1.81
$VV V$	1.77	2.05	2.74
$t\bar{t}V$	1.58	1.59	1.60
$tVV$	1.67	1.77	1.99

NNPDF\_lo\_as\_0130\_qed [95]. The outcomes are compared with the various results from refs. [117–119].

## References

- H. Georgi, S. Glashow, Unity of all elementary particle forces. *Phys. Rev. Lett.* **32**, 438–441 (1974). <https://doi.org/10.1103/PhysRevLett.32.438>
- J.C. Pati, A. Salam, Lepton number as the fourth color. *Phys. Rev. D* **10**, 275–289 (1974). <https://doi.org/10.1103/PhysRevD.10.275> [Erratum: *Phys. Rev. D* **11**, 703–703 (1975)]
- LHCb Collaboration, R. Aaij et al., Search for lepton-universality violation in  $B^+ \rightarrow K^+ \ell^+ \ell^-$  decays. *Phys. Rev. Lett.* **122**, 191801 (2019). <https://doi.org/10.1103/PhysRevLett.122.191801>. arXiv:1903.09252
- LHCb Collaboration, R. Aaij et al., Test of lepton universality in beauty-quark decays. arXiv:2103.11769
- LHCb Collaboration, R. Aaij et al., Test of lepton universality with  $B^0 \rightarrow K^{*0} \ell^+ \ell^-$  decays. *JHEP* **08**, 055 (2017). [https://doi.org/10.1007/JHEP08\(2017\)055](https://doi.org/10.1007/JHEP08(2017)055). arXiv:1705.05802
- LHCb Collaboration, R. Aaij et al., Branching fraction measurements of the rare  $B_s^0 \rightarrow \phi \mu^+ \mu^-$  and  $B_s^0 \rightarrow f_2'(1525) \mu^+ \mu^-$  decays. arXiv:2105.14007
- LHCb Collaboration, R. Aaij et al., Measurement of  $CP$ -averaged observables in the  $B^0 \rightarrow K^{*0} \mu^+ \mu^-$  decay. *Phys. Rev. Lett.* **125**, 011802 (2020). <https://doi.org/10.1103/PhysRevLett.125.011802>. arXiv:2003.04831
- HFLAV Collaboration, Y.S. Amhis et al., Averages of b-hadron, c-hadron, and  $\tau$ -lepton properties as of 2018. *Eur. Phys. J. C* **81**, 226 (2021). <https://doi.org/10.1140/epjc/s10052-020-8156-7>. arXiv:1909.12524
- J. Blumlein, E. Boos, A. Kryukov, Leptoquark pair production in hadronic interactions. *Z. Phys. C* **76**, 137–153 (1997). <https://doi.org/10.1007/s002880050538>. arXiv:hep-ph/9610408
- A. Belyaev, C. Leroy, R. Mehdiyev, A. Pukhov, Leptoquark single and pair production at LHC with CalcHEP/CompHEP in the complete model. *JHEP* **09**, 005 (2005). <https://doi.org/10.1088/1126-6708/2005/09/005>. arXiv:hep-ph/0502067
- M. Kramer, T. Plehn, M. Spira, P. Zerwas, Pair production of scalar leptoquarks at the Tevatron. *Phys. Rev. Lett.* **79**, 341–344 (1997). <https://doi.org/10.1103/PhysRevLett.79.341>. arXiv:hep-ph/9704322
- T. Plehn, H. Spiesberger, M. Spira, P. Zerwas, Formation and decay of scalar leptoquarks/squarks in ep collisions. *Z. Phys. C* **74**, 611–614 (1997). <https://doi.org/10.1007/s002880050426>. arXiv:hep-ph/9703433
- O.J.P. Eboli, R. Zukanovich Funchal, T.L. Lungov, Signal and backgrounds for leptoquarks at the CERN LHC. *Phys. Rev. D* **57**, 1715–1729 (1998). <https://doi.org/10.1103/PhysRevD.57.1715>. arXiv:hep-ph/9709319
- M. Kramer, T. Plehn, M. Spira, P.M. Zerwas, Pair production of scalar leptoquarks at the CERN LHC. *Phys. Rev. D* **71**, 057503 (2005). <https://doi.org/10.1103/PhysRevD.71.057503>. arXiv:hep-ph/0411038
- J.B. Hammett, D.A. Ross, NLO leptoquark production and decay: the narrow-width approximation and beyond. *JHEP* **07**, 148 (2015). [https://doi.org/10.1007/JHEP07\(2015\)148](https://doi.org/10.1007/JHEP07(2015)148). arXiv:1501.06719
- T. Mandal, S. Mitra, S. Seth, Single productions of colored particles at the LHC: an example with scalar leptoquarks. *JHEP* **07**, 028 (2015). [https://doi.org/10.1007/JHEP07\(2015\)028](https://doi.org/10.1007/JHEP07(2015)028). arXiv:1503.04689
- K.S. Babu, P.S.B. Dev, S. Jana, A. Thapa, Unified framework for  $B$ -anomalies, muon  $g - 2$  and neutrino masses. *JHEP* **03**, 179 (2021). [https://doi.org/10.1007/JHEP03\(2021\)179](https://doi.org/10.1007/JHEP03(2021)179). arXiv:2009.01771
- D. Marzocca, Addressing the B-physics anomalies in a fundamental Composite Higgs Model. *JHEP* **07**, 121 (2018). [https://doi.org/10.1007/JHEP07\(2018\)121](https://doi.org/10.1007/JHEP07(2018)121). arXiv:1803.10972
- S. Saad, Combined explanations of  $(g - 2)_\mu$ ,  $R_{D^{(*)}}$ ,  $R_{K^{(*)}}$  anomalies in a two-loop radiative neutrino mass model. *Phys. Rev. D* **102**, 015019 (2020). <https://doi.org/10.1103/PhysRevD.102.015019>. arXiv:2005.04352
- V. Gherardi, D. Marzocca, E. Venturini, Low-energy phenomenology of scalar leptoquarks at one-loop accuracy. *JHEP* **01**, 138 (2021). [https://doi.org/10.1007/JHEP01\(2021\)138](https://doi.org/10.1007/JHEP01(2021)138). arXiv:2008.09548
- D. Bečirević, I. Doršner, S. Fajfer, N. Košnik, D.A. Faroughy, O. Sumensari, Scalar leptoquarks from grand unified theories to accommodate the  $B$ -physics anomalies. *Phys. Rev. D* **98**, 055003 (2018). <https://doi.org/10.1103/PhysRevD.98.055003>. arXiv:1806.05689
- I. Bigaran, J. Gargalionis, R.R. Volkas, A near-minimal leptoquark model for reconciling flavour anomalies and generating radiative neutrino masses. *JHEP* **10**, 106 (2019). [https://doi.org/10.1007/JHEP10\(2019\)106](https://doi.org/10.1007/JHEP10(2019)106). arXiv:1906.01870
- A. Crivellin, D. Müller, F. Saturnino, Flavor phenomenology of the leptoquark singlet-triplet model. *JHEP* **06**, 020 (2020). [https://doi.org/10.1007/JHEP06\(2020\)020](https://doi.org/10.1007/JHEP06(2020)020). arXiv:1912.04224
- A. Crivellin, D. Müller, T. Ota, Simultaneous explanation of  $R(D^{(*)})$  and  $b \rightarrow s \mu^+ \mu^-$ : the last scalar leptoquarks standing. *JHEP* **09**, 040 (2017). [https://doi.org/10.1007/JHEP09\(2017\)040](https://doi.org/10.1007/JHEP09(2017)040). arXiv:1703.09226
- U. Aydemir, T. Mandal, S. Mitra, Addressing the  $R_{D^{(*)}}$  anomalies with an  $S_1$  leptoquark from  $SO(10)$  grand unification. *Phys. Rev. D* **101**, 015011 (2020). <https://doi.org/10.1103/PhysRevD.101.015011>. arXiv:1902.08108
- T. Mandal, S. Mitra, S. Raz,  $R_{D^{(*)}}$  motivated  $S_1$  leptoquark scenarios: impact of interference on the exclusion limits from LHC data. *Phys. Rev. D* **99**, 055028 (2019). <https://doi.org/10.1103/PhysRevD.99.055028>. arXiv:1811.03561
- S. Iguro, M. Takeuchi, R. Watanabe, Testing leptoquark/EFT in  $\bar{B} \rightarrow D^{(*)} \ell \bar{\nu}$  at the LHC. *Eur. Phys. J. C* **81**, 406 (2021). <https://doi.org/10.1140/epjc/s10052-021-09125-5>. arXiv:2011.02486
- H.M. Lee, Leptoquark option for B-meson anomalies and leptonic signatures. *Phys. Rev. D* **104**, 015007 (2021). <https://doi.org/10.1103/PhysRevD.104.015007>. arXiv:2104.02982
- M. Bordone, O. Catà, T. Feldmann, R. Mandal, Constraining flavour patterns of scalar leptoquarks in the effective field theory. *JHEP* **03**, 122 (2021). [https://doi.org/10.1007/JHEP03\(2021\)122](https://doi.org/10.1007/JHEP03(2021)122). arXiv:2010.03297
- I. Doršner, S. Fajfer, A. Lejlić, Novel leptoquark pair production at LHC. *JHEP* **05**, 167 (2021). [https://doi.org/10.1007/JHEP05\(2021\)167](https://doi.org/10.1007/JHEP05(2021)167). arXiv:2103.11702
- P. Bandyopadhyay, R. Mandal, Revisiting scalar leptoquark at the LHC. *Eur. Phys. J. C* **78**, 491 (2018). <https://doi.org/10.1140/epjc/s10052-018-5959-x>. arXiv:1801.04253
- A. Bhaskar, T. Mandal, S. Mitra, Boosting vector leptoquark searches with boosted tops. *Phys. Rev. D* **101**, 115015 (2020). <https://doi.org/10.1103/PhysRevD.101.115015>. arXiv:2004.01096
- A. Bhaskar, D. Das, T. Mandal, S. Mitra, C. Neeraj, Precise limits on the charge-2/3  $U_1$  vector leptoquark. arXiv:2101.12069
- A. Bhaskar, T. Mandal, S. Mitra, M. Sharma, Improving third-generation leptoquark searches with combined signals and boosted top. arXiv:2106.07605

35. L. Da Rold, M. Epele, A. Medina, N.I. Mileo, A. Szykman, Enhancement of the double Higgs production via leptoquarks at the LHC. [arXiv:2105.06309](#)
36. G. Hiller, D. Loose, I. Nišandžić, Flavorful leptoquarks at the LHC and beyond: spin 1. *JHEP* **06**, 080 (2021). [https://doi.org/10.1007/JHEP06\(2021\)080](https://doi.org/10.1007/JHEP06(2021)080). [arXiv:2103.12724](#)
37. U. Haisch, G. Polesello, Resonant third-generation leptoquark signatures at the Large Hadron Collider. *JHEP* **05**, 057 (2021). [https://doi.org/10.1007/JHEP05\(2021\)057](https://doi.org/10.1007/JHEP05(2021)057). [arXiv:2012.11474](#)
38. K. Chandak, T. Mandal, S. Mitra, Hunting for scalar leptoquarks with boosted tops and light leptons. *Phys. Rev. D* **100**, 075019 (2019). <https://doi.org/10.1103/PhysRevD.100.075019>. [arXiv:1907.11194](#)
39. A. Bhaskar, D. Das, B. De, S. Mitra, Enhancing scalar productions with leptoquarks at the LHC. *Phys. Rev. D* **102**, 035002 (2020). <https://doi.org/10.1103/PhysRevD.102.035002>. [arXiv:2002.12571](#)
40. A. Alves, O.Jt. Eboli, G. Grilli Di Cortona, R.R. Moreira, Indirect and monojet constraints on scalar leptoquarks. *Phys. Rev. D* **99**, 095005 (2019). <https://doi.org/10.1103/PhysRevD.99.095005>. [arXiv:1812.08632](#)
41. I. Doršner, S. Fajfer, M. Patra, A comparative study of the  $S_1$  and  $U_1$  leptoquark effects in the light quark regime. *Eur. Phys. J. C* **80**, 204 (2020). <https://doi.org/10.1140/epjc/s10052-020-7754-8>. [arXiv:1906.05660](#)
42. S. Mandal, M. Mitra, N. Sinha, Probing leptoquarks and heavy neutrinos at the LHeC. *Phys. Rev. D* **98**, 095004 (2018). <https://doi.org/10.1103/PhysRevD.98.095004>. [arXiv:1807.06455](#)
43. R. Padhan, S. Mandal, M. Mitra, N. Sinha, Signatures of  $\tilde{R}_2$  class of leptoquarks at the upcoming  $ep$  colliders. *Phys. Rev. D* **101**, 075037 (2020). <https://doi.org/10.1103/PhysRevD.101.075037>. [arXiv:1912.07236](#)
44. M.J. Baker, J. Fuentes-Martín, G. Isidori, M. König, High- $p_T$  signatures in vector-leptoquark models. *Eur. Phys. J. C* **79**, 334 (2019). <https://doi.org/10.1140/epjc/s10052-019-6853-x>. [arXiv:1901.10480](#)
45. H. Nadeau, D. London, Leptoquarks at e gamma colliders. *Phys. Rev. D* **47**, 3742–3749 (1993). <https://doi.org/10.1103/PhysRevD.47.3742>. [arXiv:hep-ph/9303238](#)
46. S. Atag, O. Cakir, Pair production of scalar leptoquarks at TeV energy gamma p colliders. *Phys. Rev. D* **49**, 5769–5772 (1994). <https://doi.org/10.1103/PhysRevD.49.5769>
47. S. Atag, A. Celikel, S. Sultansoy, Scalar leptoquark production at TeV energy gamma p colliders. *Phys. Lett. B* **326**, 185–189 (1994). [https://doi.org/10.1016/0370-2693\(94\)91212-2](https://doi.org/10.1016/0370-2693(94)91212-2)
48. W. Buchmuller, R. Ruckl, D. Wyler, Leptoquarks in lepton-quark collisions. *Phys. Lett. B* **191**, 442–448 (1987). [https://doi.org/10.1016/0370-2693\(87\)90637-X](https://doi.org/10.1016/0370-2693(87)90637-X) [Erratum: *Phys. Lett. B* **448**, 320–320 (1999)]
49. J. Hewett, T. Rizzo, Leptoquark signals at  $e^+e^-$  colliders. *Phys. Rev. D* **36**, 3367 (1987). <https://doi.org/10.1103/PhysRevD.36.3367>
50. J. Hewett, S. Pakvasa, Leptoquark production in hadron colliders. *Phys. Rev. D* **37**, 3165 (1988). <https://doi.org/10.1103/PhysRevD.37.3165>
51. F. Cuyppers, Leptoquark production in  $e^- \gamma$  scattering. *Nucl. Phys. B* **474**, 57–71 (1996). [https://doi.org/10.1016/0550-3213\(96\)00270-2](https://doi.org/10.1016/0550-3213(96)00270-2). [arXiv:hep-ph/9508397](#)
52. P. Bandyopadhyay, R. Mandal, Vacuum stability in an extended standard model with a leptoquark. *Phys. Rev. D* **95**, 035007 (2017). <https://doi.org/10.1103/PhysRevD.95.035007>. [arXiv:1609.03561](#)
53. S. Saad, A. Thapa, Common origin of neutrino masses and  $R_{D^{(*)}}$ ,  $R_{K^{(*)}}$  anomalies. *Phys. Rev. D* **102**, 015014 (2020). <https://doi.org/10.1103/PhysRevD.102.015014>. [arXiv:2004.07880](#)
54. P.S. Bhupal Dev, A. Soni, F. Xu, Hints of natural supersymmetry in flavor anomalies?. [arXiv:2106.15647](#)
55. W. Altmannshofer, P.S.B. Dev, A. Soni, Y. Sui, Addressing  $R_{D^{(*)}}$ ,  $R_{K^{(*)}}$ , muon  $g - 2$  and ANITA anomalies in a minimal  $R$ -parity violating supersymmetric framework. *Phys. Rev. D* **102**, 015031 (2020). <https://doi.org/10.1103/PhysRevD.102.015031>. [arXiv:2002.12910](#)
56. W. Altmannshofer, P.S. Bhupal Dev, A. Soni,  $R_{D^{(*)}}$  anomaly: a possible hint for natural supersymmetry with  $R$ -parity violation. *Phys. Rev. D* **96**, 095010 (2017). <https://doi.org/10.1103/PhysRevD.96.095010>. [arXiv:1704.06659](#)
57. P. Bandyopadhyay, S. Dutta, A. Karan, Investigating the production of leptoquarks by means of zeros of amplitude at photon electron collider. *Eur. Phys. J. C* **80**, 573 (2020). <https://doi.org/10.1140/epjc/s10052-020-8083-7>. [arXiv:2003.11751](#)
58. P. Bandyopadhyay, S. Dutta, A. Karan, Zeros of amplitude in the associated production of photon and leptoquark at  $e - p$  collider. *Eur. Phys. J. C* **81**, 315 (2021). <https://doi.org/10.1140/epjc/s10052-021-09090-z>. [arXiv:2012.13644](#)
59. P. Bandyopadhyay, S. Dutta, M. Jakkapu, A. Karan, Exploring spins of beyond Standard Models via angular distribution at the LHC. [arXiv:2007.12997](#)
60. S. Dutta, P. Bandyopadhyay, A. Karan, Distinguishing different BSM signatures at present and future colliders. [arXiv:2105.00893](#)
61. R. Mandal, A. Pich, Constraints on scalar leptoquarks from lepton and kaon physics. *JHEP* **12**, 089 (2019). [https://doi.org/10.1007/JHEP12\(2019\)089](https://doi.org/10.1007/JHEP12(2019)089). [arXiv:1908.11155](#)
62. S. Davidson, D.C. Bailey, B.A. Campbell, Model independent constraints on leptoquarks from rare processes. *Z. Phys. C* **61**, 613–644 (1994). <https://doi.org/10.1007/BF01552629>. [arXiv:hep-ph/9309310](#)
63. I. Doršner, S. Fajfer, A. Greljo, J. Kamenik, N. Košnik, Physics of leptoquarks in precision experiments and at particle colliders. *Phys. Rep.* **641**, 1–68 (2016). <https://doi.org/10.1016/j.physrep.2016.06.001>. [arXiv:1603.04993](#)
64. A. Crivellin, D. Müller, L. Schnell, Combined constraints on first generation leptoquarks. *Phys. Rev. D* **103**, 115023 (2021). <https://doi.org/10.1103/PhysRevD.103.115023>. [arXiv:2104.06417](#)
65. ATLAS Collaboration, G. Aad et al. Search for pairs of scalar leptoquarks decaying into quarks and electrons or muons in  $\sqrt{s} = 13$  TeV  $pp$  collisions with the ATLAS detector. *JHEP* **10**, 112 (2020). [https://doi.org/10.1007/JHEP10\(2020\)112](https://doi.org/10.1007/JHEP10(2020)112). [arXiv:2006.05872](#)
66. CMS Collaboration, A.M. Sirunyan et al., Search for singly and pair-produced leptoquarks coupling to third-generation fermions in proton-proton collisions at  $\sqrt{s} = 13$  TeV. *Phys. Lett. B* **819**, 136446 (2021). <https://doi.org/10.1016/j.physletb.2021.136446>. [arXiv:2012.04178](#)
67. ATLAS Collaboration, G. Aad et al., Search for pair production of third-generation scalar leptoquarks decaying into a top quark and a  $\tau$ -lepton in  $pp$  collisions at  $\sqrt{s} = 13$  TeV with the ATLAS detector. *JHEP* **06**, 179 (2021). [https://doi.org/10.1007/JHEP06\(2021\)179](https://doi.org/10.1007/JHEP06(2021)179). [arXiv:2101.11582](#)
68. M. Cepeda et al., Report from Working Group 2: Higgs Physics at the HL-LHC and HE-LHC. CERN Yellow Rep. Monogr. **7**, 221–584 (2019). <https://doi.org/10.23731/CYRM-2019-007.221>. [arXiv:1902.00134](#)
69. FCC Collaboration, A. Abada et al., FCC physics opportunities: future circular collider conceptual design report volume 1. *Eur. Phys. J. C* **79**, 474 (2019). <https://doi.org/10.1140/epjc/s10052-019-6904-3>
70. C.M. Ankenbrandt et al., Status of muon collider research and development and future plans. *Phys. Rev. ST Accel. Beams* **2**, 081001 (1999). <https://doi.org/10.1103/PhysRevSTAB.2.081001>. [arXiv:physics/9901022](#)
71. D. Neuffer, V. Shiltsev, On the feasibility of a pulsed 14 TeV c.m.e. muon collider in the LHC tunnel. *JINST*

- 13, T10003 (2018). <https://doi.org/10.1088/1748-0221/13/10/T10003>. arXiv:1811.10694
72. J.P. Delahaye, M. Diemoz, K. Long, B. Mansoulié, N. Pastrone, L. Rivkin et al., Muon colliders. arXiv:1901.06150
73. T. Han, Y. Ma, K. Xie, Quark and gluon contents of a lepton at high energies. arXiv:2103.09844
74. P. Bandyopadhyay, A. Costantini, Obscure Higgs boson at colliders. Phys. Rev. D **103**, 015025 (2021). <https://doi.org/10.1103/PhysRevD.103.015025>. arXiv:2010.02597
75. G.-Y. Huang, F.S. Queiroz, W. Rodejohann, Gauged  $L_\mu - L_\tau$  at a muon collider. Phys. Rev. D **103**, 095005 (2021). <https://doi.org/10.1103/PhysRevD.103.095005>. arXiv:2101.04956
76. C. Sen, P. Bandyopadhyay, S. Dutta, A. KT, Displaced Higgs production in Type-III Seesaw at the LHC/FCC, MATHUSLA and Muon collider. arXiv:2107.12442
77. A. Costantini, F. De Lillo, F. Maltoni, L. Mantani, O. Mattelaer, R. Ruiz et al., Vector boson fusion at multi-TeV muon colliders. JHEP **09**, 080 (2020). [https://doi.org/10.1007/JHEP09\(2020\)080](https://doi.org/10.1007/JHEP09(2020)080). arXiv:2005.10289
78. G.-Y. Huang, S. Jana, F.S. Queiroz, W. Rodejohann, Probing the  $R_{K^{(*)}}$  anomaly at a muon collider. arXiv:2103.01617
79. P. Asadi, R. Capdevilla, C. Cesarotti, S. Homiller, Searching for leptoquarks at future muon colliders. arXiv:2104.05720
80. N. Cabibbo, Unitary symmetry and leptonic decays. Phys. Rev. Lett. **10**, 531–533 (1963). <https://doi.org/10.1103/PhysRevLett.10.531>
81. M. Kobayashi, T. Maskawa, CP violation in the renormalizable theory of weak interaction. Prog. Theor. Phys. **49**, 652–657 (1973). <https://doi.org/10.1143/PTP.49.652>
82. R. Mandal, C. Murgui, A. Peñuelas, A. Pich, The role of right-handed neutrinos in  $b \rightarrow c\tau\bar{\nu}$  anomalies. JHEP **08**, 022 (2020). [https://doi.org/10.1007/JHEP08\(2020\)022](https://doi.org/10.1007/JHEP08(2020)022). arXiv:2004.06726
83. P. Arnan, D. Becirevic, F. Mescia, O. Sumensari, Probing low energy scalar leptoquarks by the leptonic  $W$  and  $Z$  couplings. JHEP **02**, 109 (2019). [https://doi.org/10.1007/JHEP02\(2019\)109](https://doi.org/10.1007/JHEP02(2019)109). arXiv:1901.06315
84. A. Falkowski, D. Straub, Flavourful SMEFT likelihood for Higgs and electroweak data. JHEP **04**, 066 (2020). [https://doi.org/10.1007/JHEP04\(2020\)066](https://doi.org/10.1007/JHEP04(2020)066). arXiv:1911.07866
85. E. Coluccio Leskow, G. D'Ambrosio, A. Crivellin, D. Müller,  $(g - 2)_\mu$ , lepton flavor violation, and  $Z$  decays with leptoquarks: correlations and future prospects. Phys. Rev. D **95**, 055018 (2017). <https://doi.org/10.1103/PhysRevD.95.055018>. arXiv:1612.06858
86. A. Crivellin, C. Greub, D. Müller, F. Saturnino, Scalar leptoquarks in leptonic processes. JHEP **02**, 182 (2021). [https://doi.org/10.1007/JHEP02\(2021\)182](https://doi.org/10.1007/JHEP02(2021)182). arXiv:2010.06593
87. L. Di Luzio, M. Kirk, A. Lenz, T. Rauh,  $\Delta M_s$  theory precision confronts flavour anomalies. JHEP **12**, 009 (2019). [https://doi.org/10.1007/JHEP12\(2019\)009](https://doi.org/10.1007/JHEP12(2019)009). arXiv:1909.11087
88. W. Altmannshofer, P. Stangl, New physics in rare B decays after Moriond 2021. arXiv:2103.13370
89. A. Angelescu, D. Bečirević, D. Faroughy, O. Sumensari, Closing the window on single leptoquark solutions to the  $B$ -physics anomalies. JHEP **10**, 183 (2018). [https://doi.org/10.1007/JHEP10\(2018\)183](https://doi.org/10.1007/JHEP10(2018)183). arXiv:1808.08179
90. A. Angelescu, D. Bečirević, D.A. Faroughy, F. Jaffredo, O. Sumensari, On the single leptoquark solutions to the  $B$ -physics anomalies. arXiv:2103.12504
91. F. Staub, SARAH 4: a tool for (not only SUSY) model builders. Comput. Phys. Commun. **185**, 1773–1790 (2014). <https://doi.org/10.1016/j.cpc.2014.02.018>. arXiv:1309.7223
92. A. Belyaev, N.D. Christensen, A. Pukhov, CalcHEP 3.4 for collider physics within and beyond the Standard Model. Comput. Phys. Commun. **184**, 1729–1769 (2013). <https://doi.org/10.1016/j.cpc.2013.01.014>. arXiv:1207.6082
93. T. Sjostrand, S. Mrenna, P.Z. Skands, PYTHIA 6.4 physics and manual. JHEP **05**, 026 (2006). <https://doi.org/10.1088/1126-6708/2006/05/026>. arXiv:hep-ph/0603175
94. M. Cacciari, G.P. Salam, G. Soyez, FastJet user manual. Eur. Phys. J. C **72**, 1896 (2012). <https://doi.org/10.1140/epjc/s10052-012-1896-2>. arXiv:1111.6097
95. NNPDF Collaboration, E.R. Nocera, R.D. Ball, S. Forte, G. Ridolfi, J. Rojo, A first unbiased global determination of polarized PDFs and their uncertainties. Nucl. Phys. B **887**, 276–308 (2014). <https://doi.org/10.1016/j.nuclphysb.2014.08.008>. arXiv:1406.5539
96. A. Alves, O. Eboli, T. Plehn, Stop lepton associated production at hadron colliders. Phys. Lett. B **558**, 165–172 (2003). [https://doi.org/10.1016/S0370-2693\(03\)00266-1](https://doi.org/10.1016/S0370-2693(03)00266-1). arXiv:hep-ph/0211441
97. J. Alwall, M. Herquet, F. Maltoni, O. Mattelaer, T. Stelzer, MadGraph 5: going beyond. JHEP **06**, 128 (2011). [https://doi.org/10.1007/JHEP06\(2011\)128](https://doi.org/10.1007/JHEP06(2011)128). arXiv:1106.0522
98. CMS Collaboration, A.M. Sirunyan et al., Identification of heavy-flavour jets with the CMS detector in pp collisions at 13 TeV. JINST **13**, P05011 (2018). <https://doi.org/10.1088/1748-0221/13/05/P05011>. arXiv:1712.07158
99. CMS Collaboration, I.R. Tomalin, B tagging in CMS, J. Phys. Conf. Ser. **110**, 092033 (2008). <https://doi.org/10.1088/1742-6596/110/9/092033>
100. CMS Collaboration, B-tagging performance of the CMS Legacy dataset, TWiki@ CERN (2018)
101. G. Bagliesi, Tau tagging at Atlas and CMS. In 17th Symposium on Hadron Collider Physics 2006 (HCP 2006). arXiv:0707.0928
102. CMS Collaboration, G.L. Bayatian et al., CMS technical design report, volume II: physics performance. J. Phys. G **34**, 995–1579 (2007). <https://doi.org/10.1088/0954-3899/34/6/S01>
103. ATLAS Collaboration, Performance and calibration of the Jet-FitterCharm algorithm for c-jet identification, ATL-PHYS-PUB-2015-001
104. N. Mohr, Dilepton mass edge measurement in SUSY events with CMS. In: 44th Rencontres de Moriond on Electroweak Interactions and Unified Theories. arXiv:0904.3408
105. CMS Collaboration, Discovery potential and measurement of a dilepton mass edge in SUSY events at  $\sqrt{s} = 10$  TeV, CMS-PAS-SUS-09-002
106. H. Al Ali et al., The muon smasher's guide. arXiv:2103.14043
107. A. Azatov, F. Garosi, A. Greljo, D. Marzocca, J. Salko, S. Trifinopoulos, New physics in  $b \rightarrow s\mu\mu$ : FCC-hh or a muon collider?. arXiv:2205.13552
108. P. Bandyopadhyay, E.J. Chun, C. Sen, Boosted displaced decay of right-handed neutrinos at CMS, ATLAS and MATHUSLA. arXiv:2205.12511
109. CMS Collaboration, G.L. Bayatian et al., CMS technical design report, volume II: physics performance. J. Phys. G **34**, 995–1579 (2007). <https://doi.org/10.1088/0954-3899/34/6/S01>
110. J. Hubisz, J. Lykken, M. Pierini, M. Spiropulu, Missing energy look-alikes with  $100 \text{ pb}^{-1}$  at the LHC. Phys. Rev. D **78**, 075008 (2008). <https://doi.org/10.1103/PhysRevD.78.075008>. arXiv:0805.2398
111. ATLAS Collaboration, Simulation-based extrapolation of  $b$ -tagging calibrations towards high transverse momenta in the ATLAS experiment, ATL-PHYS-PUB-2021-003 (2021)
112. ATLAS Collaboration, Direct constraint on the Higgs-charm coupling from a search for Higgs boson decays to charm quarks with the ATLAS detector, ATLAS-CONF-2021-021 (2021)
113. ATLAS, CDF, CMS, D0 Collaboration, T. Theveneaux-Pelzer and J. Fernandez Menendez, Leptons:  $e$ ,  $\mu$ ,  $\tau$  + systematic uncertainties. In 6th International Workshop on Top Quark Physics, pp. 262–271 (2014). <https://doi.org/10.3204/DESY-PROC-2014-02/3>

114. ATLAS Collaboration, G. Aad et al., Jet energy scale and resolution measured in proton–proton collisions at  $\sqrt{s} = 13$  TeV with the ATLAS detector. *Eur. Phys. J. C* **81**, 689 (2021). <https://doi.org/10.1140/epjc/s10052-021-09402-3>. [arXiv:2007.02645](https://arxiv.org/abs/2007.02645)
115. P. Bandyopadhyay, A. Datta, A. Datta, B. Mukhopadhyaya, Associated Higgs production in CP-violating supersymmetry: probing the ‘open hole’ at the large hadron collider. *Phys. Rev. D* **78**, 015017 (2008). <https://doi.org/10.1103/PhysRevD.78.015017>. [arXiv:0710.3016](https://arxiv.org/abs/0710.3016)
116. J. Alwall, R. Frederix, S. Frixione, V. Hirschi, F. Maltoni, O. Mattelaer et al., The automated computation of tree-level and next-to-leading order differential cross sections, and their matching to parton shower simulations. *JHEP* **07**, 079 (2014). [https://doi.org/10.1007/JHEP07\(2014\)079](https://doi.org/10.1007/JHEP07(2014)079). [arXiv:1405.0301](https://arxiv.org/abs/1405.0301)
117. J.M. Campbell, R.K. Ellis, C. Williams, Vector boson pair production at the LHC. *JHEP* **07**, 018 (2011). [https://doi.org/10.1007/JHEP07\(2011\)018](https://doi.org/10.1007/JHEP07(2011)018). [arXiv:1105.0020](https://arxiv.org/abs/1105.0020)
118. T. Binoth, G. Ossola, C.G. Papadopoulos, R. Pittau, NLO QCD corrections to tri-boson production. *JHEP* **06**, 082 (2008). <https://doi.org/10.1088/1126-6708/2008/06/082>. [arXiv:0804.0350](https://arxiv.org/abs/0804.0350)
119. P. Azzi et al., Report from Working Group 1: Standard Model Physics at the HL-LHC and HE-LHC. CERN Yellow Rep. Monogr. **7**, 1–220 (2019). <https://doi.org/10.23731/CYRM-2019-007.1>. [arXiv:1902.04070](https://arxiv.org/abs/1902.04070)